Radiative Cooling in the Nocturnal Boundary Layer

CENTRALE LANDBOUWCATALOGUS
0000 0312 5933

Promotoren: dr. ir. L. Wartena,
Hoogleraar in de landbouwweerkunde
en omgevingsnatuurkunde.

dr. ir. F.T.M. Nieuwstadt,
Hoogleraar in de stromingsleer aan de Technische Universiteit
van Delft.

Co-promotor: dr. J. Reiff,
wetenschappelijk medewerker aan het Koninklijk Nederlands
Meteorologisch Instituut.

NN08201, 1251

Radiative Cooling in the Nocturnal Boundary Layer

Stephen A. Tjemkes

Proefschrift
ter verkrijging van de graad van
doctor in de landbouwwetenschappen,
op gezag van de rector magnificus,
dr. H.C. van der Plas,
in het openbaar te verdedigen
op woensdag 21 december 1988
des namiddags te vier uur in de aula
van de Landbouwuniversiteit te Wageningen.

BIBLIOTHEEK
LANDBOUWUNIVERSITEIT
WAGENINGEN

ISN = 288061

Voorwoord

Dit proefschrift is een verslag van 4 jaar onderzoek aan het transport van langgolvige straling door de nachtelijke grenslaag. Gedurende deze periode heb ik gewerkt op het Koninklijk Nederlands Meteorologisch Instituut (KNMI) in dienst van de werkgemeenschap Meteorologie en Fysische Oceanografie (MFO).

Op het KNMI werd al geruime tijd onderzoek gedaan aan de nachtelijke grenslaag. Dit onderzoek concentreerde zich op het energie transport in de nachtelijke grenslaag door turbulentie. Gedurende dit onderzoek, ging men zich afvragen in hoeverre langgolvige straling bijdraagt aan dit energie transport. En vervolgens hoe langgolvige straling de structuur van de grenslaag beinvloed. Een andere groep onderzoekers op het KNMI, welke zich bezig hield met het ontwikkelen van grenslaag modellen voor de korte termijn weersverwachting, vroeg zich af hoe in een nieuw grenslaag model, het transport van langgolvige straling efficient berekend kon worden.

Bij de werkgemeenschap MFO werd, voor onderzoek aan deze vragen, een subsidie aangevraagd. Met het geld van deze subsidie, ben ik in de gelegenheid gesteld om onderzoek aan het transport van langgolvige straling door de nachtelijke grenslaag te doen. Omdat dit een omvangrijk onderzoeksterrein is heb ik mij beperkt tot de wolkenloze nachtelijke grenslaag. In dit proefschrift vindt U een verslag van mijn onderzoeksactiviteiten. Maar voordat U, geachte lezer, met hoofdstuk 1 begint wil ik eerst de volgende personen bedanken voor hun steun en samenwerking gedurende de afgelopen vier jaar.

Mijn (co) promotoren Frans Nieuwstadt, Hans Reiff en Bert Wartena voor hun opmerkingen en adviezen gedurende mijn promotie onderzoek. Bovendien wil ik Frans en Hans bedanken voor hun samenwerking bij de gemeenschappelijke publicaties.

Kamergenoot Peter Duynkerke voor de leerzame, turbulente dicussies en de prettige samenwerking bij onze gemeenschappelijke publicaties. Ik hoop dat ik in de toekomst nog vaker met je kan samenwerken.

De collega's voor het lezen en becommentariëren van de verschillende manuscripten. Met name Anton Beljaars, Han van Dop en Bert Holtslag.

De coordinator van de afdeling fysische meteorologie, Wim Schipper voor de hulp bij het aanschaffen van de MacIntosh PC en laserprinter en het bekwaam oplossen van diverse problemen.

Graeme Stephens, associate professor at the Colorado State University, for his hospitality and stimulating discussions during my two months stay at CSU. I'm looking forward to our future cooperation.

De secretaresses Sandra Klutz en Marleen Kaltofen, de studio en de drukkerij voor de vormgeving van de diverse publicaties welke de basis vormen van dit proefschrift.

Het KNMI voor de geboden faciliteiten.

Mijn ouders, welke mijn studie hebben mogelijk gemaakt.

En mijn levensgezellinen Petra Venema, Roeby en Esra Tjemkes voor de vele prettige momenten samen in het verleden, het heden en (hopenlijk) in de toekomst.

pNO8201, 7251

STELLINGEN

1. De thermodynamische structuur in het middengedeelte van de turbulente nachtelijke grenslaag wordt vrijwel niet beinvloed door directe infrarode stralingskoeling (dit proefschrift).

2. In de stationaire oppervlaktelaag is het verticale profiel van de dimensieloze turbulente warmteflux sterk gekromd (dit proefschrift).

3. Een statistische interpretatie van het Goody bandmodel kan niet worden gerechtvaardigd (dit proefschrift).

4. De vervanging van de benzinemotor door de waterstofmotor zal eerder het broeikas effect versterken dan doen afnemen.

5. Bandmodellen kunnen niet het gecombineerde effect van verstrooiing en absorptie van straling door aerosolen beschrijven.

6. Het huidige formaat van de krant nodigt niet uit om óók de binnenpagina's te lezen.

7. Ter voorbereiding op een wetenschappelijke carriere, zou een college engels rapporteren opgenomen moeten worden in het studiepakket, zodat studenten al in een vroeg stadium zich kunnen bekwamen in het schrijven van engelstalige artikelen.

8. Om het weer en klimaat realistischer te beschrijven dient in globale weer- en klimaatmodellen het één-dimensionale model van het atmosferische stralingtransport vervangen te worden door een drie-dimensionaal.

9. Goedkope agrarische produkten worden uiteindelijk duur betaald.

10. Promoveren op een meteorologisch onderwerp betekent het najagen van wind.

Stellingen behorend bij het proefschrift:

"Radiative Cooling in the
Nocturnal Boundary Layer"

van Stephen A. Tjemkes
promotie op 21 december 1988
om 16:00 in de aula van de LU-Wageningen.

Contents

Voorwoord iv

Contents v

Abstract ix

Chapter 1
Introduction 1
1.1 The atmospheric spectrum 1
1.2 Consequences of infrared radiation. 3
2. Introduction to the present work 5
2.1 Guide to this thesis 7

Chapter 2.
Infrared radiation through a cloudless sky 8
1. Problem formulation 8
2. The frequency integral 11
i) The combined absorption of two different gases. 13
ii) Finite atmospheres. 14
2.1 Emissivity models 15
2.2 Wide and narrow band model 17
2.2.1 Regular wide and narrow band 17
i) Governing equations for a regular wide band model. 20
ii) Governing equations for a regular narrow band model. . . 20
2.2.2 Pseudo-monochromatic models. 21
3. The angular integral 23
3.1 regular wide band models 26
3.2 regular narrow band models 27
4. Inhomogeneous atmospheres 28

Chapter 3.
An accurate radiation model 32
1. Abstract 32
2. Introduction 32
3. Model description 32
3.1 Governing equations 32
3.2 The transmission function 33
3.3 The height integral 35
4. Comparison study 37
4.1 Comparison with observations 37
4.2 Influence of observational errors 38
4.3 Comparison with calculations 39
5. Summary 41

Chapter 4
The nocturnal boundary layer
Model calculations compared with observations 43

1. Abstract 43
2. Introduction 43
3. The model 44
3.1 Governing equations 44
3.2 Turbulence closure 45
3.3 Radiation model 45
1) Solar radiation 45
2) Infrared radiation 45
3.4 Boundary conditions 46
1) Upper boundary 46
2) Lower boundary 47
3.5 Numerical procedure 47
4. Observational data 47
4.1 The observational site 49
4.2 Dimensionless wind shear and temperature gradient 49
4.3 Initial conditions 51
1) 30 / 31 May, 1978 51
2) 12 / 13 October 1978 54
5. Discussion of the results 54
5.1 The surface energy balance 54
5.2 The surface temperature 56
5.3 The surface stress and boundary layer height 57
5.5 Profiles of temperature and wind speed 59
5.6 The cooling rate 61
6. Summary and conclusions 63

Chapter 5
A parametrization scheme for the minimum surface temperature 65
1. Abstract 65
2. Introduction 65
3. Model calculations 67
4. Comparison with observations 69
5. Summary 70

Appendix A
A comparison of infrared radiation codes for the nocturnal boundary layer. 71
1. Introduction 71
2. Governing model equations 72
2.1 The narrow band model 72
2.2 The emissivity model 72
2.3 The k-model 73
2.4 Spectroscopic data 75
3. Preliminary Results 75
3.1 Overlap parametrization. 75
3.2 Intercomparison of the models 75
4. Conclusions 79

Appendix B.
A new look at the Goody band model 81
1. Abstract 81
2. Introduction 81
3. The mean transmission function 83
3.1 The flat line approach 83
3.2 The statistical approach 84
3.3 Test calculations 85

4. The mean equivalent width 87
4.1 A simple interpolation formula 87
4.2 Test calculations 91
5. Summary and conclusions 93

Appendix C
List of symbols 96

Appendix D
The transmission function 99
D.1 Gaseous absorption 99
D.2 Continuum absorption 100

References 101

Samenvatting en Conclusies. 106

Cirriculum Vitae 108

We work in the dark-we do what we can-we give what we have. Our doubt is our passion and our passion is our task. The rest is the madness of art.

Philip Roth

Abstract

Errata

...versiteit van Delft"

Op het schut
vervangen v

Op het sch
vervanger

Uitnodiging

voor het bijwonen van mijn promotie
op 21 december 1988 om 16.00 uur
in de aula van de Landbouwuniversiteit
Generaal Foulkesweg 1a, Wageningen.

Na afloop van de promotie is er gelegenheid tot felicitatie.

De receptie (tevens afscheidsfeest)
wordt gehouden in Stadskasteel Oudaen,
Oudegracht 99, Utrecht vanaf 21.00 uur
(voor een plattegrond z.o.z.).

Geen cadeaus, bloemen of toespraken

Petra Venema en Stephen Tjemkes
Vrieswijk 18, Heiloo

Chapter 1
Introduction

All material with a temperature above absolute zero (0 K or -273.15 °C) emit electromagnetic radiation. The wavelength of the emitted radiation depends strongly on the temperature of the emitter. The earth surface and atmosphere emit at relatively low temperatures (≈ 270 K). The wavelength of terrestrial radiation is therefore in between 3.6 and 100 μm, which is in the infrared part of the electromagnetic wavelength range. The sun emits at a much higher temperature (≈ 6500 K). The wavelength of solar radiation is between 0.3 and 3.6 μm, which is in the visible part of the electromagnetic wavelength range. Due to the wavelength difference, terrestrial and solar radiation terrestrial and solar radiation do not interact and can be considered separately. For that reason one usually concentrate only on one type of radiation only. Here we study terrestrial or infrared radiation.

In contrast to the radiation of the sun, terrestrial radiation cannot be observed by the human eye. The existence of invisible radiation has been demonstrated by W. Herschel. In 1800 he measured what he called the relative heating power of solar radiation. For that purpose he passed solar radiation through a prism, such that it was split into its components. Then he used sensitive thermometers to determine the relative heating power of light of different wavelengths. It turned out that the heating power increased from violet to red and even increased beyond the red where no visible radiation was observed. Nowadays, we are familiar with more kinds of invisible radiation. For instance we prepare our food with microwaves and use x-rays to examine broken bones.

1.1 The atmospheric spectrum

The atmosphere nor the surface emits infrared radiation uniformly over all frequencies. The distribution of radiative intensity as a function of frequency is called a spectrum. In Fig. 1.1 the spectra of upward and downward radiation measured at the surface are presented. The two spectra are similar except for the spectral region between 8 and 13 μm. In this region the upward radiation spectrum, peaks around 10 μm, whereas except for a small peak at 9.6 μm, the downward radiation spectrum exhibits a minimum. This difference in downward and upward radiation arises from the vertical thermodynamic structure and the spectral characteristics of the atmosphere.

Consider the spectral regions from 3.6 to 8 and from 13 to 20 μm where the upward and downward spectra are quite similar. In these regions strong absorption bands of infrared active gases such as water vapor and carbon dioxide exists. This means that in the atmosphere infrared radiation can travel only short distances between the successive events of emission and absorption. Downward infrared radiation received at the surface originates from the lowest levels of the atmosphere (typically 100 m above the surface). The temperature of these layers differs only slightly from the surface temperature. Therefore in strong absorption bands the downward radiation from the atmosphere differs only slightly from the upward surface radiation.

The spectral region between 8 and 13 μm is known as the atmospheric window region for infrared radiation, for in this region infrared radiation in the atmosphere is only weakly absorbed. Infrared radiation in the window region can travel long distances before being absorbed. Infrared radiation received at the surface originates

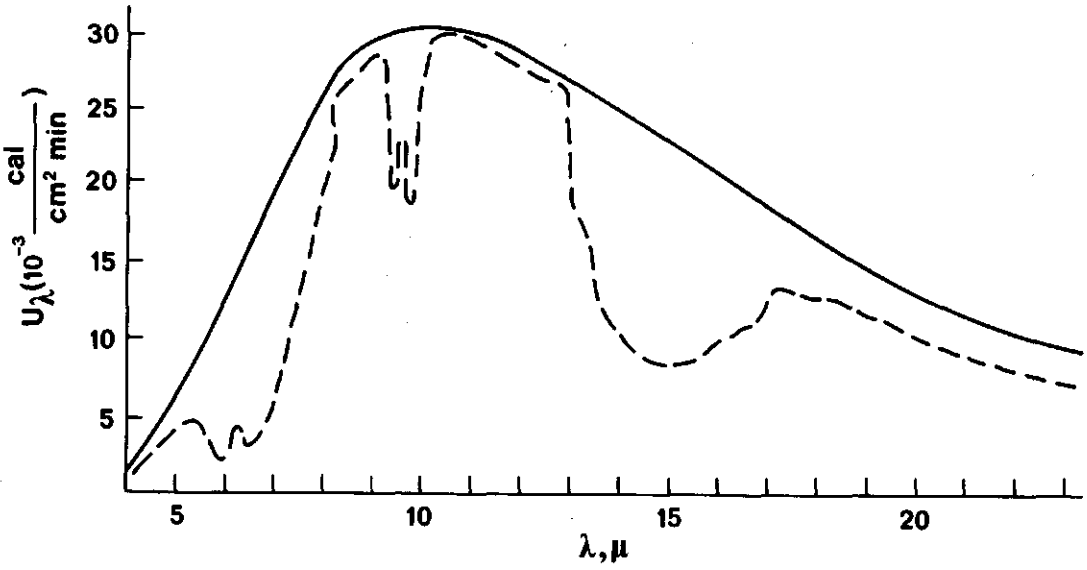

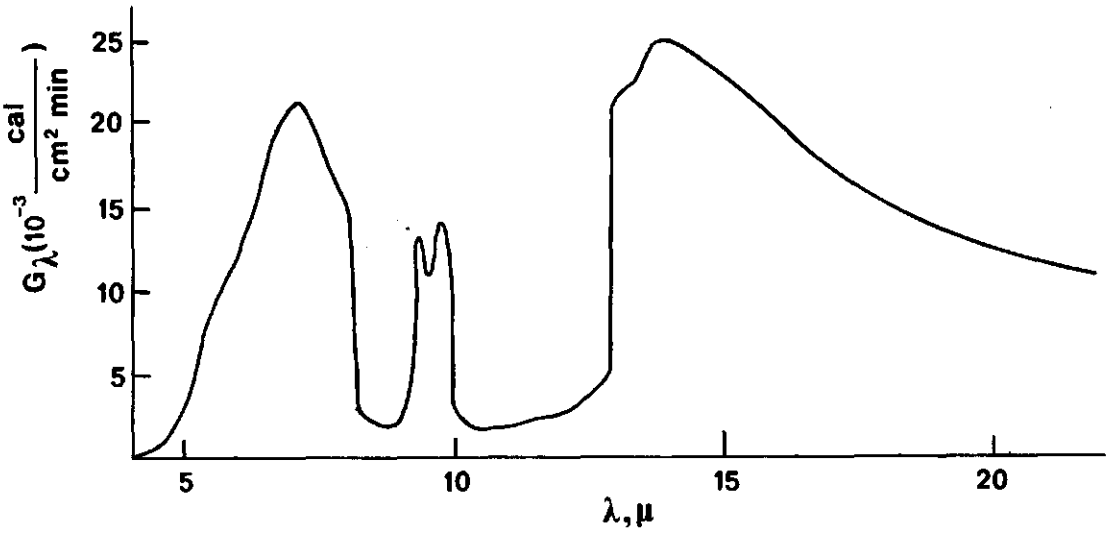

Fig. 1.1 upper fig.: *Spectral intensities of the upward radiation at the surface (solid line) and at the top of the atmosphere (dashed line) at 20:00 hr, Nov. 14, 1963 Rostov on Don (USSR).*

Fig. 1.1 lower fig.: *Spectral intensities of the downward radiation at the surface at 20:00 hr, Nov. 14, 1963 Rostov on Don (USSR). Modified from Kondratyev (1969)*

from levels high in the atmosphere (typically 30 km), where the temperature is much lower than at the surface. Therefore in the window region the intensity of downward radiation is much less than upward surface radiation. Due to the presence of the window region the surface receives less infrared radiative energy from the atmosphere than it emits into the atmosphere. Hence, the window region determines the amount of energy lost by the surface.

As discussed above, inside the window region only weak absorption lines are present, such that infrared radiation will not be diminished. Therefore, the upwelling radiation at the top of the atmosphere is similar to upward radiation at the surface (Fig. 1.1). Thus the presence of the infrared window allows us to make infrared observation of the surface using air or space born detectors.

1.2 Consequences of infrared radiation.

Our planet is continuously bathed in solar radiation. Yet, the temperature of the earth does not rise continuously. This is because the earth emits as much energy as it receives from the sun. As explained in the previous section, most of this energy is lost by infrared radiation in the window region.

However, the window region is not completely transparent. Carbon dioxide absorbs in the window region. Due to the burning of large amounts of fossil fuels, the atmospheric content of carbon dioxide is increasing monotonically since the middle of the previous century (Fig. 1.2). As a result the absorption in the window region increases and the earth loses less energy than it receives. This causes the global temperature to rise.

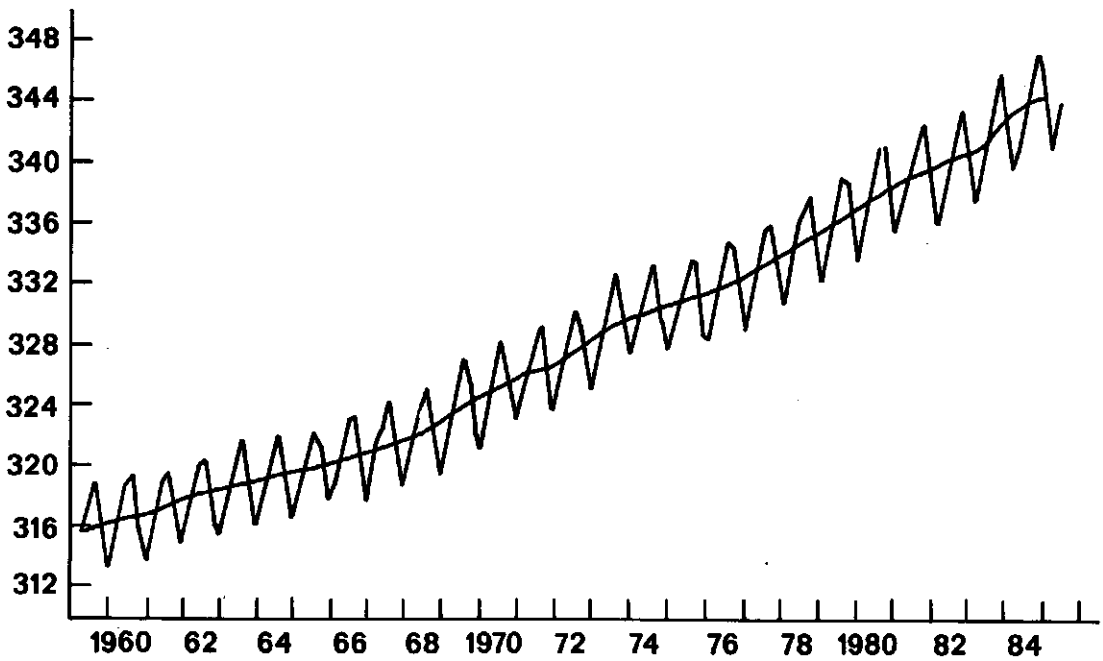

Fig. 1.2 *Carbon dioxide content in part per 10^6 parts at Mauna Loa (Hawaii, USA) since 1960. From NRC-Handelsblad (july 12, 1988)*

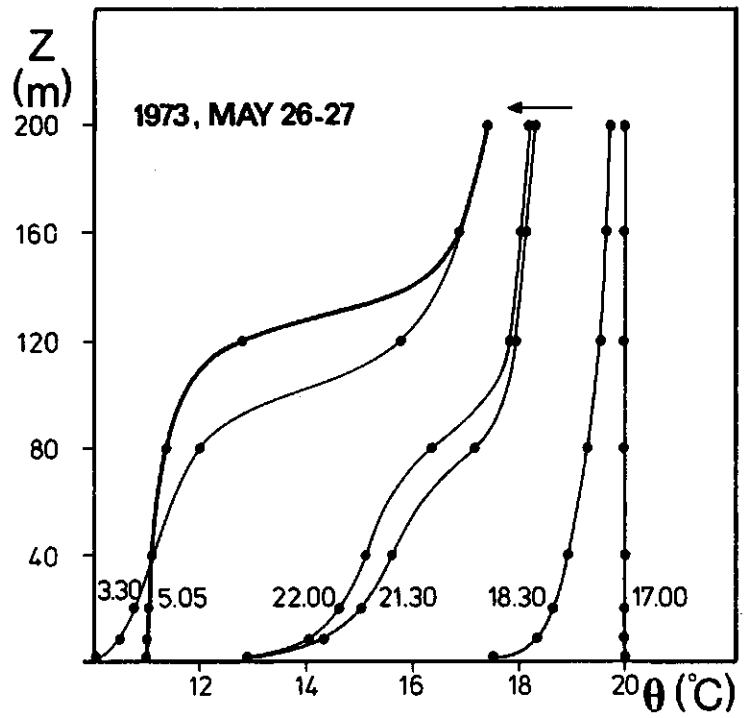

Fig. 1.3 *Potential temperature as a function of height measured at Cabauw on a clear night, with a high windvelocity U(200 m) = 10 m/s.*

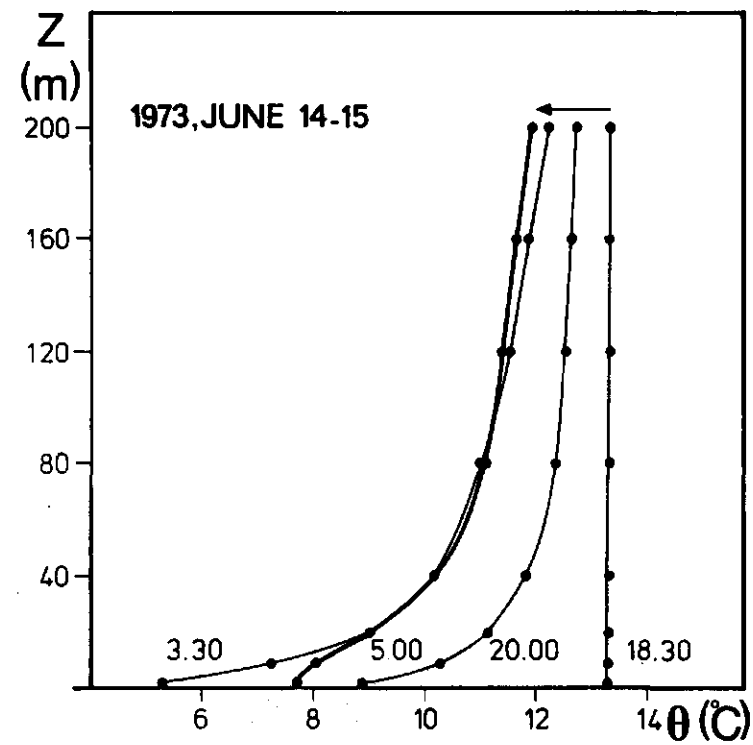

Fig. 1.3 (cont) *Potential temperature as a function of height measured at Cabauw on a clear night, with a windvelocity U(200 m) = 1 m/s (after van Ulden and Holtslag (1985).*

This scenario of global warming is referred to as the greenhouse effect, since in a greenhouse infrared energy losses is prohibit by the glass walls. Based on computer simulations the global temperature is expected to rise by 1 - 4 K due to this effect. Not only the increased carbon dioxide content is responsible for the greenhouse effect. Other gases such as methane and nitrous oxide are also able to increase the atmospheric absorption in the window.

Also on a much smaller scale the consequences of infrared radiation can be observed. To give a very local example, on mornings after a clear autumn nights, the pond on the terrain of the Royal Netherlands Meteorological Institute is covered by a tin layer of ice. However, not the entire pool is covered by ice. Near a tree, which inclines partly over the pool, generally no ice is observed. The reason is clear, the water surface cools due to emission of infrared radiation, it warms due to absorption of infrared radiation. Whether there is net radiative warming or cooling depends on the balance between emission and absorption. In the middle of the pool the water receives less radiative energy from the clear sky than that it emits into it. If the net radiative energy loss of the water surface is large enough its temperature can decrease below the freezing point. The tree emits more than the clear sky. This extra emission is sometimes just enough to prevents the water under the tree from freezing.

Finally, I would like to discuss now an example concerning my own study. At the end of a clear day, the earth surface cools due to emission of infrared radiation. The atmospheric layers within the lowest 200 m of the atmosphere, called the nocturnal surface inversion (NSI), cools at the same time, because heat is transferred from these layers towards the cooling surface. Two different processes are responsible for this heat transfer towards the surface. Turbulent mixing and infrared radiation. The structure of the NSI depends strongly on the relative contributions of these processes. If turbulent mixing dominates over radiative transfer the potential temperature varies slowly with height. (Fig. 1.3). But if radiation dominates over turbulent mixing, the potential temperature profile is rather logarithmic shaped (Fig. 1.3). While infrared radiative cooling is present throughout the entire NSI, turbulent mixing is restricted to the lower parts of the NSI. These layers are referred to as the nocturnal boundary layer. The intent of this thesis is to analyze the influence of infrared radiative cooling on the NBL.

2. Introduction to the present work

The best approach to study the influence of infrared radiation upon the NBL is to make detailed observations of the radiative cooling rate profile. This was done by Funk in 1960. He concluded that radiative transfer in the lowest 2 m of the NBL results in extremely large cooling rates, with values on the order of 50 K per day. Because his observations are restricted to the lower parts of the NBL, no conclusions on the radiative cooling rate profile through the entire NBL can be made. Except for these observations near the surface reported by Funk (1960) no accurate in situ observations of the radiative cooling rate profile exist.

As a consequence of the energy equation, the cooling rate is determined by the divergence of the radiative and turbulent heat flux. Therefore observations of the turbulent heat flux profile in connection to observations of the cooling ratio, could be used to study the influence of infrared radiative transfer indirectly. From his study of the stationary boundary layer, Nieuwstadt (1984) argued that the turbulent heat flux ($\overline{w'\theta'}$) decreases linearly with height (Fig. 2.1)

$$\overline{w'\theta'}\,(z) = \overline{w'\theta'}\,(z=z_o)\left(1 - \frac{z}{h}\right) \qquad (2.1)$$

which agrees reasonably well with observations although Nieuwstadt neglected

radiative transfer. From this work we might conclude that infrared radiative cooling has no impact on the turbulent structure of the stationary boundary layer. On the otherhand Lenschow et al. (1988) argued that infrared radiative cooling within the NBL results in an increasing slope with height of the turbulent heat flux profile. From their observations they proposed

$$\overline{w'\theta'}\,(z) = \overline{w'\theta'}\,(z=z_o)\left(1 - \frac{z}{h}\right)^{1.5} \qquad (2.2)$$

which diverge in the upper half of the NBL from Nieuwstadt's relation (Fig. 2.1).

Instead of observations, model calculations can be used. The interaction between radiation and turbulence has numerically been simulated by a variety of authors such as Garratt and Brost (1981), André and Mahrt (1982), Coantic and Simenon (1984), Estournel (1988). Estournel (1988) found that that the turbulent heat flux decreases linearly with height, which confirmes the findings of Nieuwstadt (1984). However, Garratt and Brost (1981) concluded that for layers within the bulk of the boundary layer ($0.1 < z/h < 0.7$) infrared radiation contributes only 5% to the total cooling rate. However, they concluded that in the surface layer ($z/h < 0.1$) the infrared radiative cooling rate is even larger than the total cooling rate. As a result, turbulent mixing cools the layers in the middle of the NBL, but it must warms the layers near the bottom. Such that a low level maximum in the turbulent heat flux is generated (Fig. 2.1). These findings of Garratt and Brost are in correspondence with the observations of the radiative cooling rate near the surface as reported by Funk (1960), but they disagree with the observations of the turbulent heat flux reported by Lenschow et al. (1988) and Nieuwstadt (1984). Especially in the lower half of the NBL (Fig. 2.1). Thus there remains some confusion on the impact of infrared radiative transfer on the structure of the NBL.

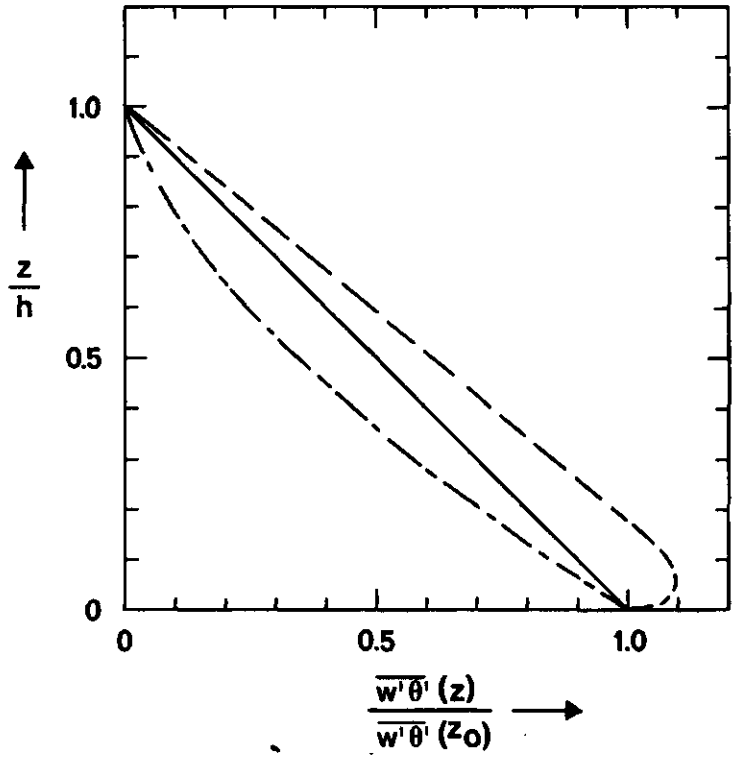

Fig. 2.1 *Normilized turbulent heat flux as a function of normilized height according to Nieuwstadt (1984) (Solid line), according to Lenschow et al. (1988, dashed dotted line) and schematic according to Garratt and Brost (1982, dashed line).*

The NBL is usually only a few hundred meters deep. Our interest in the radiative transfer is thus restricted to a rather thin layer of air. Yet, radiation in the NBL is usually described in terms of empirical relations, which are developed to describe radiative transfer in large scale numerical weather models (cf. Garratt and Brost, 1981). It is far from evident that these empirical models may be used to describe the microphysical processes within the NBL. Funk (1960) showed that especially near the surface, empirical schemes may diverge from observations. Therefore, our aim is to develop and test a radiation model which accurately simulates radiative cooling within the NBL. This radiation model will be used in combination with a turbulence model to simulate the interaction between infrared radiation and turbulence in the NBL.

2.1 Guide to this thesis

A description of the accurate radiation model is given in chapter 3, with some additional theory in Appendix B. Moreover in chapter 3 we compare the performance of the radiation model with observations and with other independent calculations. In chapter 4 this radiation model is used in combination with a turbulence model for a simulation study of the nocturnal boundary layer. In this chapter we compare the performance of the combined radiation-turbulence model with observations of two cloudless nights collected at the meteorological observational site near Cabauw in The Netherlands. The combined-radiation turbulence model is used further in a study on the influence of the geostrophic wind on the minimum surface temperature. The results of this study is given in chapter 5. In Appendix A a description of a fast radiation code for future use in boundary layer models is given, together with an comparison of this fast code with the accurate radiation model.

In the next chapter (chapter 2) an introduction to some basic radiative transfer theory is given. In this chapter we also discuss some problems related with the transfer of infrared radiation through a cloudless atmosphere. The objective of chapter 2 is to introduce some frequently used concepts to approximate the formal solution of the radiative transfer equation. As such this chapter can be considered as background for the following chapters. The objective of this chapter is not to discuss infrared radiative transfer theory in depth nor to provide an extensive overview of all possible radiation models available in the literature. The interested reader is referred to some excellent publications such as written by Chandrasekhar (1960), Goody (1964), Liou (1980), Tiwari (1978), Stephens (1984) or Cess et al. (1986).

Chapter 2.
Infrared radiation through a cloudless sky

1. Problem formulation

Consider a plane parallel horizontally homogeneous atmosphere such that all variables depend only on the height above the surface (Fig. 1.1). The energy content of a pencil of radiation traversing the atmosphere will be changed by its interaction with matter. To describe the removal of energy from the radiation field by matter we used the macroscopic variable χ (unit: m^{-1}) called the extinction coefficient. It defines the amount of energy removed from a element of material from the radiation field. Let I represents the specific intensity of a pencil of radiation (units: $Wm^{-2}Hz^{-1}sr^{-1}$) then we may write for the loss of energy

$$dI_\nu(z,\mu) = -\chi_\nu(z)\, I_\nu(z,\mu)\, dz / \mu, \qquad (1.1)$$

where $\mu = \cos\theta$, where θ the angle between the vertical and the direction of

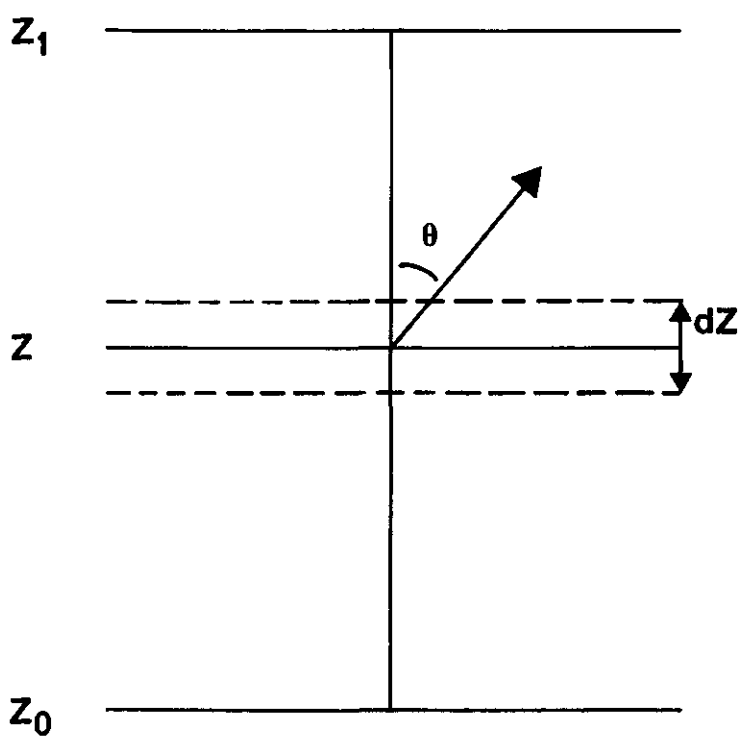

Fig. 1.1 *Plane parallel atmosphere. zo the lower boundary, z1 the upper boundary, z the reference level, dz the layer thickness. The arrow indicates the propagation direction and θ the angle between the vertical and the propagation direction.*

propagation and ν the frequency (unit: Hz). It is useful to distinguish between absorption and scattering processes . During scattering process the infrared wave is not taken from the radiation field but after a scatter event it reappear at a different propagation direction than the incident beam. During an absorption process the infrared wave is completely destroyed by a absorbing particle. If we assume that both processes occur independently, then the total extinction coefficient is found from a linear sum of the absorption coefficient κ and the scatter coefficient σ

$$\chi_\nu(z) = \kappa_\nu(z) + \sigma_\nu(z). \qquad (1.2)$$

In the atmosphere infrared radiation can be scattered by aerosols and cloud droplets and can be absorbed by infrared active molecules such as water vapor, carbon dioxide and ozone. In cloudless aerosol free atmospheres the contribution of scattering to the total extinction can thus be neglected.

To describe the emission of infrared radiation into the radiation field by matter, we use the macroscopic emission coefficient η. It defines the amount of energy released from a element of material into the radiation field. An important relation exists between the emission and absorption coefficient in the case of strict thermodynamical equilibrium. Consider an adiabatic isothermal enclosure in steady state equilibrium, which states that the energy loss of an element of the enclosure is completely compensated by the energy gain. Moreover, assume that the medium inside the enclosure is homogeneous. Then we may expect the radiation field to be isotropic and homogeneous throughout the enclosure with the thermal emission given by

$$\eta_\nu(z) = \kappa_\nu(z)\, B_\nu(T), \qquad (1.3)$$

which is known as Kirchhoff's law. In (1.3) B represents the Planck-function, which gives the emission of a black body[1]. The atmosphere as a whole is not in thermodynamical equilibrium, but in local thermodynamic equilibrium (LTE). Which states that at each point in the atmosphere we can define a local temperature such that the local emission coefficient is given by Kirchhoffs law.

Let us now consider the transfer of radiation through the atmosphere. The energy content of a pencil of radiation increases due to emission processes and decreases due to absorption processes. Counting up the gains and losses during its traversal the net energy change is given by (Chandrasekhar, 1960)

$$\frac{\partial I_\nu(z,\mu)}{\partial z} = \frac{\kappa_\nu(z)}{\mu}\Big(B_\nu\big(T(z)\big) - I_\nu(z,\mu) \Big). \qquad (1.4)$$

In (1.4) the first term on the right hand side describes the emission of infrared radiation, whereas the second term describes the absorption.

Because the radiative cooling rate is proportional to the gradient of the net flux, for all practical applications the profile of net flux is required. The net radiative flux at a reference level (F(z)) is defined as the summation over all solid angles ($d\omega$) and all

---

[1] A black body is a hypothetical object, with the property of absorbing all incident radiation, regardless its frequency. The total emission of a black body depends only on its temperature. It is independent of the composition of the black body. A black body does not emit radiation uniformly over all frequencies. The distribution of radiative intensity as a function of frequency is known as the Planck function

frequencies (dv) of the specific intensity. For a plane parallel atmosphere this yield (Chandrasekhar, 1960).

$$F(z) = 2\pi \int_0^{\infty} \int_{-1}^{1} I_\nu (z,\mu)\, \mu d\mu\, d\nu. \qquad (1.5)$$

From a solution of (1.4) we may evaluate F(z) according to

$$F(z) = F^{+}(z) - F^{-}(z), \qquad (1.6)$$

where the upward flux F+ is given by

$$F^{+}(z) = \pi \int_0^{\infty} \left\{ B_\nu\big(T(o)\big)\tau_\nu(o,z) + \int_0^{z} B_\nu\big(T(z')\big) \frac{\partial \tau_\nu(z', z)}{\partial z'} dz' \right\} d\nu \qquad (1.7^a)$$

and the downward flux F- by

$$F^{-}(z) = \pi \int_0^{\infty} \left\{ B_\nu\big(T(top)\big)\tau_\nu(top,z) + \int_{top}^{z} B_\nu\big(T(z')\big) \frac{\partial \tau_\nu(z, z')}{\partial z'} dz' \right\} d\nu \qquad (1.7^b)$$

The slab or diffuse transmission function which describes the transmission along the path between z and z' $\{\tau(z,z')\}$ is evaluated according to

$$\tau_\nu(z', z) = 2 \int_0^{1} \exp\left\{ -\int_{z'}^{z} \kappa_\nu(z'')dz''/\mu \right\} \mu d\mu. \qquad (1.8)$$

The first term of the right hand side in (1.7a,b) describes the contribution of radiation from the boundary to the upward and downward flux respectively, whereas the second term describes the contribution of radiation from the levels between the boundary and the reference level.

The evaluation of the net flux at the reference level is thus relatively straight forward. Given the distribution of the absorption coefficient with frequency and the profiles of the infrared active gases and temperature, the net flux is found from a multiple integral (1.5). Models which evaluate the net flux along this way are called "line by line" models and they are regarded as the most accurate models available. The accuracy of line by line models depends on the adopted line profile, especial in the line wings. The precise shape of the line wing is not known, therefore the error in the two flux components evaluated by line by line models is approximately 1% (WMO,1984). Line by line models require too much computer time to be used on a routine base within a numerical forecast model. To obtain a practical evaluation for the net flux, some simplification of the four integrals in (1.5) is necessary. They are

I1: The summation over all frequencies within the infrared spectrum (dv).

I2: The summation over all zenith angles ($d\mu$).
I3: The summation of the absorption coefficient along the line of sight (dz'').
I4: The summation over the contributions from the surrounding atmosphere (dz').

In most radiation schemes, the height integration (I4) is evaluated numerically. Therefore, the object of any parametrization scheme is to provide a simple, accurate and computational efficient method for any of the three remaining integrals I1, I2 and I3. The parametrization of these integrals can not be chosen independently. Once the parametrization for the frequency integral is chosen, the parametrization schemes for the other two integrals are fixed.

The absorption coefficient is a function of pressure and temperature. For simplicity we assume the absorption coefficient to be independent of z in the following two paragraphs. Then the slab transmission function over the layer of thickness Δz (= $z' - z$) is given by

$$\tau_\nu(z', z) = 2 \int_0^1 \exp\left\{-\kappa_\nu \Delta z/\mu\right\} \mu d\mu. \qquad (1.9)$$

Instead of the absorption coefficient, the mass absorption coefficient is frequently used. Let κ^* represent the mass absorption coefficient (units: m^2kg^{-1}) then the slab transmission function over a homogeneous layer is given by

$$\tau_\nu(z',z) = 2 \int_0^1 \exp\left\{-\kappa_\nu^* u / \mu\right\} \mu d\mu\,, \qquad (1.10)$$

with u the absorber amount

$$u = \int_{z'}^{z} \rho(z'')\ dz'' \qquad (1.11)$$

and ρ the density of the infrared active gas.

2. The frequency integral

Since the absorption coefficient (κ) varies rapidly with frequency, a large number of frequency points must be considered if a numerical evaluation of the frequency integral is attempted. Such a numerical evaluation is therefore not practical for a fast evaluation of the net flux. A method to reduce the computational effort, is to consider spectral intervals or bands for which an effective transmission can be defined. The two flux components are then evaluated by

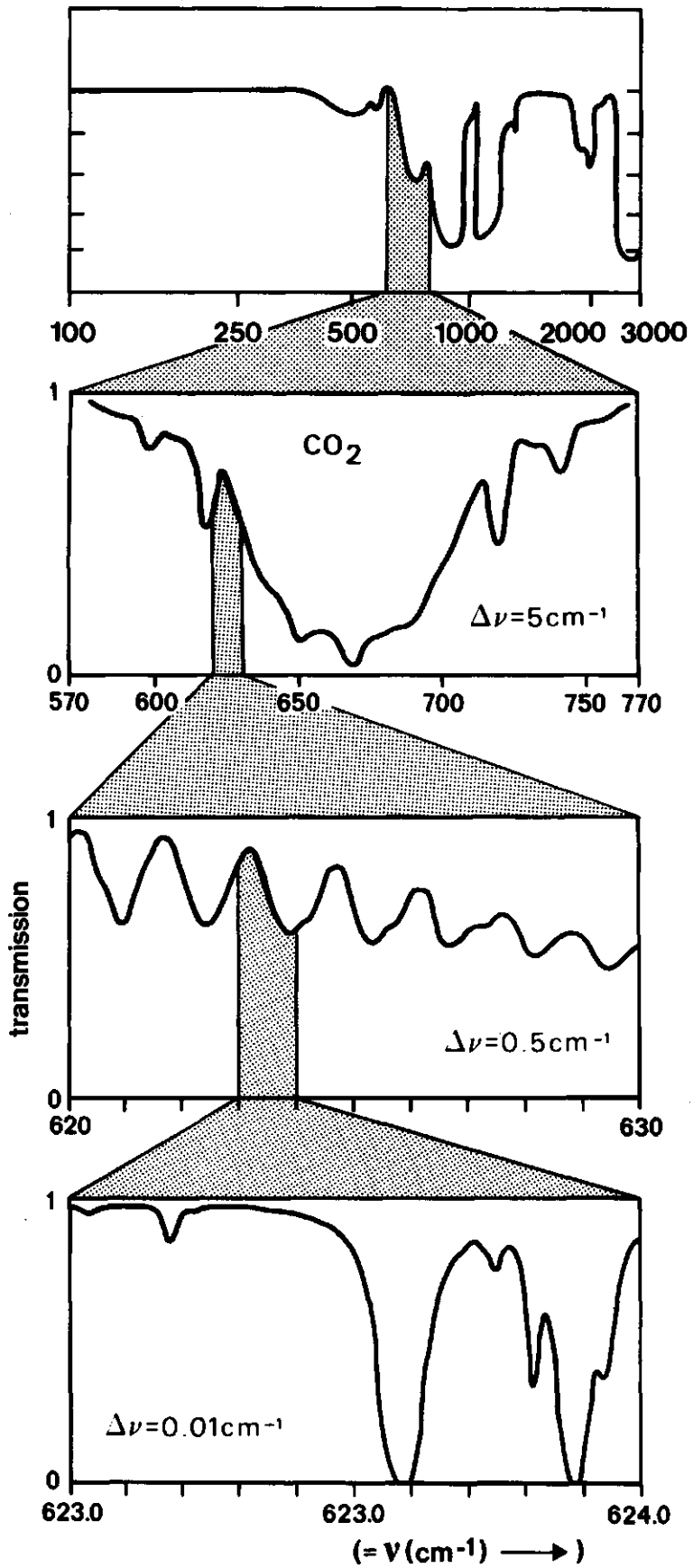

Fig. 2.1 *Transmission in the 15 μm spectral region at various spectral resolution. Top panel: the absorption coefficient for the entire long wave spectrum. Upper middle panel: complete 15 μm band. Lower middle panel 15 μm band at a higher resolution. Lower panel as above, but resolution enhanced further. Modified from Fischer (1985).*

$$F^{+}(z) = \sum_{i=1}^{n} B_i\big(T(0)\big)\,\tau_i(0,z) + \int_0^z B_i\big(T(z')\big)\,\frac{\partial \tau_i(z',\,z)}{\partial z'}\,dz' \qquad (2.1^a)$$

$$F^{-}(z) = \sum_{i=1}^{n} B_i\big(T(top)\big)\,\tau_i(top,z) + \int_{top}^{z} B_i\big(T(z')\big)\,\frac{\partial \tau_i(z,\,z')}{\partial z'}\,dz', \qquad (2.1^b)$$

with

$$B_i(z) = \pi \int_{\Delta\nu_i} B_\nu(z)\,d\nu \qquad (2.2)$$

the integrated Planck function and

$$\tau_i\,(z',\,z) = \pi \int_{\Delta\nu_i} B_\nu(z')\,\tau_\nu(z',z)\,d\nu \,/\, B_i(z') \qquad (2.3)$$

the mean transmission over the i-th spectral interval with width $\Delta\nu_i$. The summation in (2.1) is over all spectral bands inside the infrared spectrum. The complex arrangement of the spectral lines within each band prohibits an analytical evaluation of (2.3), such that the mean transmission can only be obtained from observations or from an idealized description of the real spectrum.

Complications arises because three different scales on which the slab transmission function varies with frequency can be distinguished (Fig. 2.1). The first scale refers to the low resolution variation of the absorption coefficient over the entire infrared spectrum. At a higher resolution we can distinguish the variation of the absorption over an entire absorption band. At a still higher resolution the variation of the absorption coefficient over a group of lines can be distinguished. Associated with these three different scales, we can distinguish between three different type of parametrization schemes. Emissivity models, which are associated with the variation over the entire spectrum, wide band models which are associated with the unresolved scale of an absorption band and narrow models which are associated with the separation of individual lines. Notice that a line by line model is associated with the highest resolution the variation of the transmission over a single spectral line.

It is a great practical advantage to reduce the number of calculations by increasing the width of a spectral interval. However, if the band width increases, the mean transmission becomes less exponential in nature which introduce new problems. Two examples are discussed.

i) The combined absorption of two different gases.

In several parts of the infrared spectrum, two different gases absorb simultaneously. The performance of the radiation model is sensitive to the inclusions of the combined absorption by a mixture of gases (Ohring and Josheph, 1978; Kiehl and Ramanathan, 1982). At a single frequency, it is assumed that the absorption of radiation by an infrared active gas is independent of absorption by another active gas.

Then the total absorption coefficient is found from a linear sum of the absorption coefficient of the different gasses

$$\kappa_\nu^{1+2}(z) = \kappa_\nu^1(z) + \kappa_\nu^2(z), \tag{2.4}$$

where the superscript indicates the gas number.The absorption of radiation by two different gases is found from the multiplication of the individual transmission functions. Let

$$\tau_\nu(z',z;\mu) \equiv \exp\left\{-\kappa_\nu \Delta z/\mu\right\} \tag{2.5}$$

then from (2.4) follows

$$\begin{aligned}\tau_\nu^{1+2}(z', z;\mu) &= \exp\left\{-\kappa_\nu^{1+2}\Delta z/\mu\right\} \\ &= \exp\left\{-\left(\kappa_\nu^1 + \kappa_\nu^2\right)\Delta z/\mu\right\} \\ &= \tau_\nu^1(z',z;\mu) * \tau_\nu^2(z',z;\mu).\end{aligned} \tag{2.6}$$

This multiplicative property of transmission functions is only valid for monochromatic transmission functions. It is assumed that (2.6) may also be applied to other parametrization schemes, which is not valid as can been seen from

$$\begin{aligned}\tau_i^{1+2}(z', z) &= \pi \int_{\Delta\nu_i} B_\nu(z')\tau_\nu^{1+2}(z', z)\, d\nu \,/\, B_i(z') \\ &= \pi \int_{\Delta\nu_i} B_\nu(z')\, \tau_\nu^1(z', z) * \tau_\nu^2(z', z)\, d\nu \,/\, B_i(z') \\ &\neq \pi \int_{\Delta\nu_i} B_\nu(z')\tau_\nu^1(z', z)\, d\nu \,/\, B_i(z') * \pi \int_{\Delta\nu_i} B_\nu(z')\tau_\nu^2(z', z) d\nu \,/\, B_i(z') \\ &= \tau_i^1(z', z) * \tau_i^2(z', z).\end{aligned} \tag{2.7}$$

However it is often not realized that within other schemes, this assumption is only a crude manner to parametrize the combined absorption of a mixture of gases, which may influence the model performance.

ii) Finite atmospheres.

For some applications such as considered in this thesis the nocturnal boundary layer, the simulation of radiative transfer through only the lower parts of the atmosphere is required. To avoid lengthy radiation calculations, the transfer equation is

solved for that specific part of the atmosphere only. At a single frequency, the slab transmission is a rather simple function of the absorber amount (cf. (1.10)). Such that the transmission over the lower parts of the atmosphere can be separated from the transmission over the upper parts.

$$\tau_\nu(z', z;\mu) = \exp\left\{-\kappa_\nu(z'-z)/\mu\right\} = \exp\left\{-\kappa_\nu\big((z'-Z) + (Z-z)\big)/\mu\right\}$$

$$= \tau_\nu(z', Z; \mu) * \tau_\nu(Z, z; \mu), \qquad (2.8)$$

with Z the highest calculation level. Substitution of (2.8) into (1.7b) yields

$$F^-(z) = \int_0^\infty \left\{ F^-_\nu(Z)\tau_\nu(z, Z) + \pi \int_Z^z B_\nu\big(T(z')\big)\frac{\partial \tau_\nu(z', z)}{\partial z'} dz' \right\} d\nu \qquad (2.9)$$

with

$$F^-(Z) = \pi\left\{ B_\nu\big(T(top)\big)\tau_\nu(Z, top) + \int_{top}^{Z} B_\nu\big(T(z')\big)\frac{\partial \tau_\nu(z', Z)}{\partial z'} dz' \right\}. \qquad (2.10)$$

This means that to describe the transfer of infrared radiation through the lower parts of the atmosphere with a line by line model, only the downward flux at the top of the model domain must be specified. No further information on the radiation field in the upper parts of the atmosphere is required.

The mean transmission of a spectral interval is a rather complex function of the number of absorbers along the line of sight. As a result in band models the transmission over the lower parts of the atmosphere cannot be separated from the transmission over the upper parts,

$$\tau_i(z', z; \mu) = \int_{\Delta\nu_i} \tau_\nu(z', z; \mu)\, d\nu/\Delta\nu_i = \int_{\Delta\nu_i} \tau_\nu(z', Z; \nu) * \tau_\nu(Z, z; \nu)\, d\nu/\Delta\nu_i$$

$$\neq \int_{\Delta\nu_i} \tau_\nu(z', Z; \mu)\, d\nu / \Delta\nu_i * \int_{\Delta\nu_i} \tau_\nu(Z, z; \mu)\, d\nu / \Delta\nu_i$$

$$= \tau_i(z', Z;\mu) * \tau_i(Z, z; \mu). \qquad (2.11)$$

Which means that to describe the transfer of infrared radiation through the lower parts of the atmosphere using a band model, the radiative transfer equation through the entire atmosphere must be solved.

2.1 Emissivity models

In emissivity models, the frequency integral in (1.5) is removed once and for all by defining a mean transmission for the entire infrared spectrum. Equation (1.5) is

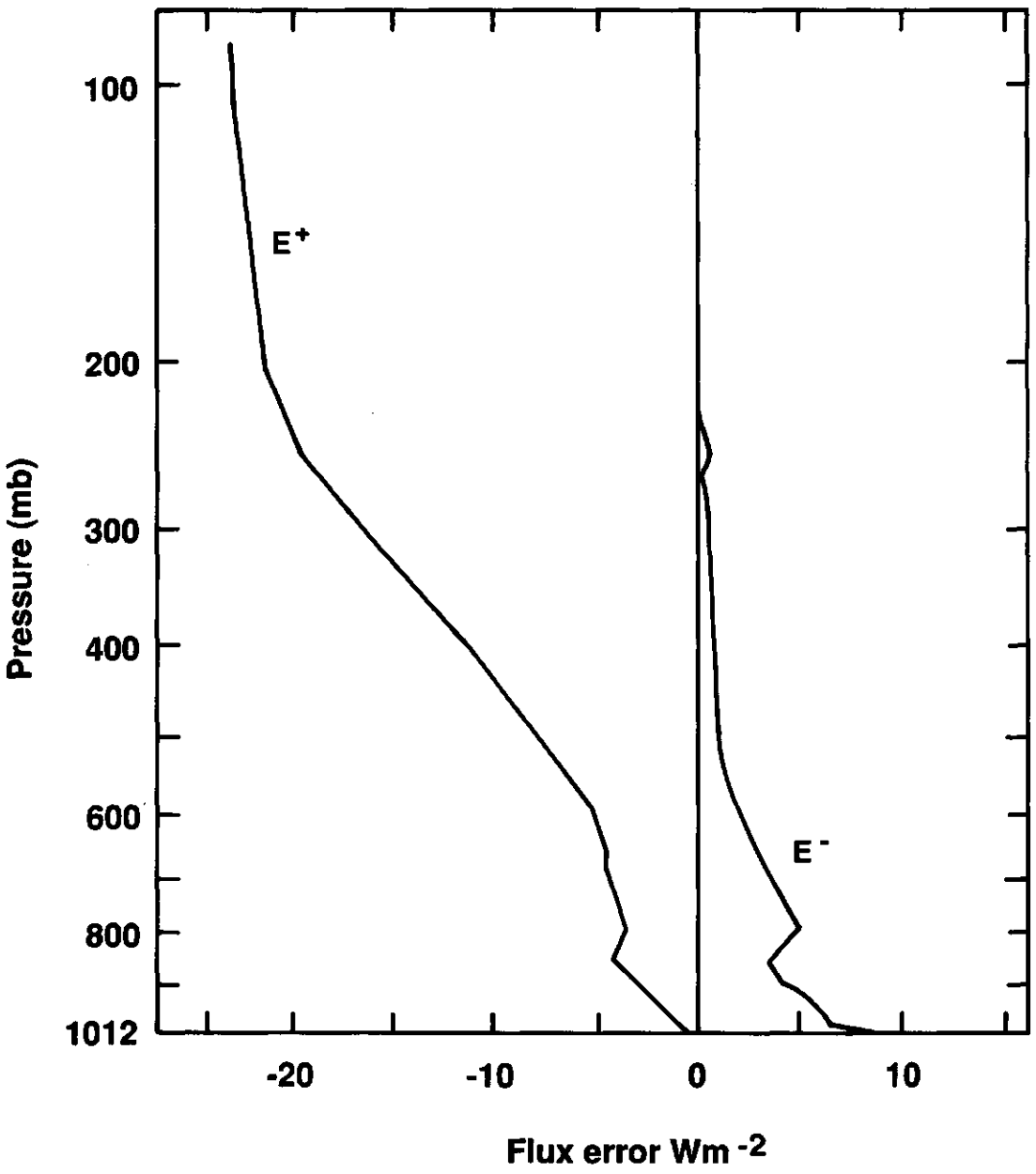

Fig. 2.2 *Typical set of error curves for flux calculations employing the emissivity approach. The error curves are based on a 21 band radiation model, which is taken to provide the exact fluxes (modified from Rodgers, 1967)*

written as

$$F^{+}(z) = \sigma T^{4}(0)\, \tau_e^{+}(0,z) + \int_0^z \sigma T^{4}(z') \frac{\partial \tau_e^{+}(z',\, z)}{\partial z'}\, dz' \qquad \left(2.12^{a}\right)$$

$$F^{-}(z) = \int_{top}^{z} \sigma T^{4}(z') \frac{\partial \tau_e^{-}(z,\, z')}{\partial z'}\, dz' \qquad \left(2.12^{b}\right)$$

with

$$\frac{\partial \tau_e^+(z', z)}{\partial z'} = \pi \int_0^\infty B_\nu(z') \frac{\partial \tau_\nu(z', z)}{\partial z'} d\nu / \sigma T^4(z') \quad z'>z \qquad (2.13^a)$$

$$\frac{\partial \tau_e^-(z, z')}{\partial z'} = \pi \int_0^\infty B_\nu(z') \frac{\partial \tau_\nu(z, z')}{\partial z'} d\nu / \sigma T^4(z') \quad z'<z \qquad (2.13^b)$$

$$\tau_e^+(0, z) = \pi \int_0^\infty B_\nu(z)\, \tau_\nu(0,z)\, d\nu / \sigma T^4(z). \qquad (2.13^c)$$

For homogeneous path $1-\tau_e(z',z)$ is the classical definition of emissivity, relating the emission of a column of gas to that of a black body at the some temperature. In principle this quantity can be measured.

Well known examples of emissivity models are the schemes proposed by Rodgers (1967) and Samori (1968). In their formulation the mean transmission is expressed as a function of the absorber amount and a few adjustable parameters. These parameters are found from a fit of the emissivity model results to the performance of an accurate radiation model (such as a line by line model) for several different standard atmospheres.

Emissivity models approximate the tropospheric and stratospheric flux components within approximately 10 Wm^{-2} (Fig. 2.2). As a result the error in the tropospheric and stratospheric cooling rate can be as large as 0.5 K/day (Stephens, 1984). However, near the surface where the radiative cooling rate is extremely large due to the large vertical temperature gradient, emissivity models diverge from observations by a factor of two (Funk, 1960).

2.2 Wide and narrow band model

If the frequency integral (2.3) involves the transmission of an entire absorption band, the parametrization scheme is called a wide band model, whereas in the case this integral extends over only a group of spectral lines, it is called a narrow band model. A typical width ($\Delta\nu$) for a wide band model is 300 Thz and for a narrow band model it is 30 Thz. Depending upon the chosen parametrization method, wide and narrow band models can be divided into two groups regular or pseudo-monochromatic.

2.2.1 Regular wide and narrow band

Let us consider the absorption of a single spectral line. Let A_{sl} (unit: Hz) represents the total absorption of a single spectral line defined by

$$A_{sl}(u) = \int_{-\infty}^{\infty} 1 - \tau_\nu(z, z'; \mu)\, d\nu = \int_{-\infty}^{\infty} 1 - e^{-\kappa_\nu^* u/\mu}\, d\nu\,. \qquad (2.14)$$

The variation of the mean absorption coefficient as a function of frequency is usually described by

$$\kappa_\nu^* = S\, f(\nu - \nu_0)\,, \tag{2.15}$$

with S the linestrength (units: $m^2kg^{-1}Hz$) and f the lineshape. Here we assume the lineshape to be given by a Lorentz-profile (Liou, 1980)

$$f(\nu - \nu_0) = \frac{\alpha/\pi}{(\nu - \nu_0)^2 + \alpha^2}\,, \tag{2.16}$$

with α the line halfwidth (unit: Hz) and ν_0 the line center. The total line absorption is then given by

$$A_{sl}(u) = 2\pi\alpha\, LR\left(\frac{Su/\mu}{2\pi\alpha}\right), \tag{2.17}$$

with LR (x) the the Ladenberg - Reiche function (Ladenberg and Reiche, 1913)

$$LR\,(x) = xe^{-x}\left(I_0(x) + I_1(x)\right), \tag{2.18}$$

in which $I_0(x)$, $I_1(x)$ represent the modified Bessel function of the zero and first order respectively.

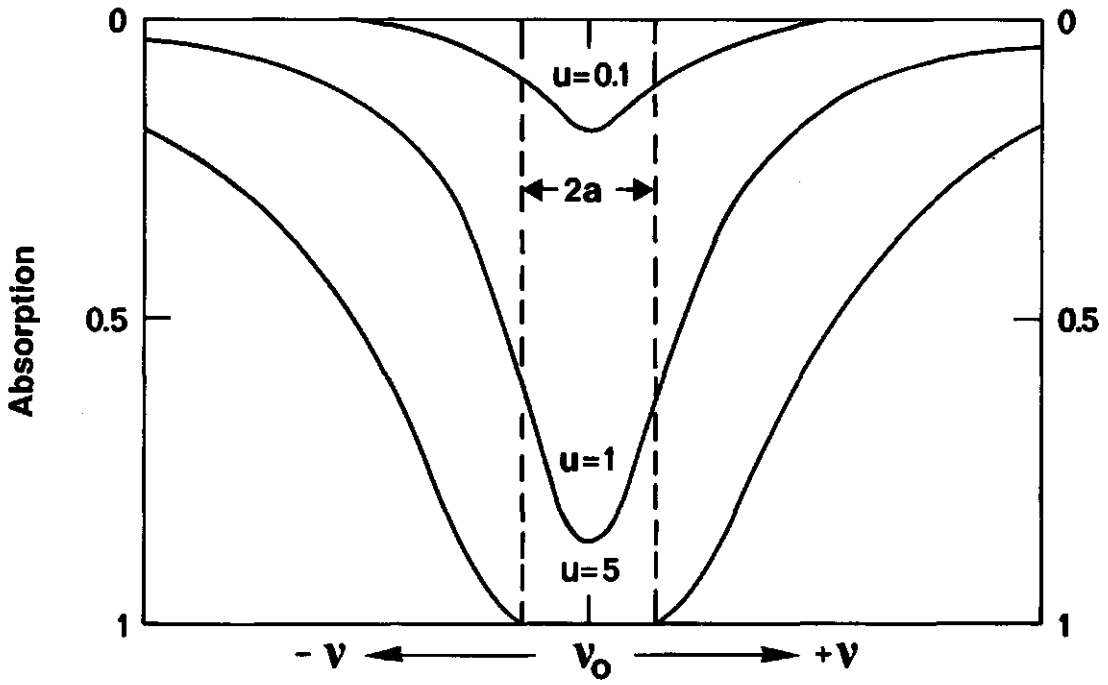

Fig. 2.3 *Single line absorption for various absorber amount (after Liou, 1980).*

Let us now consider the absorption of a single spectral line as a function of the absorber amount (Fig. 2.3). If the absorber amount is small, which states that if there are only a few absorbers along the line of sight, each will be able to remove radiation from the radiation field. Only the line center (where the absorption is highest) will contribute to the total line absorption. The line wings will be transparent and not contribute significantly to the total line absorption. Then the total line absorption should be linearly proportional to the absorber amount (*the linear absorption limit*).

$$A_{sl}(u) = Su/\mu \quad \text{if} \quad \frac{Su/\mu}{2\pi\alpha} << 1. \tag{2.19}$$

As more absorber are present only the line of sight, the line center becomes completely opaque. All radiation that can be absorbed in the line center have been. Then the dependence of the line absorption with absorber amount arises from the absorption at the line wings. From the Ladenberg - Reiche function (2.18) follows that then the line absorption should be proportional to the square root of the absorber amount (*the square root absorption limit*).

$$A_{sl}(u) = 2\sqrt{S\pi\alpha u/\mu} \quad \text{if} \quad \frac{Su/\mu}{2\pi\alpha} >> 1. \tag{2.20}$$

The dependence of the total absorption by an entire band differs only slightly from the above result of a single line. Within an absorption band, a large number of spectral lines are present, each with its own particular line characteristics. As long as the spectral lines within the band may be regarded as separated, the total absorption of an entire band is dominated by the strongest lines. If the absorber amount is small such that the spectral lines absorb in the linear absorption limit also the total band absorption is linear proportional to the absorber amount (*the non overlapping linear absorption limit*)

$$A_{wb}(u) = \sum_{j=1}^{n_{wb}} S_j \, u/\mu = S_{wb} \, u/\mu, \tag{2.21}$$

with S_{wb} the total band strength of the entire absorption band. The summation in (2.21) is over all lines inside the absorption band. If the number of absorbers increases, such that the strong lines absorb in their strong square root absorption limit, the total band absorption should also be proportional to the square root of the absorber amount (*non overlapping square root absorption limit*)

$$A_{wb}(u) = 2\sum_{j=1}^{n_{wb}} \sqrt{S_j \pi \alpha_j u/\mu} = 2\sqrt{S_{wb} \pi \alpha_{wb} u/\mu}, \tag{2.22}$$

with α_{wb} the band width. If the number of absorbers along the line of sight, increases even further, the spectral lines may not be regarded as separated. From observations it is shown that for large absorber amounts, the total band absorption should be proportional to the natural logarithm of the absorber amount (*the overlapping strong absorption limit*)

$$A_{wb}(u) = 2\Delta\nu_{wb}\ {}^{e}\log\left(\frac{S_{wb}u/\mu}{\Delta\nu_{wb}}\right), \qquad (2.23)$$

with $\Delta\nu_{wb}$ the width of the entire absorption band.

i) Governing equations for a regular wide band model.

The transmission function averaged over an entire absorption band follows from

$$\tau_{wb}(z, z'; \mu) = \left(1 - A_{wb}(u)/\Delta\nu_{wb}\right), \qquad (2.24)$$

where we assumed the band small enough such that the Planck function may be regarded as constant. The variation of the transmission for a wide band model as a function of absorber amount follow directly from the above and is given by eqs (2.21), (2.22) and (2.23) in the non overlapping weak, non overlapping strong and overlapping strong absorption limit respectively. To obtain a smooth transition from one particular absorption limit into another, the total band absorption is evaluated from an arbitrarily interpolation formula. A particular example is (Cess et al., 1986)

$$A_{wb}(u) = 2\Delta\nu_{wb}\ {}^{e}\log\left(1 + \frac{\dfrac{S_{wb}u/\mu}{\Delta\nu_{wb}}}{\sqrt{4 + \dfrac{S_{wb}u/\mu}{\Delta\nu_{wb}}\left(1 + \dfrac{\Delta\nu_{wb}}{\alpha_{wb}}\right)}}\right). \qquad (2.25)$$

S_{wb} and α_{wb} in (2.25) can be found from a comparison with line by line calculations with laboratory measurements or from quantum mechanical calculations

Although wide band models require more computational time than emissivity models, they are frequently used in atmospheric radiation studies (e.g. Ramanathan, 1976; Crisp et al., 1986). Not only because wide band models are more flexible that emissivity models but also because the spectral bands may correspond to certain satellite channels such that a convenient way to compare model calculations with satellite observations can be obtained.

ii) Governing equations for a regular narrow band model.

Before an expression for the mean transmission of a narrow spectral interval can be given, first a relation between this mean transmission and the absorption of a single spectral line must be specified. Assuming the interval small enough, such that each spectral line inside the interval absorbs uniformly and the ratio of the absorption of each spectral line and the width of the spectral interval much smaller than unity, the mean transmission of a narrow spectral interval may be evaluated according to (Tjemkes and Duynkerke, 1988a; Appendix B)

$$\tau_{nb}(z, z'; \mu) = \exp\left\{-n_{nb}\bar{A}_{nb}(u)/\Delta\nu_{nb}\right\}, \qquad (2.26)$$

with n_{nb} the number of spectral lines in the narrow interval, $\Delta\nu_{nb}$ the width of the interval and $\bar{A}_{nb}$ the mean absorption of all lines in the interval given by

$$\bar{A}_{nb}(u) = \frac{1}{n_{nb}} \sum_{j=1}^{n_{nb}} A_{sl}^{j}(u) . \qquad (2.27)$$

For the weak absorption limit the the mean absorption can be evaluated according to (2.19) and yields

$$\bar{A}_{nb}(u) = \frac{1}{n_{nb}} \sum_{j=13}^{n_{nb}} S_j u/\mu = \bar{S}_{nb} u/\mu , \qquad (2.28)$$

with $\bar{S}_{nb}$ the mean line strength, while for the strong absorption limit (2.20) it is evaluated according to

$$\bar{A}_{nb}(u) = \frac{1}{n_{nb}} \sum_{j=1}^{n_{nb}} \sqrt{S_j \pi \alpha_j u/\mu} = \sqrt{\bar{S}_{nb} \pi \bar{\alpha}_{nb} u/\mu} , \qquad (2.29)$$

with $\bar{\alpha}_{nb}$ the mean line width. In between these two limits, the mean absorption is found from an interpolation formula such as

$$\bar{A}_{nb}(u) = \left(\left(\frac{1}{\bar{S}_{nb} u/\mu} \right)^2 + \left(\frac{1}{\bar{S}_{nb} \pi \bar{\alpha}_{nb} u/\mu} \right) \right)^{-0.5} . \qquad (2.30)$$

Values for the mean line strength and line halfwidth can be obtained from a fit of (2.30) to laboratory measurements or to line by line calculations, but is more convenient to obtain the mean line strength and line halfwidth from quantum mechanical calculations (Liou, 1980). Equations (2.26) and (2.30) were originally derived by Goody (1952) therefore the combination of these two equation are known as the Goody band model.

Narrow band models are very accurate. For instance the downward flux at the surface can be approximated within 2% (Tjemkes and Nieuwstadt, 1988; Chapter 3). Unfortunately this accuracy is at the expense of a large amount of computer time. Like line by line models, regular narrow band models are rarely used in numerical forecast models.

2.2.2 Pseudo-monochromatic models.

An alternative approach has been employed more recently to approximate the frequency integration in the flux equations. This method makes use of the fact that for a homogeneous atmosphere, the transmission within a spectral interval is independent of the ordering of the value of the absorption coefficient k with respect to frequency, but depends only on the fraction of the interval that is associated with a particular value of the absorption coefficient. The k-distribution f(k), defined such that f(k)dk represents

the fraction of the spectral interval for which the absorption coefficient is between k and k + dk, is formally related to the transmission function along a homogeneous path as

$$\tau_i(z, z'; \mu) = \frac{1}{\Delta\nu_i}\int_{\Delta\nu_i} e^{-\kappa_\nu^* u/\mu}\, d\nu = \int_0^\infty f(k) e^{-ku/\mu} dk. \qquad (2.31^a)$$

For all practical applications, (2.31a) is evaluated by a quadrature formula, such that only a limited number of k-s are required.

$$\tau_i(z, z'; \mu) = \sum_{j=1}^{m} w_j e^{-k_j u/\mu}. \qquad (2.31^b)$$

The k-distribution f(k) can be obtained either from line-by-line calculations (Chou and Arking, 1980), from a non linear fit of (2.31b) to the transmission function (Pollack and Mckay, 1985) or from the inverse Laplace transform of the mean transmission function (Hansen et al. 1983; Wang and Shi, 1988; Tjemkes, 1988; Appendix A). Notice that the transmission at a specific k-value resembles the transmission at a single frequency. Therefore band models which applied the k-distribution method are also referred to as pseudo monochromatic band models.

The description of the mean transmission function using the k-distribution method has certain advantages over the regular band concept discussed in the previous section. To give an example, consider an atmospheric layer, which is divided into two sublayers. The transmission (τ_i) over the entire layer is, according to the regular band model a rather complex function of the absorber amount (cf. 2.30). such that the transmission over the entire layer, can not be evaluated by a simple method from the transmission over each sublayer. For instance the simple relation valid for monochromatic transmission function

$$\tau_\nu(\Delta u) = \tau_\nu(\Delta u_1 + \Delta u_2) = \tau_\nu(\Delta u_1) * \tau_\nu(\Delta u_2) \qquad (2.32)$$

is not valid for band transmission functions

$$\tau_{gbm}(\Delta u) = \tau_{gbm}(\Delta u_1 + \Delta u_2) \neq \tau_{gbm}(\Delta u_1) * \tau_{gbm}(\Delta u_2), \qquad (2.33)$$

where the subscript gbm refers to the Goody band model (2.30). Equation (2.33) holds for the mean transmission according to the k-distribution. But the transmission over the entire layer at a specific k-value can easily derived from the transmission over the sub layer following

$$\tau_i(z, z'; \mu) = \sum_{j=1}^{m} w_j e^{-k_j \Delta u/\mu} = \sum_{j=1}^{m} w_j e^{-k_j\left(\Delta u_1 + \Delta u_2\right)/\mu}$$

$$= \sum_{j=1}^{m} w_j \left(e^{-k_j \Delta u_1/\mu} * e^{-k_j \Delta u_2/\mu} \right). \qquad (2.34)$$

This property of the k-distribution reduces the number of calculations. As a result the k-distribution method is demonstrably faster than a regular band model, without the loss of accuracy. (Chou and Arking, 1983; Tjemkes, 1988; Appendix A). Besides its computational speed, the k-distribution has also the advantage that it is relatively straightforward to incorporate molecular absorption and scattering by aerosols and clouds in a self-consistent fashion.

On the negative side is the fact that the amount of computer time required to evaluate the mean transmission increases dramatically, if the k-distribution method is applied to spectral intervals where two different gasses absorb simultaneously. Then the transmission function averaged over a spectral interval is given by

$$\tau_i^{1+2}(z, z';\mu) = \int_0^\infty\int_0^\infty f(k^1,k^2)\, e^{-\left(k^1u^1+k^2u^2\right)/\mu}\, dk^1dk^2, \qquad (2.35^a)$$

or in discrete form

$$\tau_i^{1+2}(z, z';\mu) = \sum_{j=1}^{m}\sum_{h=1}^{M} w_{jh} e^{-\left(k_j^1u^1+k_h^2u^2\right)/\mu}, \qquad (2.35^b)$$

where a superscript 1, 2 refers to gas number 1 and 2 respectively. the transmission is now found from M x m pseudo-monochromatic transmission.

Recently, Tjemkes (1988, Appendix A) proposed an alternative method to approximate gaseous overlap. This method is based on the summation of absorber amount and is considerably faster than the summation over k-distribution (2.35) without the loss of accuracy.

3. The angular integral

To evaluate the net flux at a reference level z, we must consider the contributions to the net flux from all possible directions (cf. (1.5)). If the radiation field is isotropic (independent of zenith angle) the angular integral is trivial and the slab transmission function is given by

$$\tau_\nu(z, z') = \exp\left\{-\kappa_\nu \Delta z\right\}. \qquad (3.1)$$

In general we cannot make this simplifying assumption and the angular integral must be evaluated from a standard quadrature formula. To avoid such a tedious numerical evaluation a mean slab transmission can be defined

$$\tau_\nu(z, z'; \bar{\mu}) \equiv \int_0^1 \exp\left\{-\kappa_\nu \Delta z/\mu\right\}\mu d\mu \,/\, \int_0^1 \mu d\mu \qquad (3.2)$$

which is used as an approximation of the angular integral. Using this mean transmission, the nonisotropic radiation field is described as if it was an isotropic radiation field. The constant $1/\bar{\mu}$ is known as the difussivity factor. The numerical value for it follows from

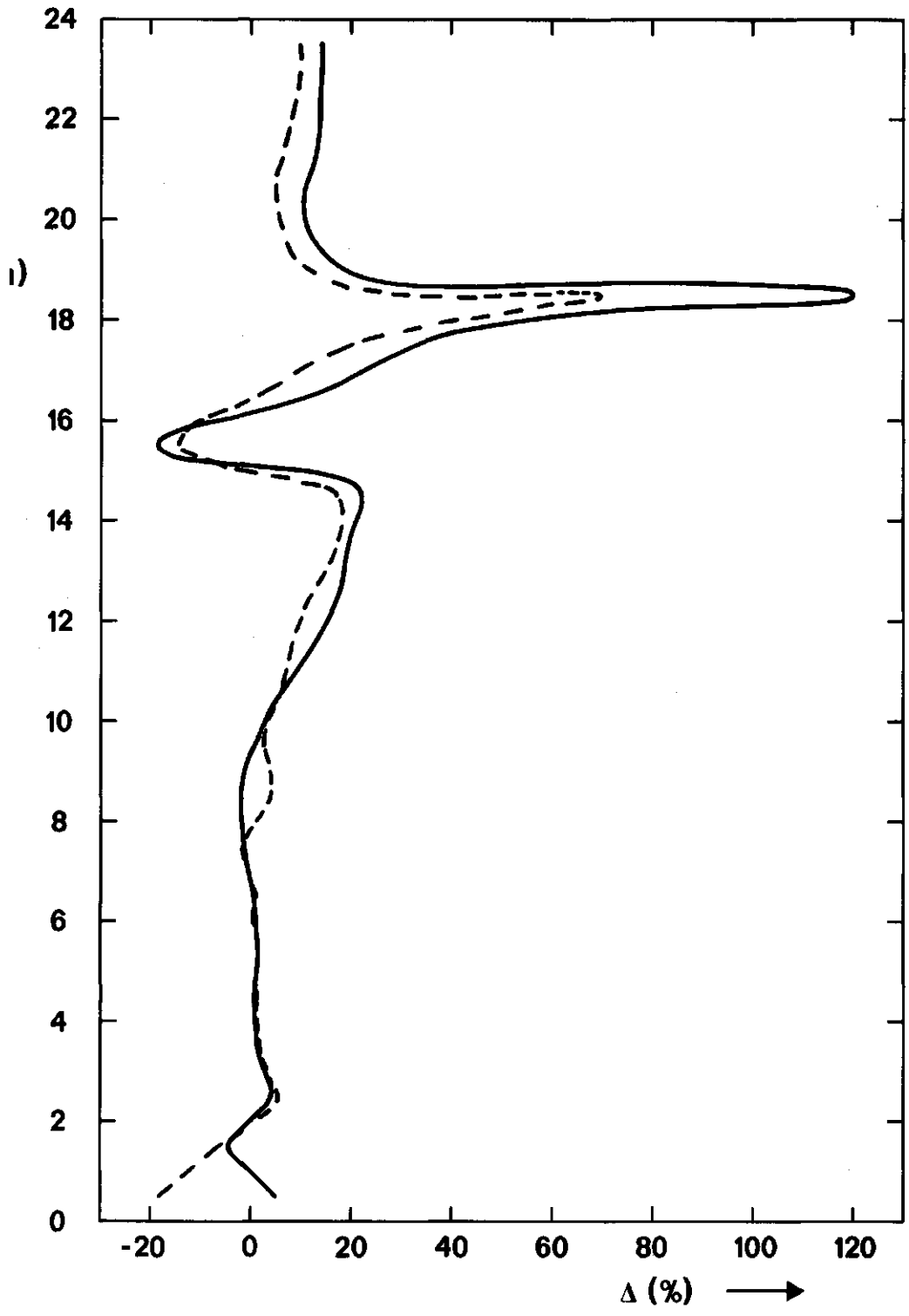

Fig. 3.1 *Error curve for flux calculations employing a fixed diffusivity factor. Calculations made with a regular narrow band model for a standard tropical atmosphere (McClatchey et al., 1972). Flux calculations using a 16-point Gauss quadrature to evaluate the angular integral are considered as exact. Solid line calculations using a fixed diffusivity factor of 1.66, dashed line with a diffusivity factor of 2.0.*

$$\bar{\mu} = \frac{\kappa_v \Delta z}{{}^{e}\log\left\{2E_3\left(\kappa_v \Delta z\right)\right\}}, \qquad (3.3)$$

with E_3 the exponential integral of the third kind given by (Abramowitz and Stegun, 1964)

$$E_n(x) = \int_1^{\infty} \frac{e^{-tx}}{t^n}\, dt\,. \qquad (3.4)$$

From (3.3) we see that in general the diffusion factor is a function of the path length $\kappa_v \Delta z$. But the commonly used value for the diffusivity factor is between 1.66 and 2.0 independent of the path length. In Fig. 3.1 a comparison is given between a numerical evaluation of the angular integral using a 16-point Gauss quadrature (Abromwitz and Stegun, 1964), which is taken to provide the exact transmission function and an approximation of the angular integral using a fixed diffusivity factor of 1.66 (solid line) and 2.0 (dashed line). Shown is the relative error in the cooling rate (Δ) defined by

$$\Delta(z) = \frac{\left(\frac{\partial T(z)}{\partial t}\right)_{exact} - \left(\frac{\partial T(z)}{\partial t}\right)_{\bar{\mu}}}{\left(\frac{\partial T(z)}{\partial t}\right)_{exact}} * 100\,\% \qquad (3.5)$$

as a function of height for a standard tropical atmosphere (McClatchey et al., 1972). In this fig. we see that near the surface and the tropopauze at 18 km, the use of a fixed diffusivity factor may lead to considerable errors in the cooling rate. The use of a diffusivity factor which varies with path is thus preferrable over a fixed one.

From an analysis of (3.2), Quanhua and Schmetz (1988) proposed an analytical expression for the diffusivity factor as a function of $\kappa_v \Delta z$ Because $\kappa_v \Delta z$ will varies rapidly with frequency, so will their expression for the diffusivity factor. The results of Quanhua and Schmetz results are limited to line by line and quasi monochromatic models. Emissivity models, regular wide and narrow bandmodels requires a band average diffusivity factor.

For emissivity models the diffusivity factor can be obtained from a comparison of the performance of the emissivity model with models that explicitly evaluate the angular integral. For regular wide and narrow band models, a numerical value for a band average diffusivity factor can be obtained from an integration of (3.2) over frequency

$$\tau_i(z, z'; \bar{\mu}) = \int_{\Delta\nu_i} \tau_\nu(z, z'; \bar{\mu})\, d\nu / \Delta\nu_i = 2 \int_{\Delta\nu_i} \int_0^1 \exp\left\{-\kappa_\nu \Delta z/\mu\right\}\, \mu d\mu\, d\nu / \Delta\nu_i$$

$$= 2 \int_0^1 \int_{\Delta\nu_i} \exp\left\{-\kappa_\nu \Delta z/\mu\right\} d\nu \,/\, \Delta\nu_i \, \mu d\mu$$

$$= 2 \int_0^1 \tau_i(z, z'; \mu)\, \mu d\mu \,. \qquad (3.6)$$

The approximation of the frequency integral is discussed in the previous paragraph here we will use some results

3.1 regular wide band models

For the non overlapping weak absorption limit (2.21) the transmission averaged over a spectral interval can be written as

$$\tau_{wb}(z, z'; \mu) = \left(1 - \frac{S_{wb} u/\mu}{\Delta\nu_{wb}}\right) . \qquad (3.7)$$

Substitution of (3.7) in (3.6) yield

$$\overline{S_{wb} u/\mu} = 2 \int_0^1 S_{wb} u/\mu \, \mu d\mu = 2 \, S_{wb} u \,. \qquad (3.8)$$

From which we find that in the nonoverlapping weak absorption limit the diffusivity factor is equal 2. In the nonoverlapping strong absorption limit the diffusivity factor follows from a substitution of (2.22) in (3.6)

$$\sqrt{\overline{S_{wb} \pi\alpha_{wb} u/\mu}} = 2 \int_0^1 \sqrt{S_{wb} \pi\alpha_{wb} u/\mu} \; \mu d\mu = \frac{4}{3} \sqrt{S_{wb} \pi\alpha_{wb} u} \,. \qquad (3.9)$$

Thus in the non overlapping strong absorption limit, the diffusivity factor is 16/9. Finally in the strong overlapping limit we have from a substitution of (2.23) into (3.6)

$$^{e}\log\left(\frac{\overline{S_{wb} u/\mu}}{\Delta\nu_{wb}}\right) = \int_0^1 2 \, ^{e}\log\left(\frac{S_{wb} u/\mu}{\Delta\nu_{wb}}\right) \mu d\mu = \, ^{e}\log\left(\frac{\sqrt{e}\, S_{wb} u}{\Delta\nu_{wb}}\right) . \qquad (3.10)$$

In the strong overlapping absorption limit the diffusivity factor is thus equals to $e^{0.5}$. To incorporate the variation of the angular integral with respect to absorber amount, in a wide band model the three limits discussed in the previous paragraph (eqs. (2.21), (2.22) and (2.23)) should thus be replaced by eqs (3.7), (3.8) and (3.9) respectively. And the particular example of a wide band model given in the previous paragraph

(2.25) should then read

$$A_{wb}(u) = 2\Delta\nu_{wb}\,{}^{e}\log\left(1 + \frac{\frac{2S_{wb}u}{\Delta\nu_{wb}}}{\sqrt{4 + \frac{2S_{wb}u}{\Delta\nu_{wb}}\left(\frac{2}{\sqrt{e}} + \frac{9}{2}\frac{\Delta\nu_{wb}}{\pi\alpha_{wb}}\right)}}\right). \qquad (3.11)$$

3.2 regular narrow band models

The diffusivity factor for a regular narrow band model follow from a substitution of (2.26) in combination with (2.28) in the weak absorption limit or (2.29) in the strong absorption limit into (3.6). For the weak absorption limit we have

$$\exp\left(-n_{nb}\bar{S}_{nb}u/\bar{\mu}\right) = 2\int_0^1 \exp\left(-n_{nb}\bar{S}_{nb}u/\mu\right)\mu d\mu\,. \qquad (3.12)$$

From a Taylor expansion of the exponential, we find that in the weak absorption limit of a narrow band model the diffusivity factor to be the same as in the non overlapping weak absorption limit of a wide band model

$$\left(1 - \frac{n_{nb}\bar{S}_{nb}u/\bar{\mu}}{\Delta\nu_{nb}}\right) = 2\int_0^1\left(1 - \frac{n_{nb}\bar{S}_{nb}u/\mu}{\Delta\nu_{nb}}\right)\mu d\mu = \left(1 - \frac{2n_{nb}\bar{S}_{nb}u}{\Delta\nu_{nb}}\right). \qquad (3.13)$$

A value for the diffusivity factor in the strong absorption limit is somewhat more difficult to obtain it follows from

$$\exp\left(-\frac{n_{nb}\sqrt{\bar{S}_{nb}\bar{\pi\alpha}_{nb}u/\bar{\mu}}}{\Delta\nu_{nb}}\right) = 2\int_0^1 \exp\left(-\frac{n_{nb}\sqrt{\bar{S}_{nb}\bar{\pi\alpha}_{nb}u/\mu}}{\Delta\nu_{nb}}\right)\mu d\mu\,. \qquad (3.14)$$

Equation (3.12) can be written using the definition of the exponential integrals (3.4) as

$$\bar{\mu} = -\frac{\frac{n_{nb}\sqrt{\bar{S}_{nb}\bar{\pi\alpha}_{nb}u}}{\Delta\nu_{nb}}}{{}^{e}\log\left\{4E_5\left(\frac{n_{nb}\sqrt{\bar{S}_{nb}\bar{\pi\alpha}_{nb}u}}{\Delta\nu_{nb}}\right)\right\}}. \qquad (3.15)$$

From an asymptotic expansion of the exponential integral for large arguments (Abramowitz and Stegun, 1964)

$$E_n(x) \approx \frac{e^{-x}}{x}, \tag{3.16}$$

we find

$$\bar{\mu} = \frac{1}{1 - \frac{{}^{e}\log 4}{x} + \frac{{}^{e}\log x}{x}}, \tag{3.17}$$

where

$$x = \frac{n_{nb}\sqrt{\bar{S}_{nb}\pi\bar{\alpha}_{nb}u}}{\Delta\nu_{nb}}. \tag{3.18}$$

For large x-values (3.17) yield a value of 1 for the diffusivity factor.

Thus to incorporate the variation of the diffusion factor with respect to the absorber amount into a regular narrow band model we have to replace the weak absorption limit (2.28) by

$$\bar{A}_{nb}(u) = 2\,\bar{S}_{nb}u \tag{3.19}$$

and the strong absorption limit (2.29) by

$$\bar{A}_{nb}(u) = \sqrt{\bar{S}_{nb}\pi\bar{\alpha}_{nb}u}\,. \tag{3.20}$$

The particular example of a narrow band model given in the previous paragraph (2.30) should then be modified into

$$\bar{A}_{nb}(u) = \left(\left(\frac{1}{2\bar{S}_{nb}u}\right)^2 + \left(\frac{1}{\bar{S}_{nb}\pi\bar{\alpha}_{nb}u}\right)\right)^{-0.5}. \tag{3.21}$$

4. Inhomogeneous atmospheres

In the previous paragraphs we assumed no variation of the temperature and pressure along the line of sight. Then the integration of the absorption coefficient is trivial (cf. (1.9)). In the atmosphere this condition is never met. Thus variation of the temperature and pressure along the line of sight has to be taken into account. Two approximation methods are commonly used to evaluate the integration of the absorption coefficient along the line of sight. Both methods assume the absorption along a non homogeneous path can be approximated by the absorption along a homogeneous path with an appropriate adjustment of absorber amount. The two approximation schemes

are known as the scaling approximation and the Curtis-Godson approximation.

The scaling approximation, used in emissivity model, is based on the assumption that the pressure and temperature dependence of the absorption coefficient is independent of the frequency dependence, such that

$$\kappa_\nu^*(z) = \kappa_\nu^* * f(p,T) \,, \tag{4.1}$$

with the absorption coefficient at a standard pressure (p_o) and temperature (T_o). The integration of the absorption coefficient along the line of sight (1.8) can now be approximated by

$$\int_{z'}^{z} \kappa_\nu^*(z'')\ \rho(z'')\ dz'' = \kappa_\nu^* \int_{z'}^{z} f(p,T)\ \rho(z'')\ dz''. \tag{4.2}$$

To incorporate the temperature and pressure variation of the absorption coefficient in emissivity models, the absorber amount u is replaced by a equivalent absorber amount $\bar{u}$ defined by

$$\bar{u} = \int_{z'}^{z} f(p,T)\ \rho(z'')\ dz''. \tag{4.3}$$

The usual form of f is

$$f(p,T) = \left(\frac{p}{p_0}\right)^n \left(\frac{T_0}{T}\right)^m . \tag{4.4}$$

Table (4.1) list several values of n and m applicable to water vapor, carbon dioxide and ozone. From the listed range of values we conclude that the "exact" values for m and n is not yet established. This influence the performance of radiation models which uses the scaling approximation.

A more sophisticated approximation of the integration of the absorption coefficient along the line of sight is the Curtis - Godson approximation. The Curtis - Godson approximation describes the pressure and temperature variation of the mean line strength and mean line half width along the line of sight. Therefore the Curtis-Godson approximation is used in regular wide and narrow bandmodels.

Gas	n	m
Water vapor	0.5-0.9	0.45
Carbon dioxide	1.75	11-8
Ozone	0.4	0.2

Table 4.1 *Generally accepted values for n and m for various infrared active gases*

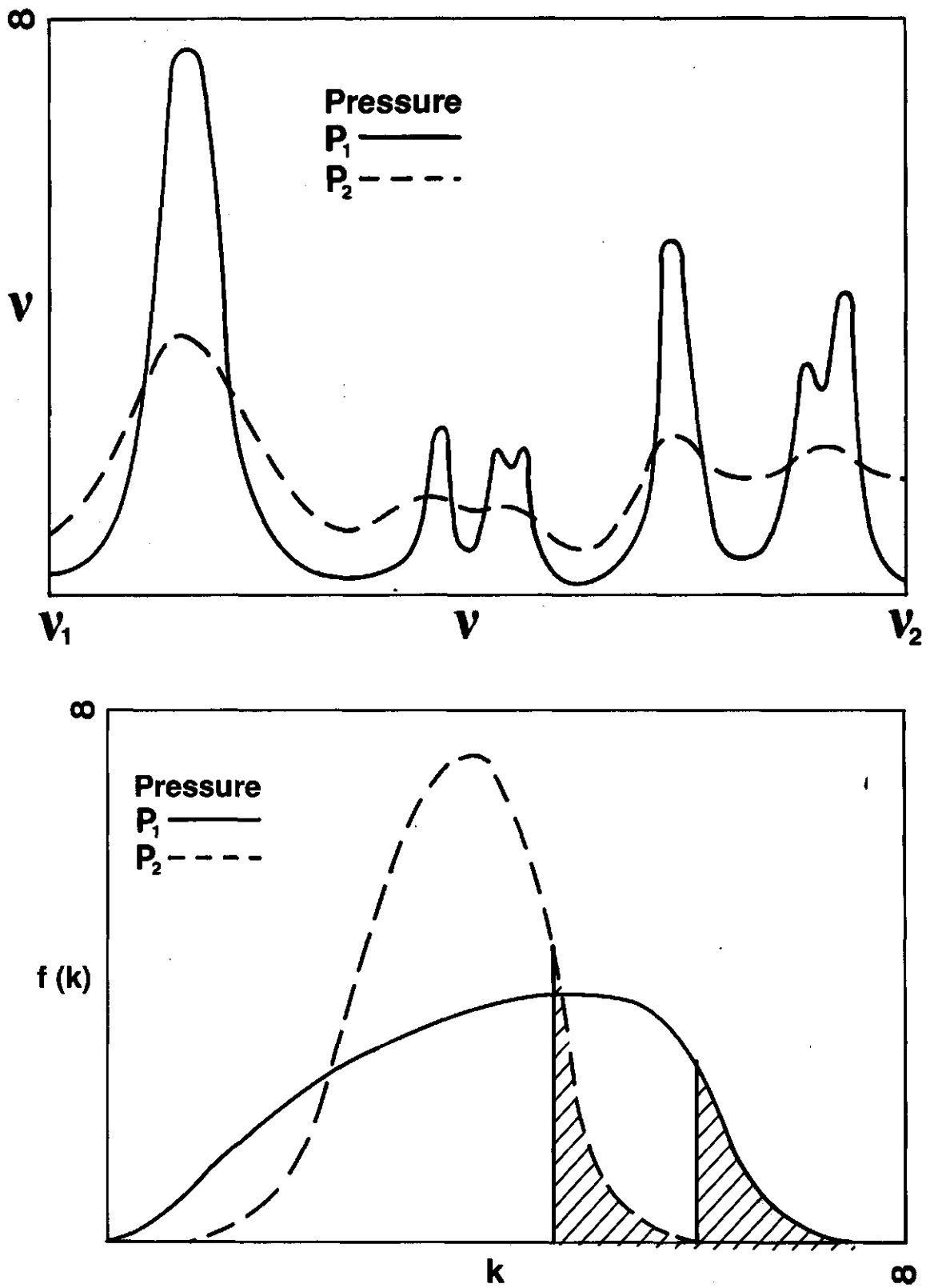

Fig. 4.1 *Schematic illustration showing the essence of the k-distribution method. Top panel: Schematic absorption line spectra at two different pressures. Bottom panel: Two probability functions f(k) associated with the left panel. The shaded area depicts the strongest absorption for the same spectral interval. (modified from Hansen et al., 1985).*

The mean line strength and line half width used in wide and narrow band models are replaced by an equivalent line strength and half width defined by (Liou, 1980)

$$\langle S \rangle = \int_{z'}^{z} S(T)\ \rho(z'')\ dz'' \Big/ \int_{z'}^{z} \rho(z'')\ dz''$$

$$= S_0 \int_{z'}^{z} f_1(T)\ \rho(z'')\ dz'' \Big/ \int_{z'}^{z} \rho(z'')\ dz'' \qquad (4.5)$$

and

$$\langle \alpha \rangle = \int_{z'}^{z} S(T)\ \alpha(p,T)\ \rho(z'')\ dz'' \Big/ \int_{z'}^{z} S(T)\ \rho(z'')\ dz''$$

$$= \alpha_0 \int_{z'}^{z} p/p_o\ f_2(T)\ \rho(z'')\ dz'' \Big/ \int_{z'}^{z} f_1(T)\ \rho(z'')\ dz'', \qquad (4.6)$$

with S_o and α_0 the mean line strength and halfwidth respectively at a standard pressure and temperature. Using simple analytical functions for f_1 and f_2 both integrals in (4.5) and (4.6) are evaluated explicitly in regular wide and narrow band models.

To account for pressure variations along the absorption path, the k-distribution provides an alternate and accurate treatment of vertical inhomogeneity. (Hansen et al., 1981). The k-distribution at all altitudes are correlated in frequency space (Fig. 4.1) i.e. the strongest and weakest absorption occurs at the same frequencies at all altitudes. Pressure effects are then included explicitly in the choice of k, used to evaluate mean transmission over a inhomogeneous path.

Chapter 3.
An accurate radiation model[2]

1. Abstract

A narrow band model is presented to simulate the transfer of infrared radiation through a cloudless atmosphere. The absorption and emission by the rotational and vibrational lines of water vapor, carbon dioxide and ozone in the spectral region from 3 to 83.3 THz is modelled using the Goody band model, while the absorption of the water vapor continuum in the atmospheric window region is evaluated using the empirical formulas of Roberts et al. (1976)

The model is tested against 44 cases of surface downward flux observations as well as against line by line calculations. From these comparison study we conclude that our narrow band model simulates the surface downward flux within ~ 3 W/m^2 (~1.5%) and the tropospheric cooling rate within 0.2 K/d (~20%)

2. Introduction

Knowledge of the infrared radiative cooling rate in the nocturnal boundary layer is important, especially since it determines the structure and evolution of layers near the surface and the boundary layer top (Garratt and Brost, 1981; Tjemkes and Duynkerke, 1988b, Chapter 4). To simulate the transfer of infrared radiation by water vapor (H_2O), carbon dioxide (CO_2) and ozone (O_3) in the spectral interval between 3 and 83.3 THz (= 3,6 and 100 μm) through the nocturnal boundary layer, we developed a regular narrow band model. In regular narrow band models, the infrared spectrum is divided into several spectral intervals for which an average net flux is evaluated from an approximate solution of the radiative transfer equation. The cooling rate is then found from the gradient of the total net flux, which is simply the linear summation over all average net flux of each spectral band. Regular narrow band models were previously used by Rodgers and Walshaw (1966), Ellingson and Gille (1978), Morcrette and Fouquart (1985), Cess et al. (1986) and Crisp et al. (1986). These authors in general claim accurate results.

The accuracy of our model is established from a comparison study. In section four we compare the performance of the model with two line by line models and with observations of the downward flux near the surface. In the last section a summary and some conclusions are given. But first we describe the covering equations of the radiation model in the next section.

3. Model description

3.1 Governing equations

The propagation of infrared radiation through a horizontally homogeneous, time independent atmosphere in local thermodynamic equilibrium, is described by

---

[2] Submitted to J. Geophys. Res. with F.T.M. Nieuwstadt as co-author

(Chandrasekhar, 1960)

$$\mu \frac{\partial I_\nu(z,\mu)}{\partial z} = \kappa_\nu(z) \left\{ B_\nu(z) - I_\nu(z,\mu) \right\} \qquad (3.1)$$

In (3.1) I represents the specific intensity for a given frequency (units: $Wm^{-2}Hz^{-1}Sr^{-1}$), B the Planck function, κ the absorption coefficient ($^{-1}$) and $\mu = \cos\theta$, with θ the angle between the direction of propagation and the vertical. Equation (3.1) states that during propagation through the atmosphere, the energy content of a pencil of radiation increases due to emission (κB) and decreases due to absorption ($-\kappa I$). Notice that in (3.1) scattering of infrared radiation by aerosols is neglected. Formally the transfer equation can be solved to yield an multiple integral for the net flux at a reference level z. But due to the rapid variation of the absorption coefficient with frequency, the evaluation of this multiple integral equation is laborious. Several approximate solutions of the transfer equation have been proposed. Here we follow Rodgers and Walshaw (1966). They assumed the spectrum to be divided into a finite number of intervals. For each of these intervals, the transfer equation (2.1) is solved to yield a mean upward (F+) and downward flux (F-) over the interval, where mean signifies an average over the interval. The resulting equations for band i reads (Rodgers and Walshaw, 1966)

$$F_i^+(z) = \tau_i(0,z) \left\{ B_i(g) - B_i(0) \right\} + B_i(z) - \int_0^z \tau_i(z', z) \frac{\partial B_i(z')}{\partial z'} dz' \qquad (3.2^a)$$

$$F_i^-(z) = \tau_i(z,Z) \left\{ B_i(Z) - B_i(\text{top}) \right\} - B_i(z) + \int_Z^z \tau_i(z', z) \frac{\partial B_i(z')}{\partial z'} dz', \qquad (3.2^b)$$

in which B_i the Planck function averaged over the interval represents and $\tau_i(z',z)$ the slab or diffuse transmission function which describes the transmission along the atmospheric path between the levels z' and z,

$$\tau_i(z',z) = \frac{2}{\Delta\nu} \int_{\Delta\nu} \int_0^1 \exp - \left\{ \int_{z'}^{z} \kappa_\nu(z'')\, dz'' / \mu \right\} \mu\, d\mu\, d\nu. \qquad (3.3)$$

In (3.2) allowance is made for the presence of temperature discontinuities at the ground (g) and a possible source of downward flux at the top of the atmosphere (top).
Given an expression for the transmission between the levels z and z', the two flux components can be calculated. The net flux is then found as $F_n = F+ - F-$ and the cooling rate from dFn / dz.

3.2 The transmission function

For the vibrational and rotational spectral lines of H_2O, CO_2 and O_3, the mean transmission function is evaluated according to the Goody band model (Goody, 1952; Tjemkes and Duynkerke, 1988a; Appendix B). For the transmission function in the atmospheric window where the water vapor continuum absorption is important, the

empirical relations proposed by Roberts et al. (1976) are used.

With the assumption that the rotational/vibrational lines of water vapor, carbon dioxide and ozone absorb uniformly over the entire spectral band and that the ratio of the line absorption and the spectral interval width is much smaller than unity, the mean transmission (3.3) can be parametrized according to (Goody, 1952; Tjemkes and Duynkerke, 1988a; Appendix B)

$$\tau_i\,(z',z) = \exp -\left\{ \frac{n_i \overline{W}_i\,(z',z)}{\Delta\nu_i} \right\} \qquad (3.4)$$

with ni the total number of lines inside the ith-interval, Δvi the spectral width and $\overline{W}_i$ the mean single line absorption given by

$$\overline{W}_i\,(z',z) = \frac{1}{n_i} \sum_{j=1}^{n_i} W_j\,(z',z). \qquad (3.5)$$

The single line absorption (Wj) can be evaluated with a Lorentz profile for the line shape according to the Ladenberg-Reiche function (Ladenberg and Reiche, 1913). Since the line strength varies from line to line and the number of lines inside the interval may be very large, the evaluation of the mean absorption from the total absorption of each individual spectral line will be very laborious. To avoid lengthy calculations we approximate the mean line absorption by a square interpolation between the small and large path length limit (Chapters 2, Appendix B).

$$\frac{n_i \overline{W}_i\,(z',\,z)}{\Delta\nu_i} = r\,\overline{S}_i\,\bar{u}\left(1 + \frac{r\,\overline{S}_i\,\bar{u}}{\pi\,\overline{\alpha}_i\,\bar{\phi}} \right)^{-0.5} . \qquad (3.6)$$

With

$$\overline{S}_i = \frac{1}{n_i} \sum_{j=1}^{n_i} S_j \qquad (3.7^a)$$

the mean line strength and

$$\overline{\alpha}_i = \frac{4\left(\sum_{j=1}^{n_i} \sqrt{S_j \alpha_j} \right)^2}{n_i \sum_{j=1}^{n_i} S_j} \qquad (3.7^b)$$

the mean line half width. In order to correct for the non-homogeneous atmosphere along the path we introduce in (3.6) $\bar{u}$ and $\bar{\phi}$ to represent the equivalent path length and pressure respectively (Rodgers van Walshaw, 1966). The equivalent path and pressure

accounts for the variation of the line strength and half width with the temperature and pressure. The r is a diffusion factor equals 5/3 which accounts for the integration over all zenith angles (Quanhua and Schmetz, 1988). Notice that we neglect any dependence of r with u.

For the band transmission function for the water vapor continuum, we use the empirical fit proposed by Roberts et al. (1976)

$$\tau_i (z',z) = \exp - \left\{ r \, \bar{\sigma}_i \, \bar{u}_c \right\} \qquad (3.8)$$

with $\bar{\sigma}$ the continuum absorption coefficient averaged over the ith band, and $\bar{u}_c$ the equivalent path length for water vapor continuum. The equivalent path accounts for the temperature dependence of the absorption coefficient.

For frequencies between 0 - 12.00 and between 45.00 - 84.00 THz, the band width was chosen to be 0.75 THz, whereas for frequencies in between 12.00 and 45.00 THz it was 0.30 THz. The mean line strength and half width are calculated from the 1980-version of the McClatchey compilation of the atmospheric absorption line parameters compiled by Rothman (1981). In spectral intervals where two or more gases (or two different types of absorption mechanisms) are active, the multiplicative formula discussed by Goody (1964) gives the total transmission as the product of the individual transmissions.

3.3 The height integral

The height integral in (3.2) between the lower (or upper) boundary and the reference level, can be written as the sum of height integrals over adjacent levels. For instance, let the integral between the lower boundary, with level number 0, and the reference level z, with level number n, be abbreviated by $I_n(o,n)$. Then this integral is evaluated according to

$$I_n(0,n) = \sum_{j=1}^{n} I_n(j-1,j), \qquad (3.9)$$

where

$$I_n (j-1,j) = \int_{z_{j-1}}^{z_j} \tau_i (z',z) \frac{\partial B_i (z')}{\partial z'} \, dz'. \qquad (3.10)$$

To evaluate the height integral $I_n(j-1, j)$, two different approximation schemes are used. If

$$\tau_i (z_n, z_{j-1}) / \tau_i (z_n, z_j) \geq 0.5 , \qquad (3.11)$$

which states that if the band transmission function does not vary rapidly with height, $I_n(j-1, j)$ may adequately be approximated by a trapezoidal rule:

$$I_n(j-1, j) \approx \frac{1}{2} \left\{ \tau_i(z_n, z_{j-1}) + \tau_i (z_n, z_j) \right\} \left\{ B_i(z_{j-1}) - B_i (z_j) \right\}. \qquad (3.12)$$

	model	NBM	Brunt	Swinbank	Brutsaert
Correlation Coefficient	day	0.993 (3)	0.995 (2)	0.926 (6)	0.996 (2)
	night	0.993 (3)	0.987 (5)	0.983 (7)	0.988 (5)
	day + night	0.990 (3)	0.990 (3)	0.979 (6)	0.993 (2)
Regression Slope	day	1.00 (3)	0.95 (2)	0.94 (4)	0.93 (2)
	night	0.90 (2)	0.92 (3)	1.02 (4)	0.91 (3)
	day + night	0.97 (2)	0.91 (2)	0.90 (2)	0.92 (2)
Regression Constant (Wm^{-2})	day	9.2 (8.5)	17.0 (7.1)	11.8 (12.1)	16.7 (6.4)
	night	29.5 (6.2)	29.6 (8.6)	2.4 (11.0)	26.4 (8.4)
	day + night	14.6 (6.1)	31.3 (5.4)	29.2 (6.5)	22.6 (5.0)
Difference (Wm^{-2})	day	9.6 (7.3)	3.1 (6.7)	-8.6 (11.2)	-4.0 (6.2)
	night	2.9 (7.9)	8.3 (8.7)	7.6 (9.0)	0.6 (8.5)
	day + night	6.0 (8.0)	5.9 (7.9)	-0.2 (12.3)	-1.5 (7.5)

Brunts formula

$$F^{-}(z=0) = \left(0.52 + 0.065\sqrt{e}\right)\sigma T^{4}(z=z_a)$$

Swinbanks formula

$$F^{-}(z=0) = 5.31\ 10^{-14}\sigma T^{4}(z=z_a)$$

Brutsaerts formula

$$F^{-}(z=0) = 1.24\left(\frac{e}{T}\right)^{1/7}\sigma T^{4}(z=z_a)$$

Table 4.1 *Results of the linear regression analysis. The numbers in brace for the correlation coefficient and the regression slop indicates the uncertainty in the last shown decimal while for the regression constant and difference it indicates the root mean square error.*

This integration scheme is fast and simple. However, if

$$\tau_i (z_n, z_{j-1}) / \tau_i (z_n, z_j) < 0.5, \qquad (3.13)$$

which states that if the band transmission function varies rapidly with height, the use of a trapezoidal rule to approximate I_n (j-1, j) would introduce non-acceptable errors in the flux calculation. In this case we use

$$I_n(j-1, j) \approx \frac{\left\{B_i (z_j) - B_i (z_{j-1})\right\} \left\{ \tau_i (z_n, z_j) - \tau_i (z_n, z_{j-1}) \right\}}{\ln\left\{\tau_i (z_n, z_j)\right\} - \ln \left\{\tau_i (z_n, z_{j-1})\right\}}. \qquad (3.14)$$

This equation is derived based on the assumption that the band transmission function can be approximated by an exponential function and that the Planck function dependents linear of z'. Several numerical tests showed that with the above described method an error of less than 1% is introduced in the surface downward flux.

4. Comparison study

The radiation model described in the previous section, is tested in two ways. First we performed a comparison between observed and calculated downward fluxes at the surface. Secondly, we used the results of the international comparison study of radiation codes used in climate models (ICRCCM; WMO, 1984) to compare the performance of our narrow band model against two line by line models.

4.1 Comparison with observations

In 1983 44 observations of the downward infrared flux at the surface were collected. These radiation observations were performed in the vicinity of the 200 m high meteorological observational site located at the Cabauw. The observational error was estimated from the radiation balance to be ± 10 Wm-2. The measurements were selected for cloudless conditions only at day- and nighttime at all four seasons of the year. Each of these 44 observations were simulated with our radiation model. For the calculations we modelled the absorption and emission of infrared radiation by water vapor, carbon dioxide and ozone. The distribution of water vapor and temperature with height for layers below 200 m were taken from the observations along the tower. For layers above 200 m they were taken from rawinsonding observations launched in De Bilt (approximately 60 km from Cabauw) at approximately the time of the observation. For carbon dioxide we adopted a mixing ration equals 330 ppmv independent of height and for ozone we adopted the standard midlatitude summer profile as given by McClatchey et al. (1972). In Fig. 4.1 we present the result of this comparison study. In addition to this fig. in Table 4.1 the results of a linear regression analysis can be found.

Table 4.1 shows that the band model underestimates the observations by about 6 Wm-2, which is within the estimated observational error. The difference between observations and simulations is smaller during the night than during the day. Which could be explained by direct solar irradiance on the instruments during daytime.

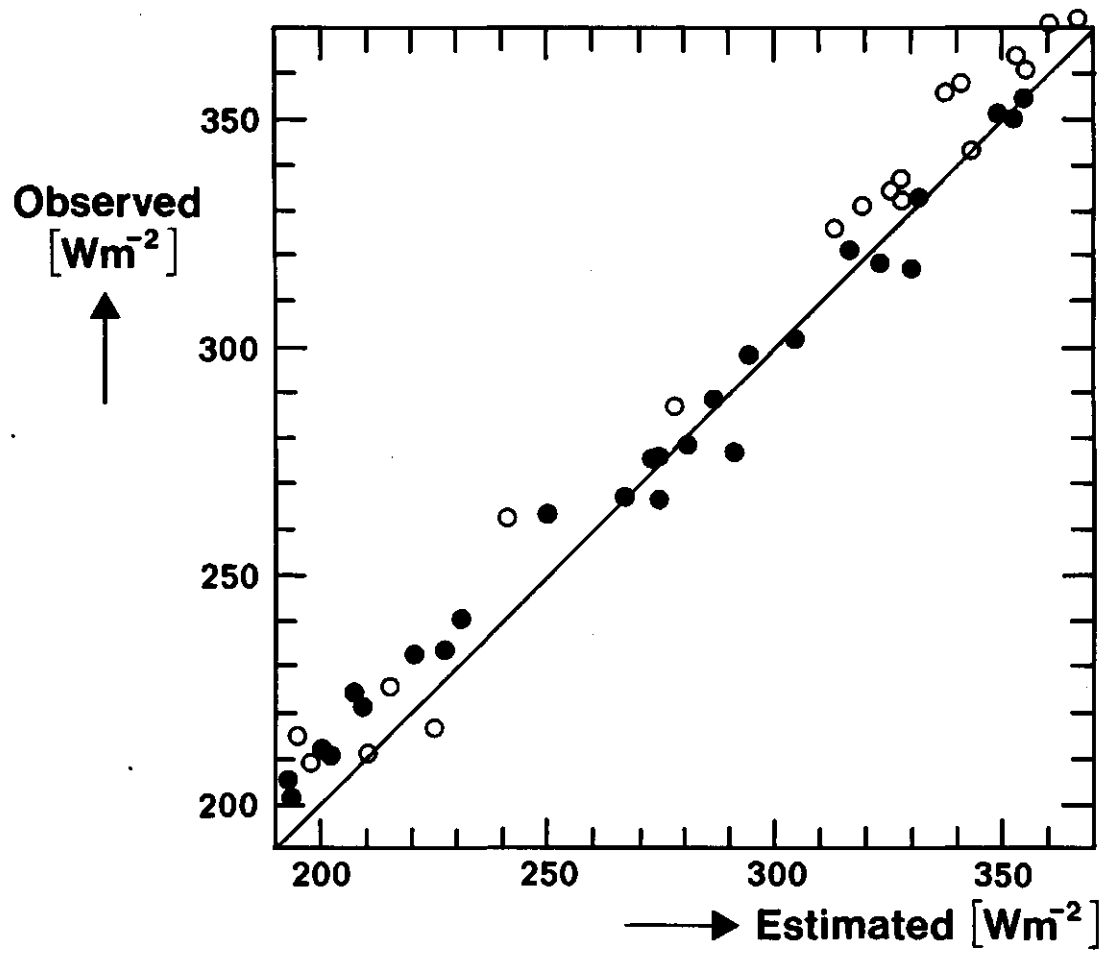

Fig. 4.1 *Comparison of the observed and simulated downward flux at the surface. Open circles denotes the day-time observations, filled circles the night-time.*

For the calculation of infrared downward flux at the surface, several relatively simple formulas exist. We have simulated the 44 observations with the empirical relations proposed by Brunt (1932), Swinbank (1963) and Brutsaert (1975). The results of this comparison study are also given in Table 4.1. Apparently, these simple formulas are at least as good as our complex band model. This means that the downward flux at the surface can be calculated not only very accurately, but also much faster and simpler than by using a complex band model. As a result these empirical relations are often used in surface energy balance models (e.g. Holtslag and de Bruin, 1988). However, it must be stressed that our band model is not used for the evaluation of the surface downward flux only, but also to estimate the cooling rate in the atmosphere for which no simple equation exists to our knowledge.

4.2 Influence of observational errors

Test calculations were performed to study the effect of observational errors on the calculated downward surface flux. For these tests we add random errors to the temperature and humidity profile, although most of the observational errors are probably caused by instrumental responds and thus these errors may be systematical. Our procedure was to change at each observational level the temperature and humidity with the observational error of 1 K and 5% for the temperature and humidity respectively. The sign of these changes were randomly chosen at every level. In total

25 calculations were performed. From these test calculations we conclude that due to random errors the calculated surface flux can vary by about 2%. Because the observational errors in temperature and humidity at levels below 200 m are significantly less than the 1K or 5% the 2% variation in the surface flux is considered as an upper limit.

4.3 Comparison with calculations

Radiation models that explicitly evaluate the frequency integral over the monochromatic transfer equation (eq. (1.5) in Chapter 1) are called "line by line" models. These models are regarded as the benchmarks of infrared flux calculations. Therefore they are frequently used as a reference for less detailed radiation models (e.g. Crisp et al., 1986).

We used the results of the intercomparison study of radiation codes used in climate models (ICRCCM; WMO, 1984) to compare the performance of our narrow band model against the line by line model of the geophysical fluid dynamics laboratory (GFDL) and the 4A-model of Scott and Chedin (1981). In Fig. 4.2 (modified from WMO, 1984), we present the cooling rate for a standard midlatitude summer profile (McClatchey et al., 1972). For these calculations only the absorption and emission by the rotational/vibrational lines of water vapor, carbon dioxide and ozone in the frequency region from 0 to 78.0 THz are taken into account. From this figure we see for layers in the troposphere (tropopauze at 13 km or 179 hPa), the difference between the two line by line models and our narrow band model is approximately 0.2 K/d. The correspondence between the GFDL-model and ours is slightly better than between the 4A-model and ours.

	Surface			Troposphere			Top
	F+	F-	NET	F+	F-	NET	F+
CO_2 - only 300 ppmv							
narrow band model	421.0	80.0	341.0	376.7	13.9	362.8	377.6
4A-model	421.0	76.4	344.6	380.2	11.7	368.5	380.9
H_2O - only without continuum							
narrow band model	421.0	265.8	155.2	331.2	6.3	324.9	331.1
4A-model	421.0	267.3	153.7	331.0	6.3	324.7	329.5
H_2O without continuum, CO_2 and O_2							
narrow band model	421.0	303.0	118.1	293.2	20.7	272.5	292.0
4A-model	421.0	300.7	120.3	296.0	19.8	276.2	292.1

Table 4.2 *Comparison between the narrow band model and the 4A line by line model of Scott and Chedin (1984). Calculations are performed for the standard midlatitude summer profile of McClatchey et al. (1972). All numbers are in Wm^{-2}. For these calculations the spectral interval is changed to 100 to 2200 cm^{-1}.*

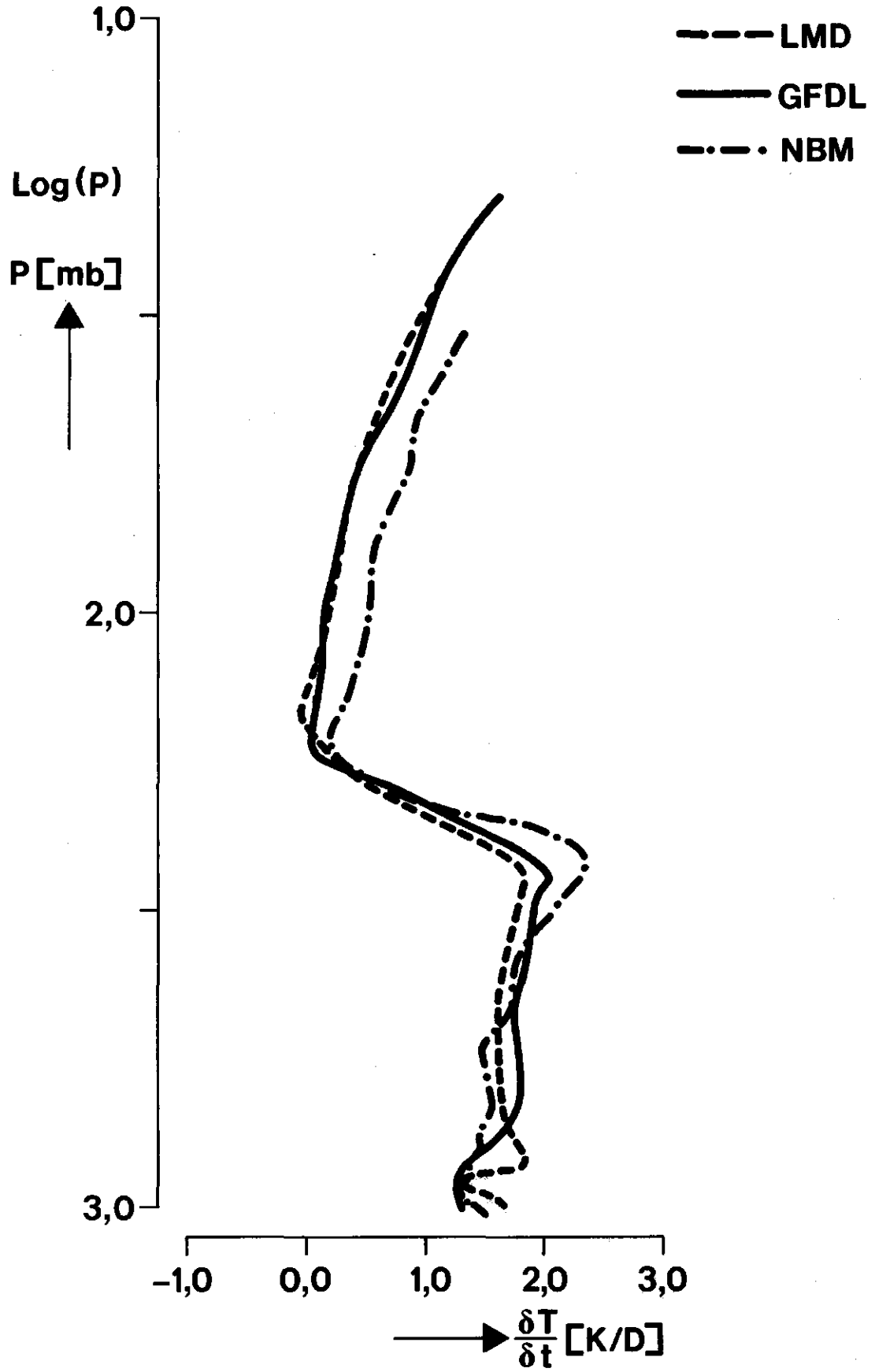

Fig. 4.2 *Cooling rate of a midlatitude simmer atmosphere according to the GFDL line by line model (solid line), the 4A line by line model (dashed line) and according to our narrow band model (dashed dotted line). For these calculations absorption by the water vapor continuum is omitted. Only the absorption by the rotational / vibrational lines of water vapor, carbon dioxide and ozone is modelled. (modified from WMO, 1984)*

Above the tropopauze, the narrow band model diverges from the two line by line models. At low levels, the line profile is formed by collisions between the molecules. The line shape is then adequately described by a Lorentz profile (Liou, 1980). At high altitudes the density becomes so low that the collisions do no longer determine the line profile. Instead, the line profile is formed as a result of the frequency shift due to moving radiation sources (Doppler effect). Then the line shape is described by the Doppler profile (Liou, 1980) . In between these two cases a combined profile should be used (the so-called Voigt-profile). Since we adopted a Lorentz line profile at all altitudes, our model will diverge from other models in which the transition from Lorentz to Doppler is taken into account as shown in Fig. 4.2.

If we look at the performance of the NBM into more detail, we see that with respect to the 4A-model our NBM underestimates the transmission due to the CO_2-lines. This is clearly demonstrated by the downward flux at the surface (Table 4.2). Since there is no downward flux of infrared radiation at the top of the atmosphere, the presented overestimation of the surface downward flux arises from a overestimation of the atmospheric emission. Because in a scatterless atmosphere, the transmission and emission should sum to unity, we conclude that the NBM underestimates the atmospheric transmission.

From the same table we notice that the band model overestimates the transmission due to the rotational and vibrational lines of water vapor. But it underestimates the transmission due to the combined absorption and emission by water vapor, carbon dioxide and ozone. The performance of the model could probably be improved if a different interpolation formula between the small and large path length limit is chosen. Tjemkes and Duynkerke (1988a; also Appendix B) demonstrated that for instance a linear interpolation formula yield better result for the 15 μm CO_2 band than the square interpolation formula. However it must be noticed that the uncertainty in the surface downward flux by line by line models is on the order of 2 Wm-2 (WMO, 1984). Which is of the same order as the difference between our NBM and the 4A-model.

5. Summary

In this paper we present an accurate narrow band radiation model to simulate infrared radiative transfer through the troposphere. The infrared spectrum between 0 and 84.00 THz is divided into 178 bands. For each of these bands the infrared transfer equation is solved. The mean transmission function of water vapor, carbon dioxide and ozone rotational / vibrational lines, is evaluated according to the Goody band model with a square interpolation between the small and large path length limit. For the water vapor continuum we use the empirical schemes of Roberts et al. (1976). To approximate the integration the absorption coefficient over the inhomogeneous path, the Curtis-Godson method is used and to approximate the integration over all zenith angles a diffusion factor of 5/3 independent of path length is adopted.

The performance of this radiation model is tested in two ways. From a comparison with 44 cases of observed downward flux at the surface, it is shown that our radiation model underestimates this flux by about 6 Wm-2 (≈2%) with a root mean square error of 8 Wm-2. Since the observational error is already 10 Wm-2 we also compared the performance of our model with calculations performed by two different line by line models. From this comparison we notice that our model only slightly overestimates the transmission due to water vapor, but underestimates the transmission due to carbon dioxide. As a result our NBM diverge approximately 3 Wm-2 in the surface downward flux from the line by line model results. Moreover from the comparison between the narrow band model and the line by line model it is shown that the error in the radiative cooling rate below the tropopauze is about 0.2 K/d (≈20%).

ACKNOWLEDGEMENTS

We thank Sandra Klutz for preparing the paper and Cees van Stralen for drawing the figures. One of us (S.A.T.) acknowledges financial support by the organization of scientific research in the Netherlands (N.W.O.) under contract # 752-365-008.

Chapter 4
The nocturnal boundary layer Model calculations compared with observations[3]

1. Abstract

The structure and evolution of the nocturnal boundary layer (NBL) is simulated using a model which includes the transfer of energy by radiation and turbulence. The radiation scheme is an accurate narrow band model which simulates the absorption and emission of infrared radiation by water vapor and carbon dioxide. For the transfer of energy by turbulence we used a model in which a prognostic equation for the turbulent kinetic energy is solved together with a diagnostic length scale equation for the turbulence. Moreover, we adopted the "force restore method" to account for the transfer of energy through the soil. For the vegetation layer a simple scheme was used to describe the energy flux.

The performance of this combined model is compared with detailed observations of the mean thermodynamic and turbulence structure throughout the NBL (up to 200 m) for two cloudless nights in 1978. These observations were collected at the meteorological observational site near the village of Cabauw in the Netherlands. During the first night the wind speed above the NBL was approximately 10 m/s, while during the second night it was 6 m/s.

From the comparison we conclude that the agreement between the calculated and observed profiles of turbulence and mean thermodynamic variables and between the calculated and observed evolution of the surface fluxes is satisfactory. However, the detailed structure of these profiles depends upon the local terrain inhomogeneities. Because the model simulates a horizontally homogeneous flow, these detailed structures cannot be reproduced accurately. Moreover, we find that the inclusion of radiative cooling within the atmosphere, increases the calculated boundary layer height by about 25%.

2. Introduction

The nocturnal boundary layer (NBL) is a thin atmospheric layer, located adjacent to the earth's surface, which develops during the night. The structure and evolution of the NBL is determined by a variety of processes, such as infrared radiation, turbulent mixing, gravity waves and advection. In this paper we study the structure and evolution of the NBL due to the combined effect of radiation and turbulent mixing. In previous studies, the interaction between radiation and turbulence is studied analytically (Coantic and Seguin, 1971; Coantic and Simonin, 1984), numerically (André et al., 1978; Garratt and Brost, 1981; Estournel and Guedalia, 1985) and observationally (André and Mahrt, 1982). It was generally concluded that radiative cooling within the atmosphere can be neglected to describe the evolution of bulk of the

---

[3] Accepted for publication in J. Appl. Meteor. with P.G. Duynkerke as co-author

turbulent mixed layer. However, they also state that radiative cooling determines the evolution of the inversion layer, which usually extends to higher levels than the NBL itself.

The cooling rate due to radiative transfer is usually calculated as the gradient of the net flux, which is determined by the difference between the upward- and downward flux, two almost equally large numbers. A relatively small error in one of these two flux components will cause a relatively large error in the net flux and thus in the cooling rate. This is especially the case near the surface, where the cooling rate is calculated over thin atmospheric layers. It is therefore very important to calculate the upward- and downward flux as accurately as possible.

With respect to the radiation calculations, most of the above mentioned studies adopt an emissivity approach for the calculation of the radiative cooling rate. This method parameterizes the variability of the absorption coefficient as a function of frequency to achieve computational efficiency (Rodgers, 1967, Sasamori, 1968). The ICRCCM- study (WMO, 1984) reveals that the computations performed by several emissivity models diverge from computations performed by accurate line by line models. For instance for a standard midlatitude summer profile, the difference in the downward flux near the surface between the two models can be as large as 20 Wm^{-2}. This difference may lead to unacceptable errors in the cooling rate within the NBL.

In this paper we present calculations for the NBL using a combined model which consists of an accurate radiation model and an E-l turbulence model in which a prognostic equation for the turbulent kinetic energy is solved together with a diagnostic equation for the turbulent mixing length. The major goal of this study is to test the model using observations of temperature, wind speed, boundary layer height and friction velocity within the NBL (up to 200 m) as well as observations of the surface energy balance of two cloudless nights, collected at the Cabauw meteorological observational site in 1978.

In the next section we present the governing equations together with the turbulence and radiation scheme. Emphasis will be on the radiation scheme, since the turbulence model is described in detail by Duynkerke and Driedonks (1987). In section 4 we briefly describe the observations and the initial conditions. In section 5 discussion of the results is given and finally in section 6 we summarize our findings.

3. The model

In this section we discuss the details of our coupled radiation/turbulence model. Except for the schemes of the surface temperature and the transfer of infrared radiation through the atmosphere, this model is similar to the model used by Duynkerke and Driedonks (1987; DD87 hereafter).

3.1 Governing equations

We consider a horizontally homogeneous flow with mean velocity components $(\bar{u}, \bar{v})$ in the (x, y) direction. The equations of motion, mean potential temperature $(\bar{\theta})$ and specific humidity $(\bar{q}_v)$ can be written as (DD87)

$$\frac{\partial \bar{u}}{\partial t} = -\frac{\partial \overline{u'w'}}{\partial z} + f(\bar{v} - v_g) \qquad (3.1^a)$$

$$\frac{\partial \bar{v}}{\partial t} = -\frac{\partial \overline{v'w'}}{\partial z} - f(\bar{u} - u_g) \qquad (3.1^b)$$

$$\frac{\partial \bar{\theta}}{\partial t} = -\frac{\partial \overline{\theta' w'}}{\partial z} - \frac{1}{\rho C_p}\frac{\partial F_n}{\partial z} \qquad (3.1^c)$$

$$\frac{\partial \overline{q_v}}{\partial t} = -\frac{\partial \overline{q'_v w'}}{\partial z}, \qquad (3.1^d)$$

where primes denote turbulent fluctuations, (u_g, v_g) the geostrophic wind, f the Coriolis parameter and F_n the net radiation. The overbar denotes ensemble averages. For a complete list of all variables we refer to Appendix C.

To solve this set of equations we must specify a closure relationship for the turbulent fluxes and the net radiative flux. Moreover, a solution is only possible when a set of boundary conditions is given. In section (3.3) we describe the radiation model and in section (3.4) the boundary conditions. In the next section (3.2) only a brief description of the turbulence closure is given, since a full discussion can be found in DD87.

3.2 Turbulence closure

Following K-theory all turbulent fluxes are related to the gradient of the mean variables. For instance for the vertical momentum flux we have

$$\overline{u'w'} = -K_m \frac{\partial \bar{u}}{\partial z}. \qquad (3.2)$$

with K_m the exchange coefficient for momentum. This exchange coefficient is proportional to the product of a mixing length scale and a velocity scale. For our computations we use (DD87)

$$K_m = c\, l_m E^{1/2}, \qquad (3.3)$$

with l_m a mixing length, and E the turbulent kinetic energy. Both l_m (given by a diagnostic equation) and E (given by a prognostic equation) are calculated in combination with the set of (3.1). For further details we refer to DD87.

3.3 Radiation model

1) Solar radiation

For our simulations of the NBL, we initialize our model during daytime (section 4). Therefore we have to consider the forcing of the planetary boundary layer by solar radiation. To simulate the transfer of short wave radiation through the atmosphere, we used the model presented by Fouquart and Bonnel (1980). This model involves Rayleigh scattering as well as absorption by water vapor and carbon dioxide.

2) Infrared radiation

The absorption and emission of infrared radiation by water vapor and carbon dioxide is simulated using a narrow band model (NBM-hereafter). The infrared spectrum between 3.6 and 100 μm is divided into 178 spectral bands. The mean

upward (F+) and downward (F-) flux for each of these bands are calculated from a solution of the transfer equation given by Rodgers and Walshaw (1966),

$$F_i^+(z) = \tau_i(0,z)\left\{B_i(g) - B_i(0)\right\} + B_i(z) - \int_0^z \tau_i(z', z)\frac{\partial B_i(z')}{\partial z'}\,dz' \qquad (3.4^a)$$

$$F_i^-(z) = \tau_i(z,Z)\left\{B_i(Z) - B_i(top)\right\} - B_i(z) + \int_Z^z \tau_i(z', z)\frac{\partial B_i(z')}{\partial z'}\,dz'. \qquad (3.4^b)$$

In these equations $\tau_i(z,z')$ represents the slab or diffuse transmission function (Liou, 1980) and

$$B_i = \pi \int_{\Delta\nu_i} B_\nu\, d\nu / \Delta\nu_i \qquad (3.5)$$

the Planck function integrated over the frequency interval $\Delta\nu_i$. Allowance is made for the presence of a temperature discontinuity at the ground and a source of downward flux at the upper boundary ($B_i(top)$). The total upward and downward flux is found as a sum of the fluxes over all bands.

For the vibrational/rotational lines of water vapor and carbon dioxide, the slab transmission function is parametrized according to the Goody band model (Goody, 1952; Tjemkes and Duynkerke, 1988a, Appendix B). For the water vapor continuum in the region between 8-12 μm we adopted the empirical relation proposed by Roberts et al. (1976). For more details concerning the transmission functions we refer to Appendix D and Tjemkes and Nieuwstadt (1988, Chapter 3).

The radiation scheme was tested in two comparison studies (Tjemkes and Nieuwstadt, 1988). In the first, we compared the calculated downward flux near the surface with the observed flux for 24 cases, in the second we compared the performance of the NBM with the performance of two line by line models. From these two comparison studies we conclude that the calculated downward flux near the surface has an error of 3 Wm-2 (= 1,5%) whereas the error in the cooling rate is of the order of 0.2 K/d (= 20%).

3.4 Boundary conditions

1) Upper boundary

At the upper boundary of our model domain (Z) we set the wind equal to the geostrophic wind and the vertical gradients of the potential temperature, the specific humidity and the turbulent kinetic energy to zero. During our simulations, we did not perform any infrared flux calculation above z = Z. Therefore, we have to specify the downward flux in each spectral interval at the upper boundary. These fluxes are calculated for a standard midlatitude summer profile (McClatchey et al., 1972) using our detailed narrow band model in advance of our NBL-simulations. This choice introduces errors in the calculated cooling rate. However, these errors will mainly occur near the upper boundary, which is well above the boundary layer (cf. Table 4.2).

2) Lower boundary

At the surface we used the force restore method to calculate the rate of change of the surface temperature (Deardorff, 1978). The force restore method is based on a solution of the diffusion equation for heat transfer through a homogeneous soil for sinusoidal temperature wave with a period of one day. The time rate of change for the surface temperature can be written as

$$\frac{\partial T_s(t)}{\partial t} = \sqrt{\frac{2\omega}{\lambda_d \rho C_d}}\, G(t) - \omega \left\{ T_s(t) - T_d(t) \right\} \qquad (3.6)$$

where G is the soil heat flux, T_d the deep soil temperature, ω a period of one day ($2\pi/86400$ Hz.), λ_d the thermal conductivity and ρC_d heat capacity of the soil.

The soil heat flux is calculated from the surface energy balance, which states that the soil heat flux, the net radiation, the latent and the sensible heat flux should sum to zero. The surface level is within the vegetation layer. To relate the surface temperature (T_s) with a temperature (T_0) just above the vegetation level (at z_0) we used a scheme proposed by Holtslag and De Bruin (1988):

$$\frac{T_0 - T_s}{\theta_*} = c_v + \frac{u_0}{u_*} \qquad (3.7)$$

here, T_0 is the temperature at $z = z_0$, c_v and u_0 are empirical constants with values of 10 and 4.2 m/s respectively.
The specific humidity at $z = z_0$ is specified according to

$$\overline{q_v} = q_{sat}(T_0) - \max\left(0, R_c\left(\overline{q_v' w'}\right)_s\right) \qquad (3.8)$$

with R_c the canopy resistance. Finally the turbulent kinetic energy at z_0 is specified according to (DD87)

$$E = 0.033^{-1/2}\, u_*^2 + 0.35\, w_*^2 \qquad (3.9)$$

Using Monin-Obukhov similarity theory, we extrapolate the temperature and humidity from $z = z_0$ to the lowest calculation level at 1 m above the surface. The fluxes are assumed to be constant between the surface and the lowest calculation level.

3.5 Numerical procedure

The set of partial differential equations given in the previous sections, are solved on a staggered grid with a resolution of 1 m near the surface and 10 m near the top of the NBL (DD87). A standard discretization in time and a central discretization in place with the diffusion terms lagging in time, was chosen. In order to remove any tendency towards decoupling the odd and even time steps, the time filter proposed by Robert (1966) was adapted.

4. Observational data

Parameter	Measuring device	Measuring height (m)	Comment
Wind speed	Cup anemometer 20., 40, 80, 120, 160, 200	1.47, 5.63, 10.61, averaged	30 min
Wind direction	Wind vane 20, 40, 80, 120, 160, 200	1.47, 5.63, 10.61, averaged	30 min
Temperature thermocouples	Ventilated 9.69, 20, 40, 80, 120, 160, 200	0.51, 2.00, 4.72, averaged	30 min
Turbulence statistics	Trivane, fast thermocouple	20, 40, 80, 120, 160, 200	30 min averaged
Surface energy balance		surface	30 min averaged
Boundary layer height	acoustic sounder		30 min averaged
Geostrophic wind			60 min averaged
radio sounding	VIZ-1207		

Table 4.1 *Instruments and measuring heights used during the observations*

4.1 The observational site

From September 1977 until February 1979 an observational campaign was held to study the formation and evolution of the NBL. (Nieuwstadt, 1984). During this campaign profiles of temperature, wind speed, wind direction and various turbulence variances and covariances were measured along the 200 m meteorological mast near the village of Cabauw in the Netherlands. In addition to these profiles the components of the surface energy balance were measured on a terrain in the vicinity of this mast and the boundary layer height was monitored by an acoustic sounder. The geostrophic wind was calculated using pressure observations at 19 meteorological stations in the Netherlands (Nieuwstadt, 1984). The surroundings of the mast is flat and homogeneous on a scale of ~ 20 km, with a roughness length which varies from 0.05 - 0.35 m depending upon wind-direction (Monna and v/d Vliet, 1987). During the campaign several rawinsondes were launched to establish the structure of the atmosphere above the mast at the beginning of the day (Driedonks, 1981). In Table 4.1 we summarize the observed variables.

4.2 Dimensionless wind shear and temperature gradient

From the complete data set, Nieuwstadt (1984) extracted 103 half hour observations. This subset was used to calculate the dimensionless windshear (ϕ_h) and temperature gradient (ϕ_m) as a function of the dimensionless height z/Λ, with Λ the local Monin-Obukhov length defined by (Nieuwstadt, 1984)

$$\Lambda = -\frac{\tau^{1.5}}{k\frac{g}{T}\overline{w'\theta'}}. \qquad (4.1)$$

In Fig 4.1 and Fig 4.2 we plotted ϕ_m and ϕ_h as a function of z/Λ.
We see that for $z/\Lambda < 2$, ϕ_m and ϕ_h can be reasonably well approximated by a linear function

$$\phi_{m,h} \approx 1 + \beta_{m,h}\frac{z}{\Lambda}, \qquad (4.2)$$

with

$$\beta_m \approx 8 \qquad (4.3^a)$$

$$\beta_h \approx 12. \qquad (4.3^b)$$

These values for β are larger than the values proposed by Businger et al. (1971) ($\beta_m = \beta_h \approx 4.7$), which are commonly used by various authors (eg. Garratt and Brost, 1981; Estournel and Guedalia, 1985). But also larger values for β are also proposed (Yaglom, 1977).

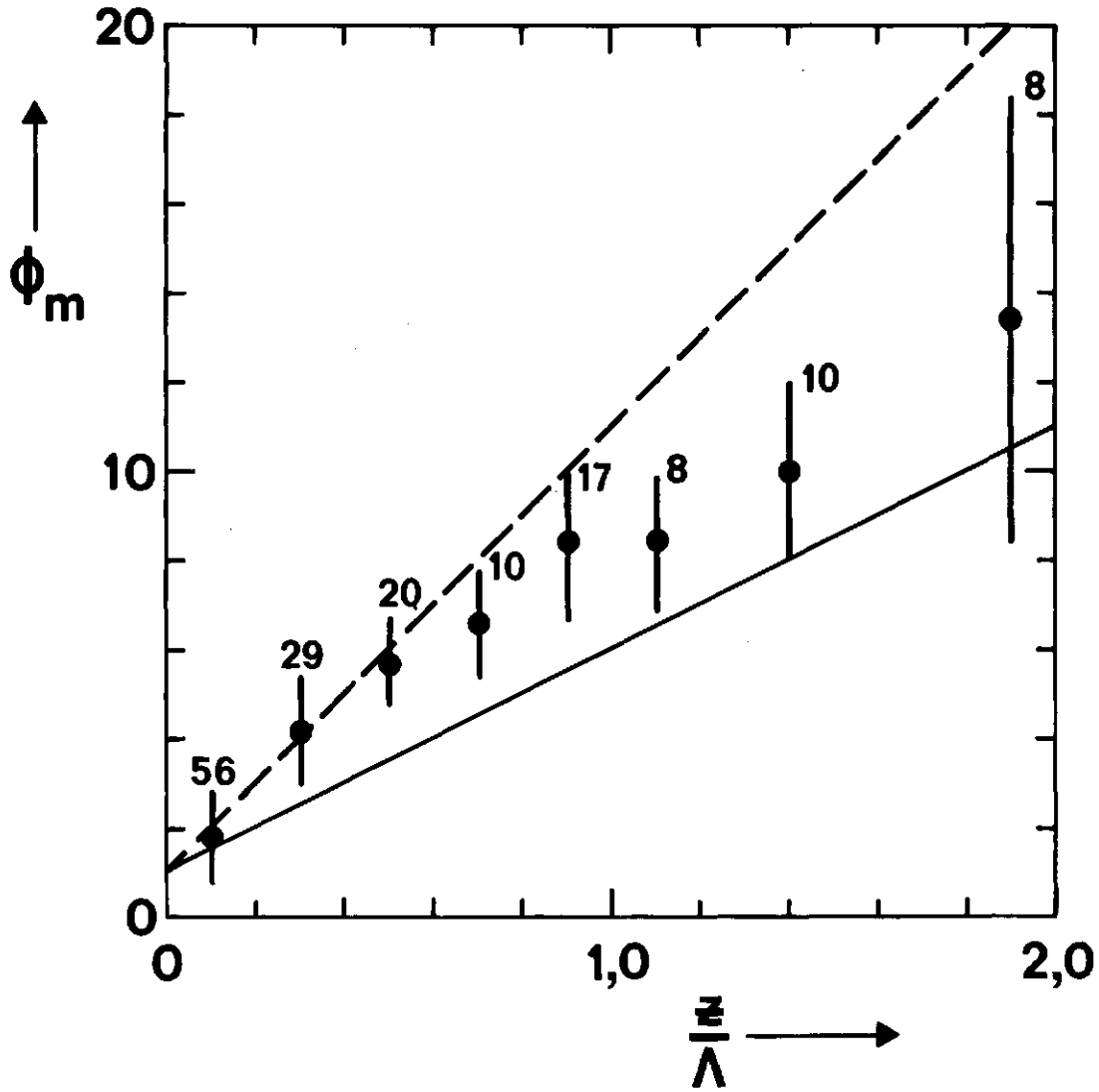

Fig. 4.1 *Dimensionless windshear (ϕ_m) as a function of the dimensionless height (z/Λ). Dots represent the observed ϕ_m averaged over a z/Λ interval. The length of the bar equals the standard deviation and the number represent the number of data points within each z/Λ interval. Also shown is the linear function*

$$\phi_m = 1 + \beta_m \frac{z}{\Lambda}$$

with $\beta = 5$ (solid line) and $\beta = 10$ (dashed line).

Based upon the same data set, Lacser and Arya (1986) found

$$\beta_m = \beta_h \approx 5, \qquad (4.4)$$

in correspondence with the β of Businger et al. (1971). These values proposed by Lacser and Arya are primarily based upon observations for larger values of z/Λ ($z/\Lambda > 2$). If we assume that heat and momentum are transferred the same, the two proportionality constants β_h, β_m must be equal. For our computations we will adopt the average of the observed values within the surface layer,

$$\beta_m = \beta_h = 10. \qquad (4.5)$$

4.3 Initial conditions

1) 30 / 31 May, 1978

During the night of 30 / 31 May 1978 (NT 1-hereafter) a high pressure zone was located over the North-Sea. As a result the wind over the Netherlands was from

Parameter	Numerical value Nt 1	Nt 2	units
Geostrophic wind velocity	10	6	m/s
Highest calculation level (Z)	2200	1000	m
Number of levels	20	40	
Roughness length (z_0)	0.15	0.15	m
Short wave radiation albedo	0.30	0.35	
Soil density (ρ_d)	$1.6*10^3$	$1.65*10^3$	kg m^{-3}
Soil specific heat	$0.89*10^3$	$1.00*10^3$	Jkg^{-1}
Deep soil temperature (T_d)	287	286	K
Soil thermal diffusivity (κ)	$0.18*10^{-6}$	$0.2*10^{-6}$	m^2/s
Canopy resistance (R_c)	100	140	s/m
Geostropic wind direction	80-100	110-140	degrees

Table 4.2 *Numerical values of the constants used for the two simulations*

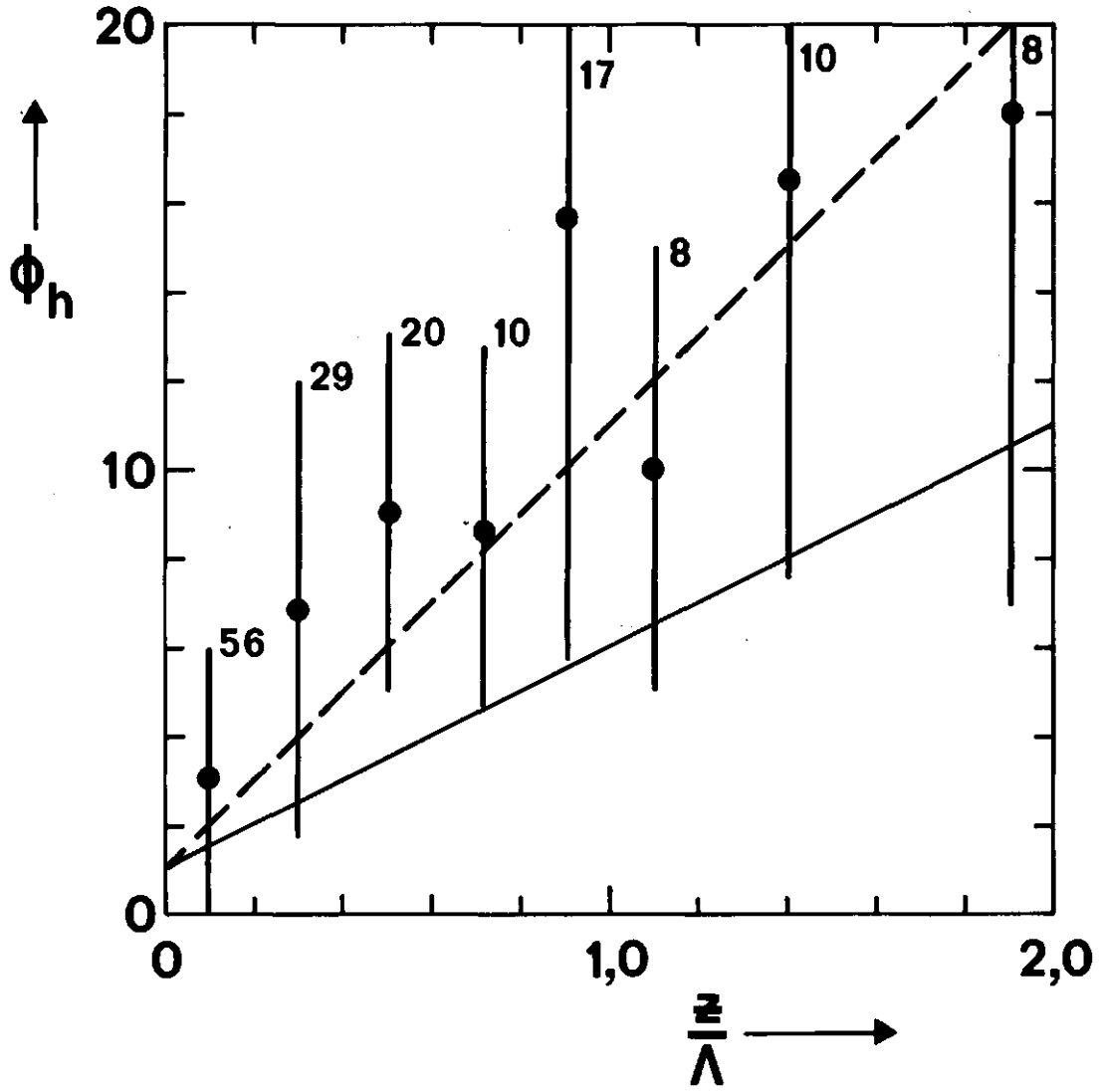

Fig. 4.2 *As fig. 4.1 but now for the dimensionless temperature gradient (ϕ_h).*

the east with a magnitude of ~ 12 m/s. At Cabauw some Cu-type clouds were observed during the afternoon which disappeared at the end of the day. From a comparison between the radio sounding at 0750 GMT 30 May and at 0748 GMT 31 May we found temperature differences of about 1K therefore we conclude that advection can be neglected during this night.

We initialize our model at 1000 GMT, with the profiles for temperature and humidity shown in Fig. 4.3. These profiles are composed from measurements along the mast, a radio sounding launched at the observational site and a radio sounding launched at the meteorological station of De Bilt (60 km from Cabauw).

No observations of the soil properties were reported. Therefore we have to estimate a value of the heat capacity ρC_d, and thermal conductivity (λ_d). Because no rain was reported during the previous 10 days, we adopted the values for a dry clay soil as given by Oke (1978; Table 4.2).

The geostrophic wind was calculated using pressure observations of 19 stations in the Netherlands (Nieuwstadt, 1984). This geostrophic wind is a mesoscale wind. Observations of the wind along the mast indicated that the wind above the NBL is less than the calculated geostrophic wind. We therefore used a value of 10 m/s for the wind velocity as an upper boundary condition in our computations. In Table 4.2 we summarize the numerical values for the various constants.

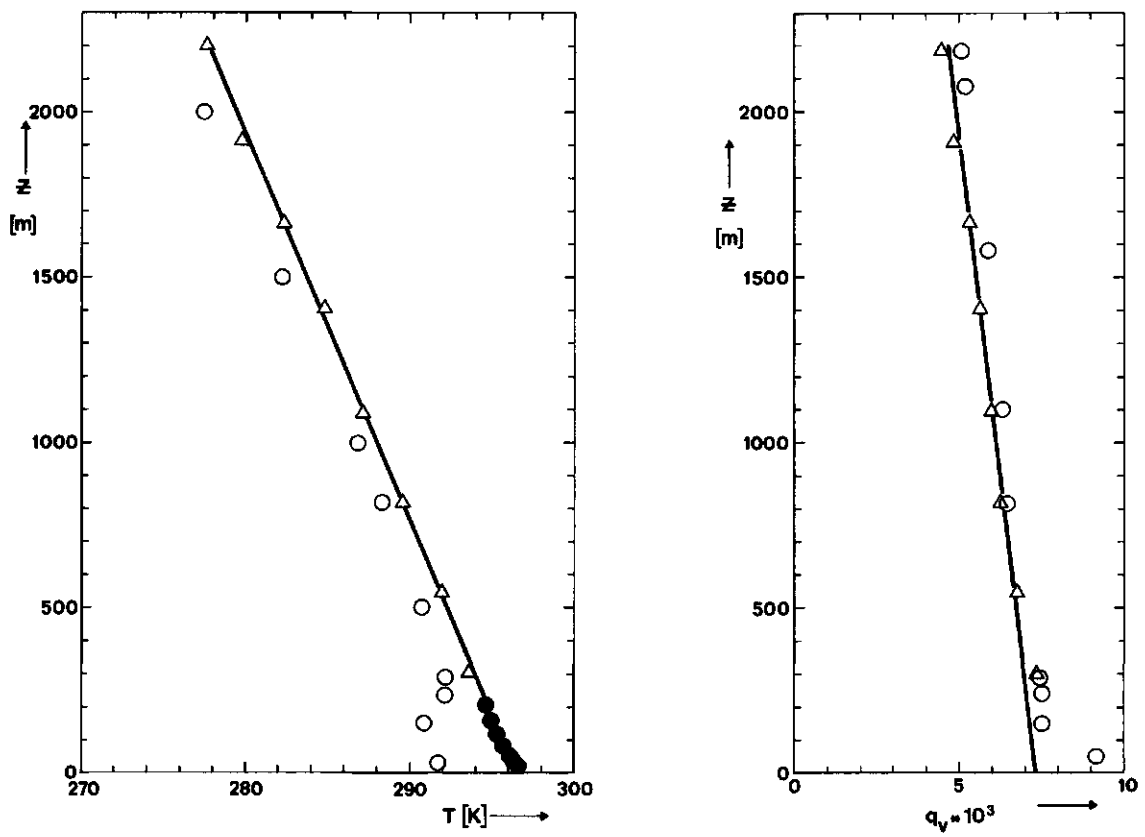

Fig. 4.3 *Initial profile for temperature (left) and humidity (right) for the simulation of NT 1.*

Triangles	:	*observations by a locally launched radiosonde*
open circles	:	*observations by a radiosonde launched at De Bilt*
closed circles	:	*observations along the mast*
solid line	:	*profile used to initialize the model.*

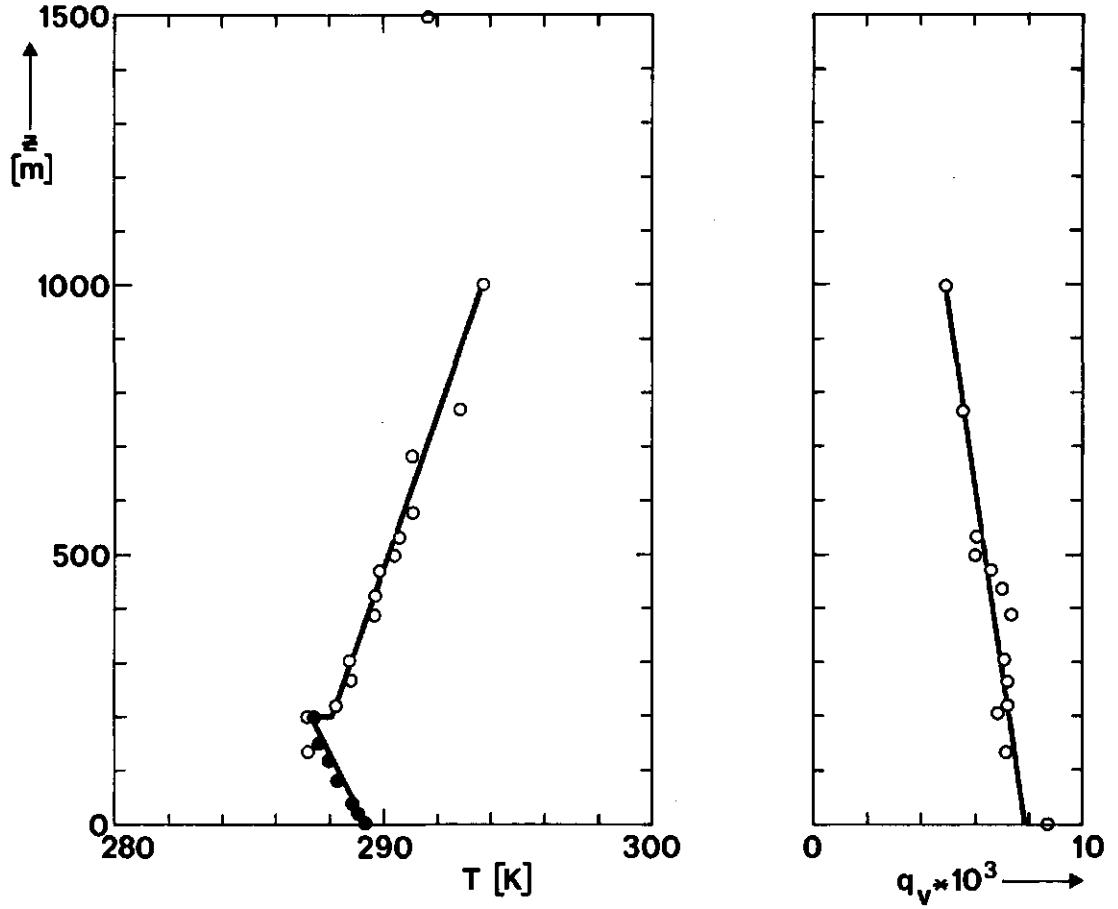

Fig. 4.4 *As Fig. 4.3, but now for NT 2.*

2) 12 / 13 October 1978

During the night of 12 / 13 October 1978 (NT 2 - hereafter) the circulation over the Netherlands was again forced by a high pressure zone. This time the center was located near Poland, such that the geostrophic wind was directed from the south-east, with a magnitude of 6 m/s. During NT 2, a front stretched out from Scandinavia over the North-Sea and Great-Britain towards the Azores, which caused some cirrus clouds over the Netherlands. From a comparison between two radio soundings, at 1200 GMT 12 October and at 0600 GMT 13 October we conclude that advection of cold air was important. However from observations along the mast, we see that this advection starts around midnight. As a result we may neglect the influence of advection upon the NBL for the beginning of the night.

We initialized the model at 1100 GMT, with the profiles of temperature and humidity given in Fig. 4.4. To estimate the thermal properties of the soil we used the values for ρC_d, and λ_d as given by Oke (1978) for a dry soil, because no rain was reported for 10 days. We obtained good results with the values for soil properties as given in Table 4.2.

5. Discussion of the results

5.1 The surface energy balance

During the transition period, when the boundary layer adjusts itself from the

unstable daytime to stable nighttime conditions the surface fluxes change rapidly with time (Fig. 5.1). Two hours after the net radiation becomes positive, the rate of change decreases and the surface fluxes become independent of time. This stationary value for the surface fluxes is reproduced well by the model (Fig. 5.1). During the transition period however, the calculated soil heat flux (G) shows a large dip which is not present in the observations. In our model we assume the turbulent heat flux to be proportional to the gradient of the mean temperature (cf. Eq. 3.2). This assumption generates a non-realistic negative temperature gradient in the bulk of the boundary layer during the day to sustain an upward turbulent heat flux.

In the transition period this temperature gradient disappears only gradually, such that the calculated net radiation and turbulent flux will be slightly out of phase. When the net radiation changes sign (around 1900 GMT) the turbulence will still transfer ~ 25 Wm^{-2} into the atmosphere while at 1930 when the turbulent fluxes changes sign, the net radiation will already transfer ~ 50 Wm^{-2} away from the surface. Both energy losses are compensated by the soil heat flux, which becomes extremely large during this transition period.

During NT 2 the geostrophic wind velocity is smaller than during NT 1. We see that for NT 2 the turbulent heat flux and the soil heat flux transfer an equal amount of energy towards the surface to compensate the energy losses of the surface by radiation, whereas during NT 1 this energy loss is almost entirely compensated by the turbulent heat flux alone.

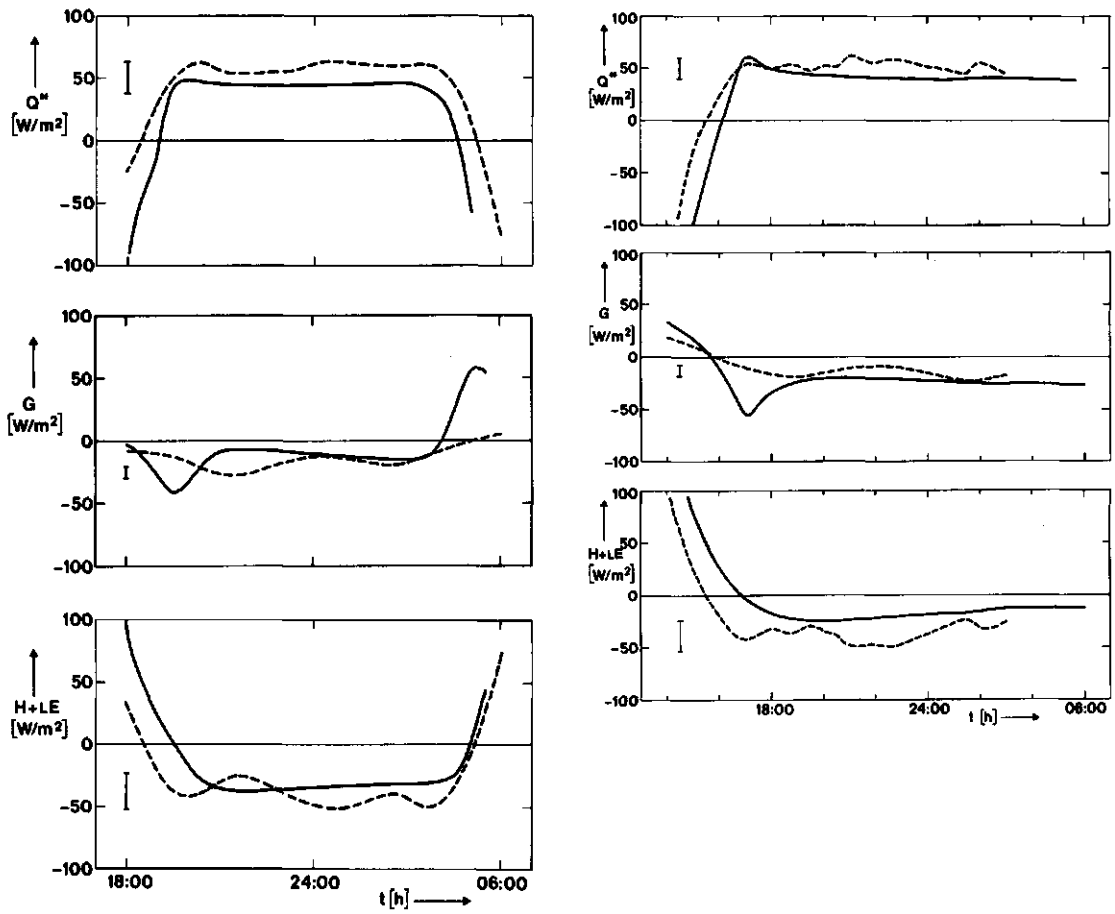

Fig. 5.1 *The evolution of the surface energy components as a function of time in GMT for NT 1 (a, left) and NT 2 (b, right). Upper Fig: net radiation. Middle Fig: soil heat flux. Lower Fig: sum of latent and sensible heat flux. Dashed line represent the observation, solid line the simulations, a vertical bar denotes the observational error.*

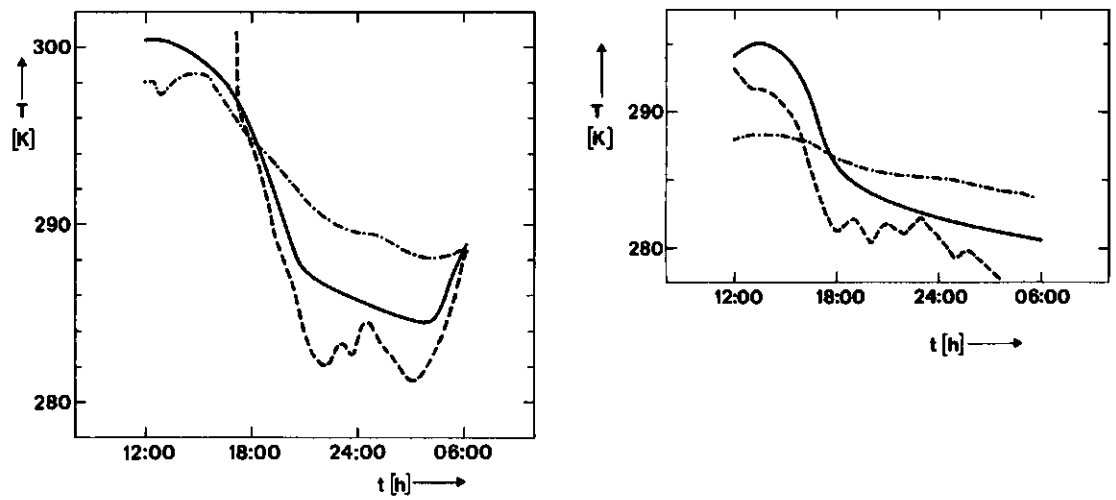

Fig. 5.2 *The time evolution of the surface temperature for NT 1 (a, left) and NT 2 (b, right). The solid line represent the simulated temperature, the dashed line the observations at 3 cm above the surface and the dashed dot line the observations at 1 cm below the surface.*

5.2 The surface temperature

As discussed in section 3.4, the surface temperature is calculated by means of the force restore method (Eq. 3.6). This method gives the temperature at the level where the surface energy balance applies and this level is usually within the vegetation layer. The exact location of this level cannot be located since we do not consider energy transfer through a vegetation layer in detail. From Fig. (5.2) we see that the calculated surface temperature falls roughly between the observed temperature at 3 cm above and 1 cm below the surface.

In contrast to the model calculations, the observed surface temperature decreases not at a constant rate. We observe several periods in which the surface temperature suddenly rises by 1 or 2 K and then decreases again. We attribute this behavior of the surface temperature to the complexity of the upstream terrain.

On length scales of the order of 1 km the upstream terrain is not homogeneous. The direct surrounding of the mast is covered by grass, whereas on remotely located areas in the east and south-east sector also some bushes can be found (Monna and Van der Vliet, 1987). These differences in terrain generate a difference in the surface temperature. The grass surface will be colder than the surface beneath the bushes. If due to advection, some warm air originated from the areas covered by bushes passes

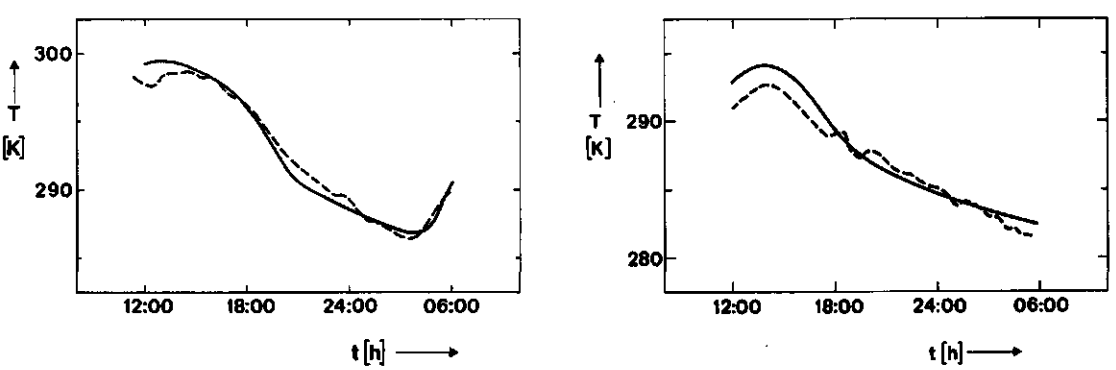

Fig. 5.3 *The time evolution of the air temperature 2 m above the surface. The solid line represent the simulations, the dashed line the observations.*

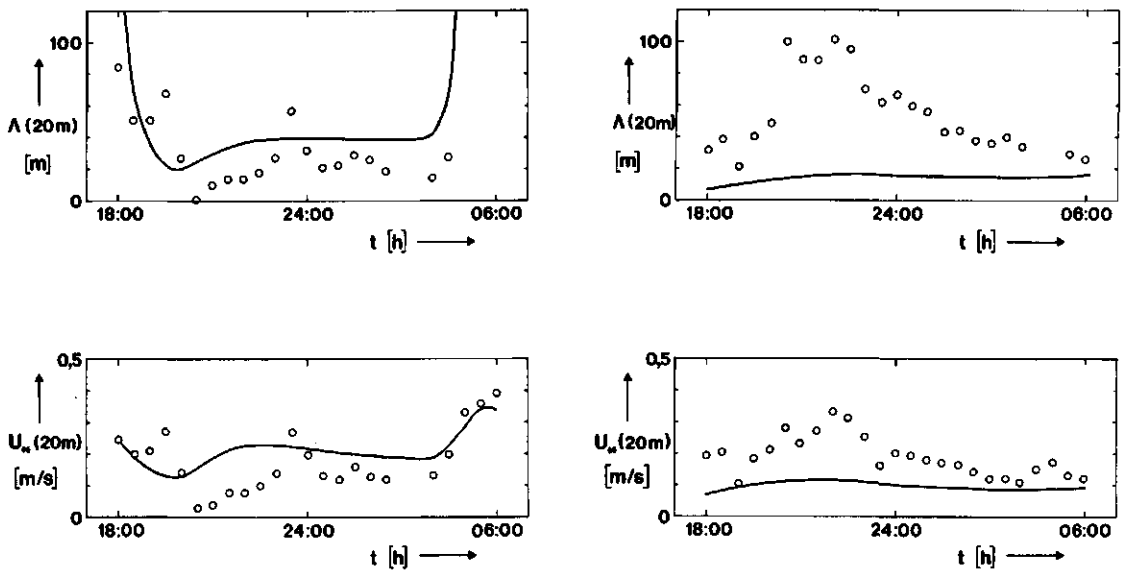

Fig. 5.4 *The time evolution of the local Monin-Obukhov length (upper Fig.) and the friction velocity (lower Fig.) at 20 m above the surface for NT 1 (a, left) and NT 2 (b, right). Open circles represent the observations and the solid line the simulations.*

the observational site, a sudden increase of the temperature can be observed. Because the amplitude of the temperature fluctuations is much less at 2 m above the surface than at the surface, the correspondence between the observed and calculated 2 m air temperature becomes much better (Fig. 5.3). For instance, the minimum temperature, which occurs shortly before sunrise is simulated within 1K.
The change is surface temperature will change the stability not only of the layers near the surface, but also of layers higher in the atmosphere as can be seen from a comparison of the simulated with the observed stress at 20 m (see Fig. 5.4 and text below).

5.3 The surface stress and boundary layer height

In Fig. 5.4 we have compared the calculated with the observed Monin-Obukhov length for NT 1 (a) and NT 2 (b). For NT 1 the agreement is quite reasonable while for NT 2 large difference occur, especially around 2200 GMT. At the beginning of NT 1, the observed stress decreases from approximately 0.25 m/s to 0. m/s at 2000 GMT. Then it increases to a peak value of 0.25 m/s around midnight and then levels off to a stationary value of 0.15 m/s. During the second night, the shear stress increases from a value of 0.2 m/s to a peak value of 0.3 m/s around 2300 GMT, then it decreases to a constant level of 0.1 m/s.

Using a roughness length of 0.15 m (Table 4.2) for both nights, the model calculates a friction velocity of 0.2 m/s for NT 1 and 0.1 m/s for NT 2 (Fig. 5.4). These values differ by about 50% from the observed after midnight. At the beginning of NT 1, the model overestimates the observed stress, while at the beginning of NT 2, it underestimates the stress. We attribute these differences to the fluctuations of the surface temperature shown in Fig. 5.2. Enger et al. (1986) have shown that these temperature fluctuations can have great influence on the fluxes in the boundary layer.

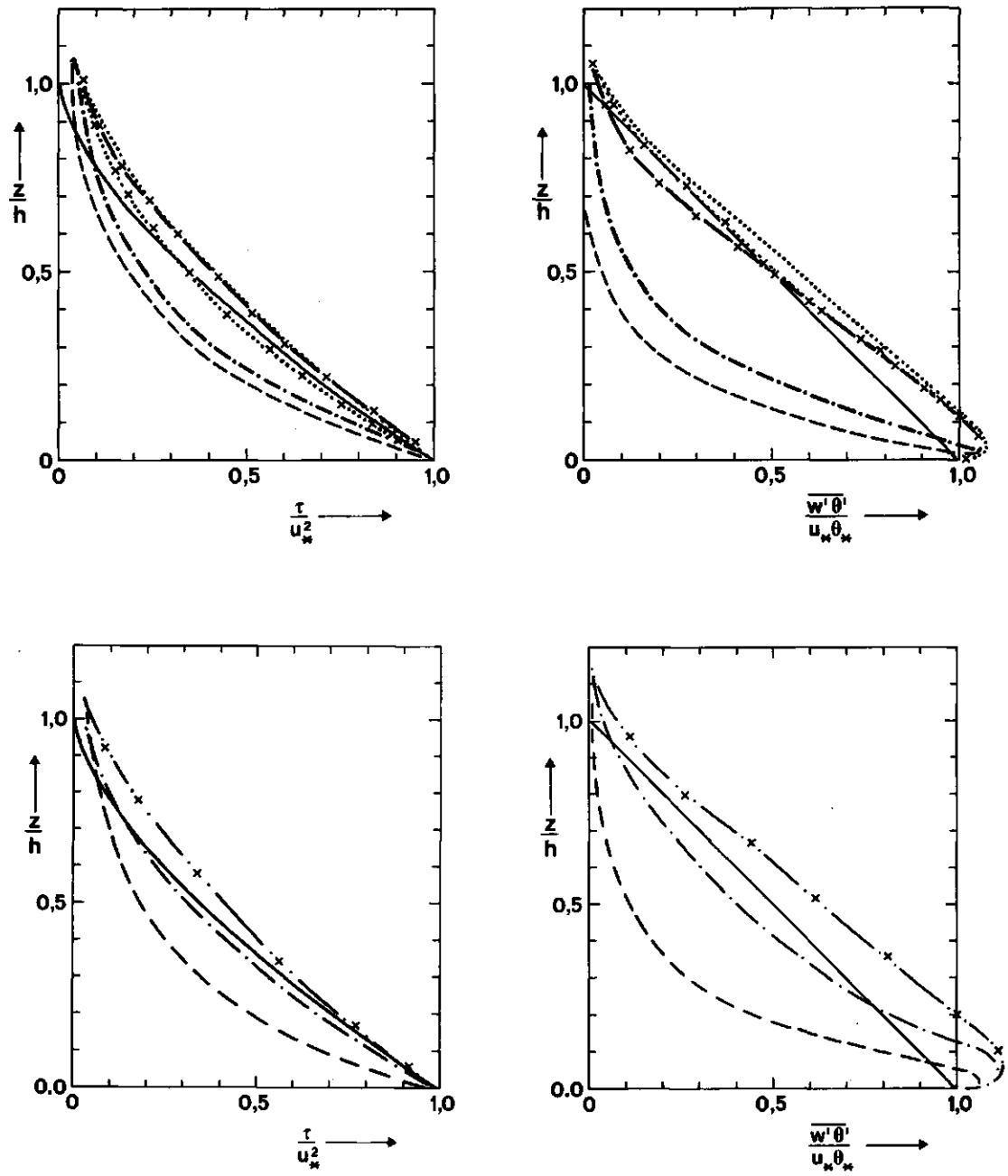

Fig. 5.6 a *Profiles of the normalized shear stress and normalized heat flux as a function of z/h.*

For NT 1 (Fig. 4.6 a, upper fig.): - - - at 1800 GMT,- . - . at 2000 GMT, -x-x at 2200 GMT, . . . at 2400 GMT, x.x. at 0200 GMT.

For NT 2 (Fig. 4.6 b, lower fig.): - - - at 1700 GMT, - . - . at 1900 GMT, - . + . - at 2100, 2300 and 0100 GMT.

The relations proposed by Nieuwstadt (1984) are given by a solid line.

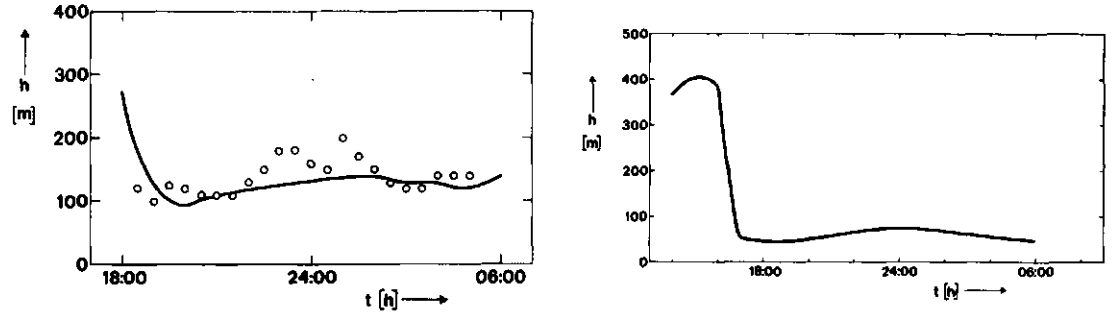

Fig. 5.5 *The time evolution of the nocturnal boundary layer height (h) for NT 1 (a, left) and NT 2 (b, right). Open circles represent the observations, solid line the simulations. The simulated h is defined as the level at which the turbulent kinetic energy is decreased to 5% of its surface value.*

From the above given discussion, we conclude that the simulated surface fluxes correspond to the observations. Therefore, the simulated NBL height, defined as the level where the turbulent kinetic energy has decreased to 5% of its surface value, diverges only little from the observed boundary layer height (Fig. 5.5). However, we notice that the NBL-height is not determined by the surface fluxes alone. Also the radiative cooling near the boundary layer top contributes significantly to the value of the nocturnal boundary layer height (section 5.6).

5.4 Turbulence profile

Nieuwstadt (1984) averaged 103 half hour observations and obtained relations between various dimensionless turbulence (co)variances and the dimensionless height z/h. We used his relations as a comparison for the present model calculations with (Fig. 5.6). Nieuwstadts relations are limited to stationary situations only, whereas we performed calculations for the evolution of the NBL. Our model results indicate that approximately two hours after the calculated net surface radiation changes sign, an almost stationary state is reached (cf. Fig. 5.1). During the hours when the NBL is evolving towards a stationary state, our model results diverge from Nieuwstadts relations. But after the transition his relations and our model results are in close agreement (see also Estournel and Guedalia, 1985).

The low level maximum in the turbulent heat profile arises from the cooling of layers above 10 m and a warming of layers below 10 m by turbulence (cf. section 5.6)

5.5 Profiles of temperature and wind speed

In Fig. 5.7 we present the calculated and observed potential temperature profiles at six different times in the night. This Fig. shows that the model is able to reproduce the rough shape of the temperature profile properly. The correspondence for NT 1 is somewhat better than for NT 2. The detailed structure in the profiles however, can not be reproduced accurately: for instance, below 10 m the curvature in the simulated profiles. We attribute this and other differences in the temperature profile to the complexity of the upstream terrain. These terrain transitions discussed in section 5.2 influence the NBL structure such that the flow in the NBL cannot be regarded as horizontally homogeneous, especially at low heights (Bosveld and Beljaars, 1988; Beljaars et al., 1983).

The roughness length of the grass near the mast is of the order of 1 cm, which is much smaller than the 15 cm used for the simulations which is considered to be representative for the exchange processes above the surface layer. Below 10 m, where

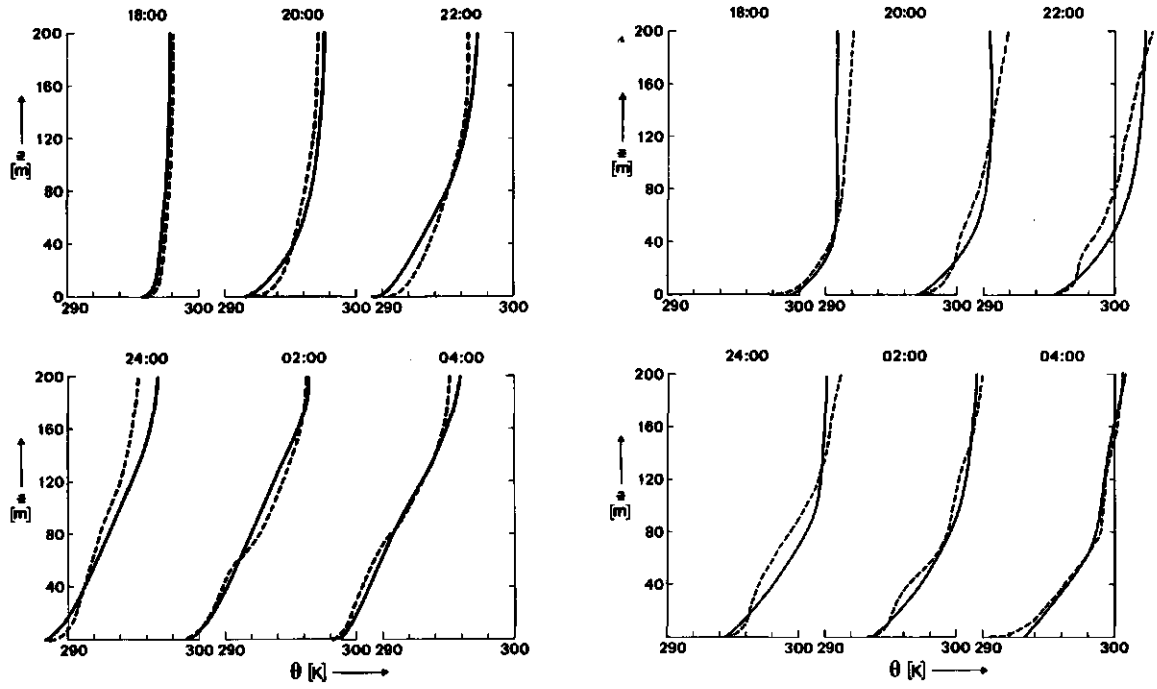

Fig. 5.7 *Profiles of the mean potential temperature as a function of height. For several times in the night for NT 1(a, left) and NT 2 (b, right). Dashed lines represent the observations, solid line the simulations.*

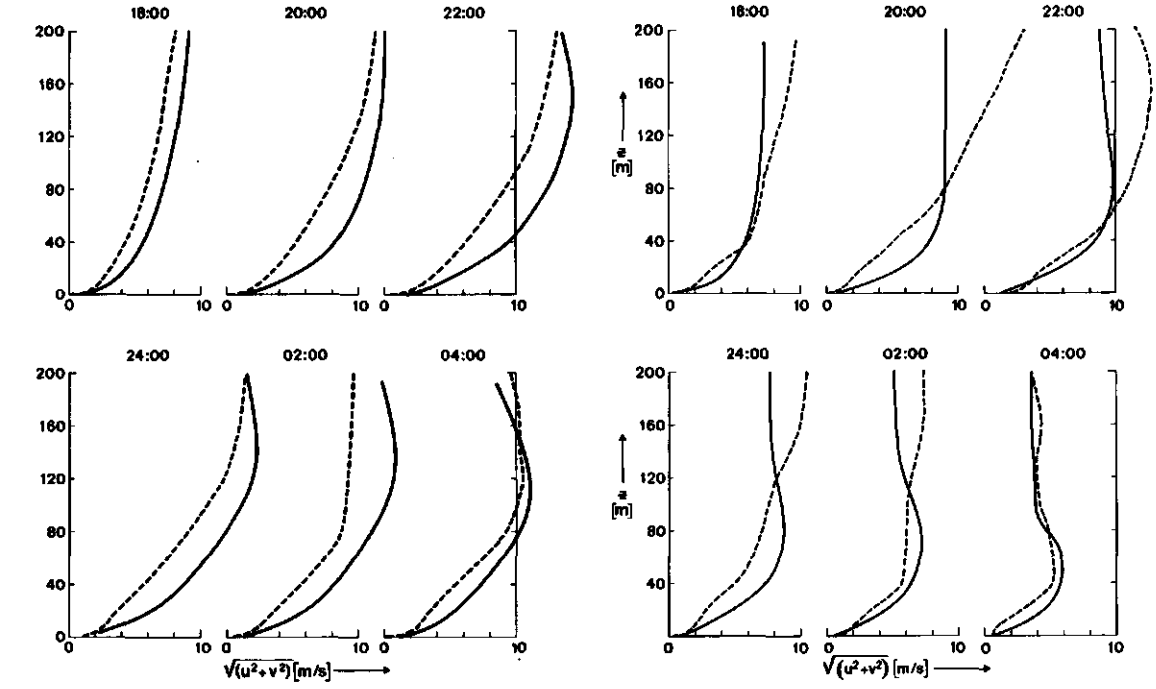

Fig. 5.8 *As fig. 5.7 but for the mean wind velocity.*

the heat exchange is determined by the grass, the model will therefore overestimate the actual exchange coefficient. To transfer the same amount of energy as observed (Fig. 5.1) the model generates a smaller temperature gradient than observed, since our model the turbulent heat flux is proportional to the gradient of the mean temperature.

Besides the roughness transitions, the wind profiles (Fig. 5.8) are also influenced by inertial oscillations. When the turbulent exchange becomes weak, the wind tends to oscillate around the geostrophic wind with a period of $2\pi/f \approx 15$ hours (mid latitudes). The amplitude of this inertial oscillation is sensitive to the wind profile at the beginning of the night. If at the beginning of the night a slight difference in the observed and simulated wind profile is present, the inertial oscillation tends to enlarge this difference during the first hours of the night.

5.6 The cooling rate

Finally we present in Figs. (5.9) and (5.10) the calculated cooling rate at different stages in the development of the NBL. The solid lines represent the cooling rate due to turbulence while the dashed lines represent the cooling rate due to radiation. The NBL tends to evolves towards a stationary state in which the total $\partial q/\partial t$ becomes independent of height. Due to the temperature discontinuity at the surface we obtain a large cooling rate due to radiation (up to ~ 100 K/d) near the surface. This radiative cooling rate is much larger than the total cooling rate in the bulk of the boundary layer, therefore the turbulence has to warm the layer close to the surface. As a result the dimensionless turbulent heat flux shows a low level maximum just above the surface.

These results are in correspondence with the results reported by Garratt and Brost (1981) but disagree with the results reported by Estournel and Guedalia (1985). Garratt and Brost used a surface emissivity of 0.8. In that case they get a strong radiative cooling of a layer close to the surface and therefore they also obtain a maximum in the dimensionless turbulent heat flux. Estournel and Guedalia do not include a temperature discontinuity at the surface as in the present study and they use a surface emissivity of 1.0. As a result they do not obtain strong radiative cooling near the surface and thus no low level maximum in the dimensionless turbulent heat flux.

Above the surface layer, the radiative cooling rate becomes independent of height and is approximately 20% of the cooling rate due to turbulent mixing. This means that within the surface layer the dimensionless turbulent heat flux increases with height while above the surface layer the dimensionless turbulent heat flux decreases with height.

The most important effect of radiation upon the NBL is probably that it decreases the temperature gradient over the NBL. The NBL becomes less stable and can therefore become thicker. In order to estimate the effect of radiation upon the boundary layer height we note that Garratt and Brost (1981) showed that the bulk Richardson number (Ri_b) in a stationary boundary layer is the same with and without radiation. We have

$$h = \frac{Ri_b (\Delta u)^2}{\frac{g}{T}\Delta\theta}. \qquad (5.1)$$

Using a Taylor expansion for $\Delta\theta$

$$\Delta\theta \approx \frac{\partial\theta}{\partial t}\Delta t$$

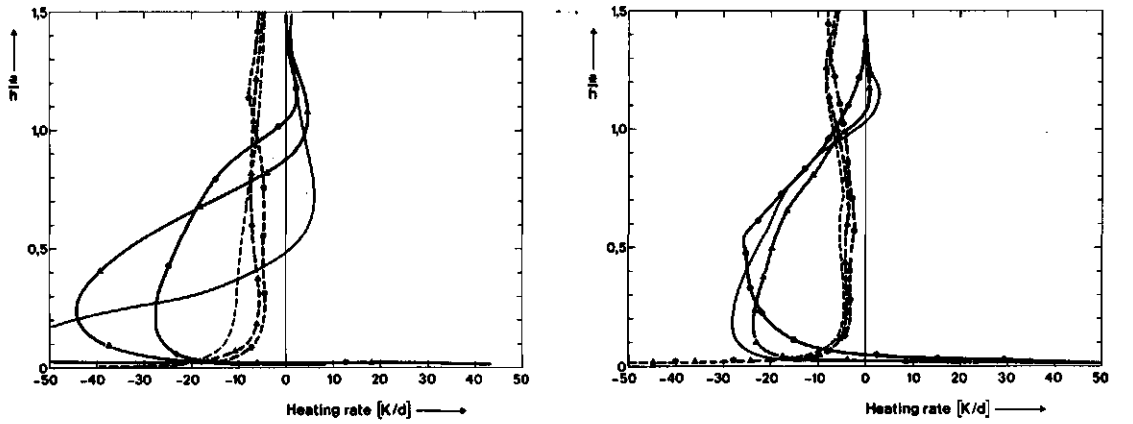

Fig. 5.9 *Profiles of the heating rate at several times in the night for NT 1.*

Heating rate due to turbulent mixing full lines and due to radiative transfer as dashes lines.

Fig. 5.9 a left _____ at 2000 GMT, -Δ-Δ- at 2200 GMT, - 0 - 0 - at 2400 GMT

Fig. 5.9 b right _____ at 2400 GMT , -Δ-Δ- at 0200 GMT, - 0 - 0 - at 0400 GMT

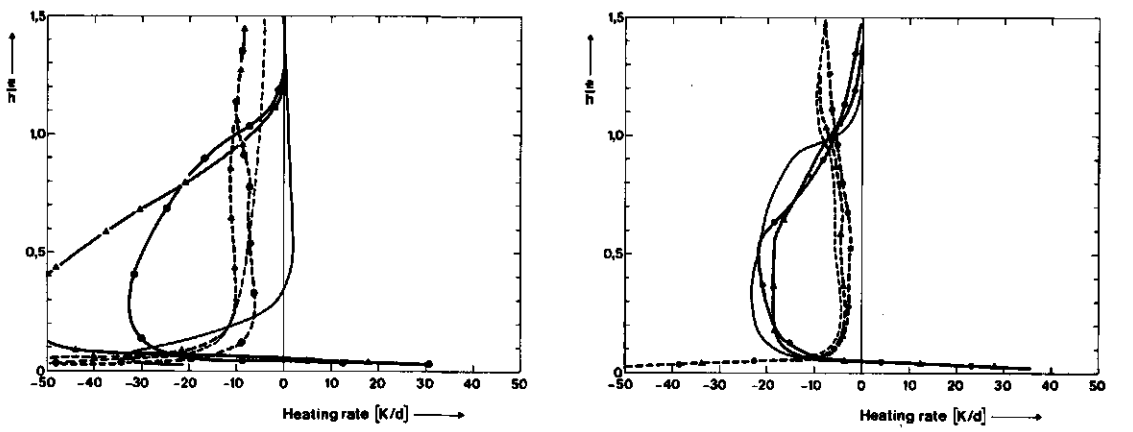

Fig. 5.10 *As Fig. 5.9 but now for NT 2.*

Fig 5.10 a left _____ at 1700 GMT , -Δ-Δ- at 1900 GMT, - 0 - 0 - at 2100 GMT

Fig. 5.10 b right _____ at 2300 GMT , -Δ-Δ- at 0100 GMT, - 0 - 0 - at 0300 GMT

we find a simple relation between the NBL height and the cooling rate at the NBL top and bottom.

$$h \approx \frac{Ri_b (\Delta u)^2}{\frac{g}{T}\left\{\left(\frac{\partial\theta}{\partial t}\right)_h - \left(\frac{\partial\theta}{\partial t}\right)_s\right\}\Delta t} \qquad (5.2)$$

Let hrad and hnorad represent the boundary layer height with and without radiative cooling within the atmosphere respectively, then we can express the ratio hrad/hnorad as

$$\frac{h_{rad}}{h_{norad}} \approx \frac{-\left(\frac{\partial\theta}{\partial t}\right)_s}{\left(\frac{\partial\theta}{\partial t}\right)_h - \left(\frac{\partial\theta}{\partial t}\right)_s}, \qquad (5.3)$$

where we assumed Δu to be constant, and $(\partial\theta/\partial t)_h$ equal zero if no radiative cooling of the atmosphere is taken into account. From Figs. (5.9) and (5.10) we find typically

$$\left(\frac{\partial\theta}{\partial t}\right)_s \approx -25\ \mathrm{Kd}^{-1} \qquad (5.4^a)$$

and

$$\left(\frac{\partial\theta}{\partial t}\right)_h \approx -5\ \mathrm{Kd}^{-1} \qquad (5.4^b)$$

such that

$$\frac{h_{rad}}{h_{norad}} \approx 1.25\ . \qquad (5.5)$$

The result (5.5) should be viewed as a very coarse estimate. However from additional model calculations presented by Tjemkes and Duynkerke (1988c) we find that the radiative cooling near the top of the NBL increases the height by about 25%.

6. Summary and conclusions

In this paper we presented a narrow band radiation model coupled with a turbulence model in which a prognostic equation for the turbulent kinetic energy is solved together with a diagnostic equation for a mixing length scale. The performance of this combined model is tested against detailed observations of the mean thermodynamic and turbulence structure within the nocturnal boundary layer (up to 200 m) for two nights, collected at the Cabauw meteorological mast in 1978. During the

first night the structure and evolution of the NBL was forced by a wind with a magnitude above the NBL of
10 m/s, whereas during the second night this magnitude was only 6 m/s.

For most variables a satisfactory correspondence between the simulations and the observations exists. However, the detailed structure of the mean wind, mean temperature profiles and friction velocity measured at 20 m cannot be reproduced properly, possibly due to terrain inhomogeneities.

Our model results indicate that within the bulk of the boundary layer ($0.1 < z/h < 0.8$), radiative cooling is less than 20% of the turbulent cooling, whereas for layers near and above the boundary layer top radiative cooling dominates. These results are in correspondence with previous results reported by Garratt and Brost (1981). Our calculations also show that near the surface radiative cooling is at least as important as turbulent cooling. However, this result should be interpreted with care because near the surface the radiative cooling rate is afflicted with a large error.

Probably the most important effect of radiation upon the structure of the NBL is to reduce the temperature jump across the boundary layer, such that the boundary layer as a whole becomes less stable. As a consequence of this effect the boundary layer height increases by about 25%.

ACKNOWLEDGEMENTS

We thank Anton Beljaars, Han van Dop, Bert Holtslag, Frans Nieuwstadt and Hans Reiff for reading the manuscript and stimulating discussions, Sandra Klutz for preparing the paper and Cees van Stralen for drawing the figures. One of us (S.A.T.) acknowledges financial support by the organization of scientific research in the Netherlands (N.W.O.) under contract # 752-365-008.

Chapter 5
A parametrization scheme for the minimum surface temperature[4]

1. Abstract

Based on model calculations with a combined radiation-turbulence model a simple relation to estimate the minimum surface temperature for a moist clay soil from the 2m air temperature averaged over 24 hours is proposed. The parametrization scheme is tested against observations taken at the meteorological observational site near the village of Cabauw in the Netherlands. From which we conclude that the parametrization scheme is able to reproduce the minimum surface temperature within 2.5 K.

2. Introduction

In a recent paper Estournel and Guedalia (1985; EG85 hereafter) studied the influence of the geostrophic wind upon the atmospheric cooling within the nocturnal boundary layer (NBL). For their study they used a coupled radiation/turbulence model and they showed that the NBL-height, as well as the potential temperature profile in the inversion layer, which extends to higher altitude than the NBL, are dependent upon the geostrophic wind velocity. At high geostrophic wind velocities, the NBL is almost as thick as the inversion layer. Then the potential temperature in the inversion layer dependents approximately linear with height. At low geostrophic wind velocities the NBL is shallow and occupies only a small fraction of the inversion layer. Then the potential temperature profile in the inversion layer is rather logarithmic shaped.

Although the shape of the potential temperature profile depends upon the geostrophic wind velocity, careful analysis of the results of EG85 revealed that the surface temperature depends only weakly upon this wind velocity. According to their calculations after ten hours integration the inversion layer losses 35% less energy while the surface cools 11 instead of 9 K if they lower the geostrophic wind velocity from 10 m/s to 3 m/s.

In this note we study the influence of the geostrophic wind upon the minimum surface temperature into more detail. In the next paragraph, (paragraph 3) we present the minimum surface temperature as a function of the geostrophic wind according to calculations performed with a boundary layer model. From the presented results we propose a simple parametrization scheme for the minimum surface temperature for a saturated clay soil. In paragraph 4 a test of this scheme against observations performed at the meteorological observational site near the village of Cabauw in the Netherlands is given. In paragraph 5 we summarize our findings.

---

[4] Submitted to J. Appl. Meteor. with J. Reiff as co-author

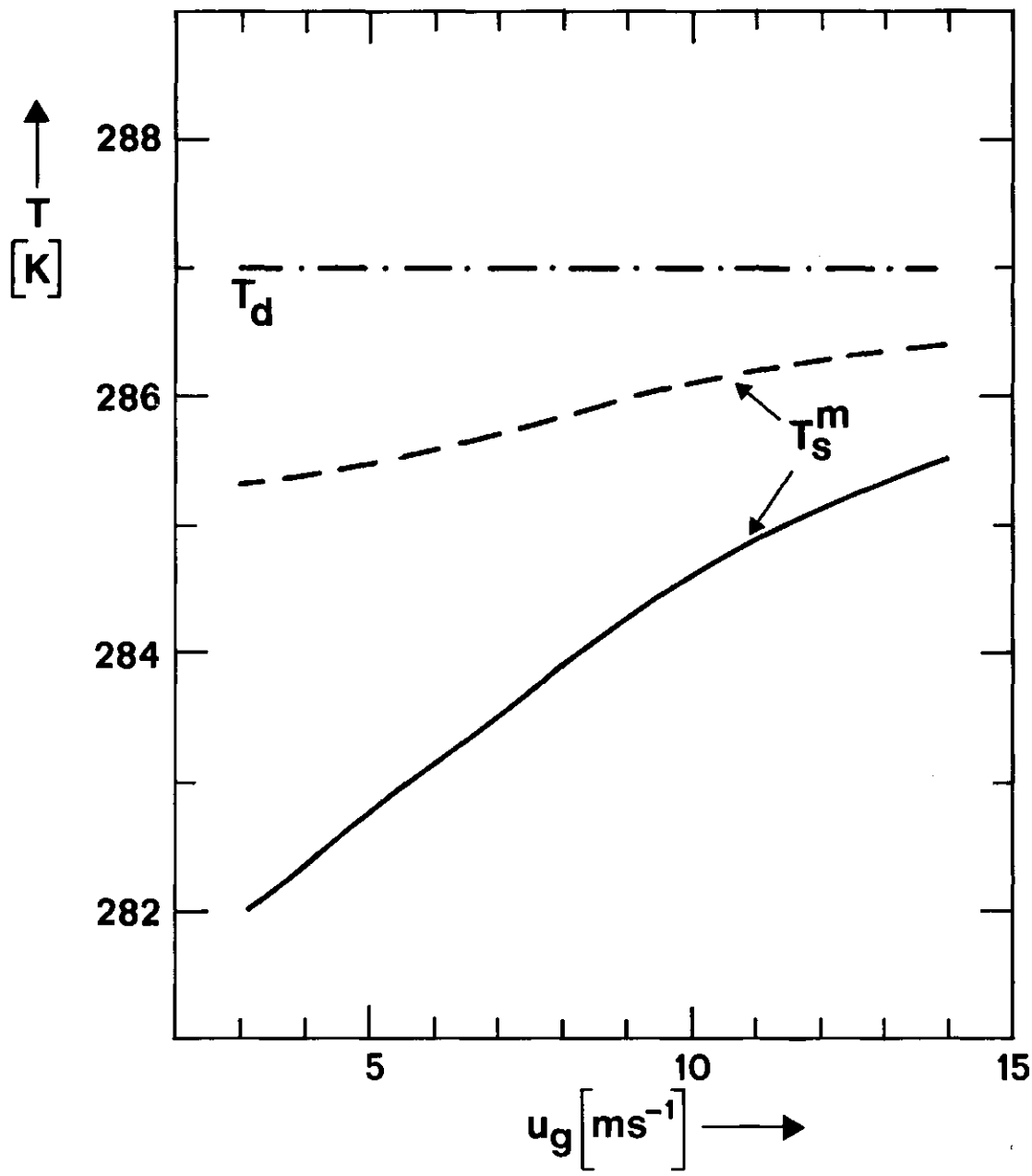

Fig. 3.1 *Minimum surface temperature (T_{m_s}) as a function of the geostrophic wind for a dry clay soil (solid lines) and for a saturated clay soil (dashed lines). Also shown by a dashed dotted line is the deep soil temperature (T_d).*

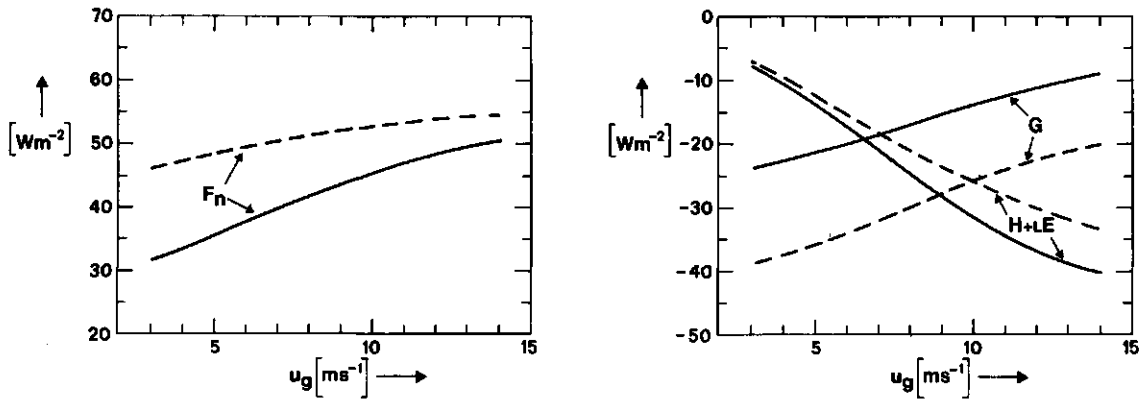

Fig. 3.2 *Three components of the surface energy balance. The net radiation (F_n) the sensible and latent heat flux ($H + LE$) and the soil heat flux (G) for the dry clay soil simulation (solid line) and for the saturated clay simulation (dashed line).*

3. Model calculations

To calculate the variation of the minimum surface temperature as a function of the geostrophic wind velocity, we used the model described by Tjemkes and Duynkerke (1988b; TD88 hereafter; Chapter 4). This model is a combined radiation-turbulence model, which simulates a horizontally homogeneous flow together with the transfer of longwave radiation through a cloudless sky. In the model, the turbulent fluxes are taken proportional to the gradient of mean thermodynamic variables, with a constant of proportionality evaluated according to the product of a mixing length scale (determined from a diagnostic equation) and the square root of the turbulent kinetic energy (determined from a prognostic equation). The radiation model is a so-called narrow band model which models the absorption and emission of longwave radiation by water vapor and carbon dioxide. Moreover, the force restore method (Deardorff, 1978) is adopted to simulate the transfer of heat through the soil.

The model used in the present study differs only slightly from the model used by EG85. They applied the same type of turbulence closure as we and their infrared radiation scheme is also a narrow band model. EG85 differs from the present study with respect to the description of the heat transfer through the soil. EG85 solved numerically the diffusion equation for a homogeneous soil, whereas here we use an analytical solution (the Force restore method, note that in this method an apparent thermal conductivity is used, which differs from the actual conductivity due to water vapor movements (Ten Berge, 1986)). Moreover we applied a simple relation proposed by Holtslag and de Bruin (1988) to approximate the heat transfer through the vegetation layer. The inclusion of a vegetation layer results in a large vertical temperature gradient over the vegetation layer. This generates a low level maximum in the dimensionless turbulent heat flux profile (TD88). EG85 simulated a NBL over bare soil. Thus they do not find such a temperature gradient near the surface as in the present study.

In Figs. 3.1 and 3.2 we present model calculations for different values of the geostrophic wind. In Fig 3.1 we show the minimum surface temperature variation with respect to the geostrophic velocity and in Fig. 3.2 the three components of the surface energy balance. Note that the soil heat flux is calculated from the surface energy balance, which states that the soil heat flux, the net radiation, the latent and the sensible heat flux should sum to zero. The integration of the soil heat flux over time can thus be interpret as the amount of energy loss by the soil. In the Figs 3.1 and 3.2 the solid line represents the model calculations for a dry clay soil (porosity (x_t) = 0.4, volumetric water content (x_v) = 0.0), whereas the dashed line represents the model calculations for

a saturated clay soil ($x_t = 0.4$, $x_v = 0.4$, parameters according to van Wijk and de Vries, 1963). The constant deep soil temperature was chosen 287 K.

According to Fig. 3.1, we see that the temperature difference between the minimum surface temperature and the deep soil temperature decreases with increasing geostrophic wind. For a dry clay soil this path is steeper than for a saturated clay soil.

The minimum surface temperature is approximately equals to the stationary solution of the force restore method. The minimum surface temperature can be evaluated from

$$T_s^m \approx T_d + \sqrt{\frac{2}{\lambda \rho C \omega}}\, G(t) \qquad (3.1)$$

In (3.1) T_{m_s} denotes the surface minimum temperature, T_d the deep soil temperature at ≈ 0.50 m below the surface, G the soil heat flux, ω the angular frequency of one day, λ the thermal conductivity and ρC the heat capacity. From this simple equation we conclude the following

At low wind velocities the turbulence within the NBL is strongly suppressed, such that the energy losses of the surface by longwave radiation cannot be compensated by the turbulent heat flux from the boundary layer (cf. Fig. 3.2). This means that at low wind velocities the soil heat flux is large causing a large energy loss of the surface and a large difference between the surface minimum temperature and the deep soil temperature is generated (cf. Fig. 3.1). At high wind velocities, the energy of the surface by radiation is almost entirely compensated by the turbulent heat flux (cf. Fig. 3.2). Thus at high wind velocities the soil heat flux is only small causing the energy loss of the surface to be small too. This results in a small temperature difference between the surface minimum temperature and the deep soil temperature (cf. Fig. 3.1). Note that the presented variation of the surface energy balance components with respect to the wind velocity is in correspondence with observations as reported by Holtslag and de Bruin (1988)

From Fig 3.1 and 3.2 we see that if the geostrophic wind velocity is decreased from 10 to 3 m/s the soil losses approximately 40 % more energy, whereas the surface minimum temperature decreases from 286 to 286.9 K. The presented decrease in temperature is slightly less than according to EG85. For their simulation study EG85 adopted a moist clay soil whereas in the above mentioned results are for a saturated clay soil. A saturated clay soil is less sensitive to the energy loss by the surface than a moist clay soil (cf. Fig. 3.1).

If we look at a particular value for the geostrophic wind, we notice that the saturated soil is warmer than the dry soil although the saturated soil losses more energy than the dry soil. In the saturated clay soil, the flow of energy from deep layers towards the surface is much faster than in a dry soil. Which states that for the saturated soil the energy loss at the surface extends over a thicker layer than for the dry clay soil. The saturated soil cools slower, causing a smaller temperature difference between the surface and the deep layers than the dry soil.

Apparently, the dependence of the minimum temperature with geostrophic wind is dominated by the soil properties. Although the magnitude of the soil heat flux is in absolute value larger for a saturated soil than for a dry soil, the minimum surface temperature of a saturated clay soil is almost independent of the geostrophic wind.

On bases of these model results we propose

$$T_s^m = T_d - C \qquad (3.2)$$

with $C \approx 1.5$ K (see Fig. 3.1) as a parametrization scheme for the surface minimum temperature of a saturated clay soil. In the next paragraph we compared the performance of this parametrization scheme against observations.

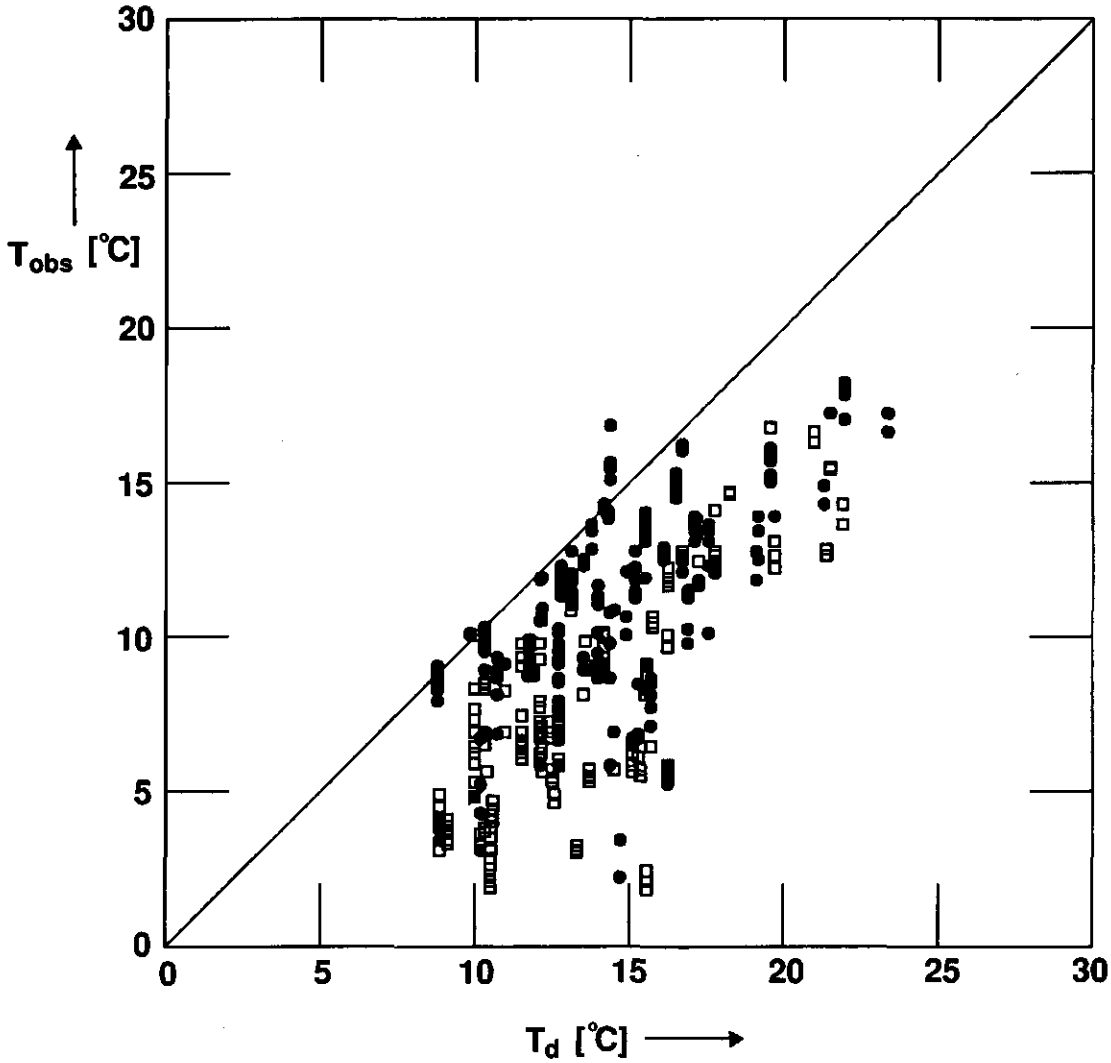

Fig. 4.1 *Scatter plot of the observed minimum surface temperature (T_{obs}) and the deep soil temperature (T_d). Open squares represent the observations at clear skies ($N < 0.25$) closed circles represent observations at cloudy skies ($N > 0.25$)*

4. Comparison with observations

We used routine weather observations taken at the meteorological observational site near the village of Cabauw in the Netherlands, which has a moist river clay soil (40 - 60 % lutum, 6-12 % humus, 40 - 55 % soil moisture; Wessels, 1983). Following Blackadar (1976), we estimate the deep soil temperature (T_d) from the mean air temperature at 2 m over the previous 24 hours. The surface temperature was measured at approximately 3 cm above the surface. The minimum temperature occurs around sunrise. We used observations of the surface temperature between a time period from 1.5 hour before sunrise and sunrise to represent the minimum surface temperature.

In Fig. 4.1 the results of our comparison study for the period from may 1986 to october 1986 are presented a scatter plot and in Table 4.1 the results of a linear regression analysis can be found. From this regression analysis, we conclude that the mean difference between the 2m air temperature averaged over 24 hours is equal to 5.9 K with a root mean square error of 2.4 K and a correlation coefficient of 0,74 over a wide range of temperatures. The constant is slightly larger than expected from the

model calculations, which can be explained from the rough representation of the vegetation layer.

As discussed in section 3 the surface temperature is calculated by means of the force restore method. This method gives the temperature at the level where the surface energy balance applies and this level is usually within the vegetation layer. The exact location of this level cannot be located since we do not consider energy transfer through a vegetation layer in detail. TD88 showed that the temperature observed at 3 cm above the surface is about 2 K less than the modeled surface temperature.

The data is selected for cloud amount. The open squares represent the observations for cloudless skies (N< 0.25), whereas the closed circles represent the cloudy skies (N>0.25). Although the proposed parametrization scheme is based on clear sky calculations, we see from Fig. 4.1 and Table 4.1 that the scheme may also be used for clouded skies, with a smaller value for the constant C. This is due to the fact that at clear skies the soil humidity is less than at cloudy skies causing the differences between the deep soil temperature and the minimum surface temperature to be large (Fig. 3.1). Based on all data point we find the constant of 4.5 K with a rms of 2.8 and a correlation coefficient of 0.7.

	clear sky (N<0.25)	cloudy sky (N>0.25)	all data
number of data points	190	238	428
mean temperature difference [K]	5.9	3.4	4.5
root mean square error [K]	2.4	2.6	2.8
correlation coefficient	0.745	0.666	0.699

Table 4.1 *Results of the linear regression analysis*

5. Summary

Based on model calculations with a combined radiation-turbulence model a simple relation to estimate the surface minimum temperature of a vegetated saturated clay soil from the 2m air temperature averaged over 24 hours is proposed. The parametrization scheme is tested against observations taken at the meteorological observational site near the village of Cabauw in the Netherlands. From which we conclude that the parametrization scheme is able to predict the minimum surface temperature within approximately 2.5 K for a vegetated saturated clay soil.

When this parametrization scheme is applied to other vegetated saturated surfaces, a different value for C must be determined. In practice this can be done from a correlation of 2m temperature averaged over 24 hours, to the minimum surface temperature.

ACKNOWLEDGEMENTS

We would like to thank Sandra Klutz for preparing the manuscript, Milco Latupeirissa for preparing the figures Bert Wartena and Bert Holtslag for reading a first draft of the manuscript and stimulating discussion. S.A.T. acknowledge financial support by the Netherlands organization for scientific research (NWO) under contract # 752-365-008.

Appendix A
A comparison of infrared radiation codes for the nocturnal boundary layer.[5]

1. Introduction

As a part of my Ph.D.- thesis on the transfer of infrared radiation through the cloudless nocturnal boundary layer (NBL) I developed a fast radiation code which employs the k-distribution method. The nocturnal boundary layer is a layer located adjacent to the earth surface, which evolves during the night. The structure and evolution of the NBL depends on a variety of processes such as infrared radiative transfer and turbulent mixing. Infrared radiative transfer couples directly to the thermal structure of the NBL, such that inclusion of atmospheric radiative cooling affects the turbulent heat flux. Especially near the surface, where the radiative cooling rate is extremely large (Funk, 1960; Garratt and Brost, 1981; Tjemkes and Duynkerke, 1988 b; Chapter 4) and near the NBL-top, where turbulent intensity is only weak (André and Mahrt, 1982; Garratt and Brost, 1981). Model calculations in which the interaction between turbulence and radiation was simulated, showed that in a stationary boundary layer (total cooling rate independent with height) leads to a low level maximum in the non-dimensional tur-bulent heat flux (Elliot, 1963; Garratt and Brost, 1981; Tjemkes and Duynkerke, 1988b; Chapter 4). Moreover infrared radiation tends to reduce the stability in the NBL. As a result turbulence can penetrate deeper into layers aloft the NBL.

The NBL is only a few hundred meters thick. Our interest in the transfer of infrared radiation is thus restricted to a rather thin layer of air. André and Mahrt (1982) and Garratt and Brost (1981) used an emissivity model to simulate the infrared radiative trans-fer through the NBL whereas Estournel and Guedalia (1985) and Tjemkes and Duynkerke (1988a) used a narrow band model. Here we will use an alternative approach namely the k-distribution method. Mainly for its propery that the inclusion of scattering by aerosols and cloud droplets is relatively straight forward (Stephens, 1984).

In this paper I present some preliminary results of a comparison study between an emissivity model, a narrow band model and a k-model. For this comparison study I modeled the absorption and emission by the rotational/vibrational lines of water vapor and carbon dioxide. The water vapor continuum absorption in the window region (from 8-12 μm) is omitted as well as temperature and pressure scaling to approximate the integration of the absorption coefficient over the inhomogeneous path.

2. Governing model equations

[5] Paper presented at the International Radiation Symposium, Lille (France)

2.1 The narrow band model

The narrow band model (NBM) described by Tjemkes and Nieuwstadt (1988) was adopted for its accuracy. The infrared spectrum is divided into 178-bands for which a mean upward (F_i+) and downward (F_i-) flux is evaluated according to

$$F_i^+(z) = B_i(0)\tau_i(0,z) + \int_0^z B_i(z')\frac{\partial \tau_i(z', z)}{\partial z'}\, dz' \qquad (3.1)$$

$$F_i^-(z) = \int_{top}^z B_i(z')\frac{\partial \tau_i(z', z)}{\partial z'}\, dz', \qquad (3.2)$$

with τ_i the transmission averaged over the spectral interval. The mean transmission for the vibrational / rotational lines of water vapor and carbon dioxide is evaluated according to the Goody band model with a Malkmus interpolation between the weak and strong absorption limit of a Lorentz shaped line (Goody, 1952; Tjemkes and Duynkerke, 1988b)

$$\tau_i(u) = \exp -\left\{ n_i\, \pi\alpha_i \left\{ \left(1 + \frac{S_i u}{\pi\alpha_i} \right)^{0.5} - 1 \right\} / \Delta\nu_i \right\} \qquad (3.3)$$

with n_i the number of lines in the interval S_i the mean line strength and α_i the mean line half width.

The narrow band model was tested in two comparison studies (Tjemkes and Nieuwstadt, 1988). In the first we compare the calculated downward flux near the surface with the observed flux for 44 cases, in the second we compared the performance of the NBM with the performance of two line by line models. From these two comparison studies we conclude that the calculated downward flux near the surface has an error of 3 W/m2 ($\approx$ 1.5%) whereas the error in the cooling rate is of the order of 0.2 k/day ($\approx$20 %).

2.2 The emissivity model

We adopted the emissivity model of Rodgers (1967) for our comparison study mainly for its com-putational speed. In the emissivity model the upward and downward flux are evaluated from

$$F^+(z) = \sigma T^4(0)\,(1-\varepsilon(0,z)) + \int_0^z \sigma T^4(z')\frac{\partial \varepsilon(z',z)}{\partial z'}\, dz' \qquad (3.4)$$

$$F^{-}(z) = \int_{top}^{z} \sigma T^4(z') \frac{\partial \epsilon(z', z)}{\partial z'} dz', \qquad (3.5)$$

with ε the emissivity evaluated according to Rodgers (1967) with the coefficients taken from Welch and Zdunkowski (1979).

2.3 The k-model

The mean transmission over a spectral interval in the k-distribution method is given by

$$\tau_i(z', z) = \int_0^{\infty} f(k)\, e^{-ku} dk\,, \qquad (3.6)$$

with f(k)dk the k-distribution, which represents the fraction of the spectral interval associated with an absorption coefficient between k and k + dk. The k-distribution is found from the inverse Laplace transform of the mean transmission. Assuming that the mean transmission is given by the Goody band model with a Malkmus interpolation (cf section 2a) the k distribution is given by (Domoto, 1974)

$$f(k) = \left(S_i\alpha_i\right)^{0.5} k^{-1.5} \exp\left(\pi\alpha_i(2\text{-}k/S_i\text{-}S_i/k)\right). \qquad (3.7)$$

For practical applications the integral in (3.6) is evaluated using a quadrature formula such that the mean transmission is found from a finite sum over pseudo-monochromatic transmissions.

$$\tau_i(z', z) = \sum_{j=1}^{N} w_j e^{-k_j u}. \qquad (3.8)$$

In the 15 μm region water vapor as well as carbon dioxide has strong absorption lines. To include the combined absorption in the k-model eq. (3.6) should be modified into

$$\tau_i(z', z) = \int_0^{\infty}\int_0^{\infty} f(k^1, k^2)\, e^{-k^1 u_1 - k^2 u_2} dk^1 dk^2, \qquad (3.9)$$

with f(k1,k2) the combined distribution function. The superscript 1 represents water vapor the superscript 2 carbon dioxide. f(k1,k2) is found from a multiplication of the individual distribution function of water vapor and carbon dioxide. For all applications the double integral in (3.9) is approximated by a quadra-ture formula to yield

$$\tau_i(z', z) = \sum_{j=1}^{N}\sum_{h=1}^{M} w_{jh}\, e^{-k_j^1 u_1 - k_h^2 u_2}. \qquad (3.10)$$

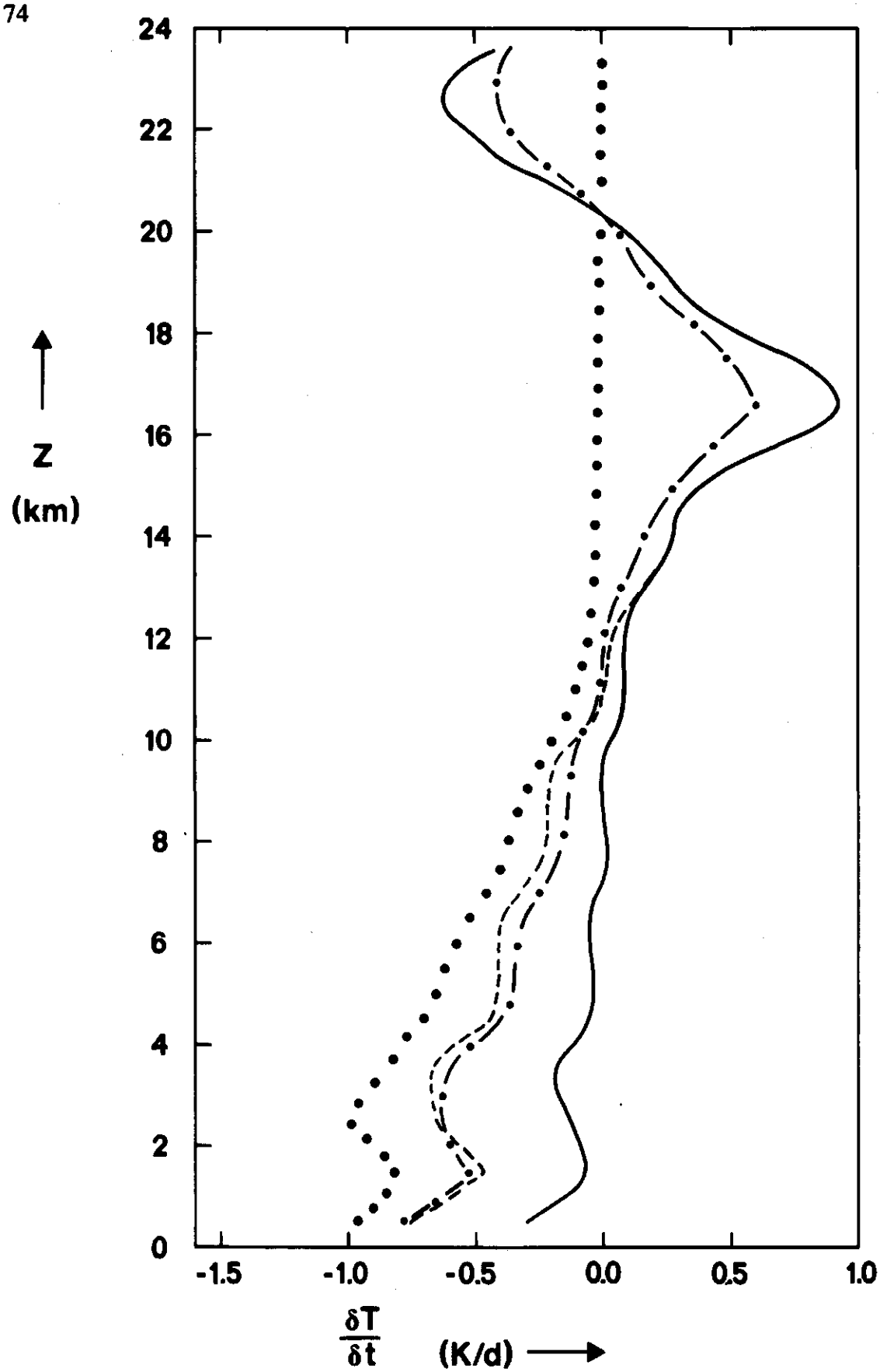

Fig. 3.1 *The infrared cooling rate profiles in a tropical atmosphere in the 15μm band region showing the contribution by CO_2 alone (solid line), the contribution by H_2O alone (dotted line) and the combined contribution of H_2O and CO_2 according to the double sum approximation (dashed line) and the single sum approximation (dashed dotted line).*

Thus the combined absorption of water vapor and carbon dioxide requires the computation of N*M pseudo-monochromatic transmissions. To our opinion such a tedious calculation is not in relation to the N pseudo-monochromatic transmission required for an interval with only one infrared active gas. A fast method to approximate gaseous overlap is found from a summation over the absorber amount

$$\tau_i(z', z) = \sum_{j=1}^{N} w_j \, e^{-k_j (u_1 + u_2)},$$

where the weights (w_j) are evaluated from a linear sum of the distribution function of water vapor and carbon dioxide

$$w_j = (w_j^1 + w_j^2) / 2. \qquad (3.12)$$

2.4 Spectroscopic data

The mean line strength and line half width are evaluated from the 1980-version of the atmospheric line parameters compiled by Rothman (1981). For the k-model the infrared spectrum is divided into 4 broad bands. For each band 32 k-values are evaluated.

3. Preliminary Results

3.1 Overlap parametrization.

Before we discuss the performance of the different radiation codes, first we analyze the two different gaseous overlap parametrizations discussed in section 2c. In Fig. 3.1 we present model calculations with our k-model for a standard tropical atmosphere (McClatchey et al., 1972). Shown is the heating rate due to absorption and emission in the 15 μm region.

In this fig. we see that in the troposphere the single sum approximation (eq (3.11)) agrees reasonably well with the double sum approximation (eq (3.10)). But above the troposphere, the single sum approximation diverge from the double sum. This can be explained from the chosen formulation to evaluate the weights (eq. (3.12)). In the troposphere the water vapor content is very small. For these layers no combined absorption is present and thus the weights in (3.11) should be given by the weights of carbon dioxide only. However in the single sum approximation the weights are evaluated as the linear sum of the weights of carbon dioxide and water vapor, which affects the model performance (cf. section 3b)

3.2 Intercomparison of the models

The downward flux at the surface is an important quantity because it is directly related to the ground heating. In 1983 44 cases of the surface downward flux were observed at the meteorological observational site at Cabauw in the Netherlands. These observa-tions were used to test the narrow band model. For each of these observations a temperature and humidity profile was constructed using observations along a 200m high mast and radiosoundings. For the present study only the night time observations were used.

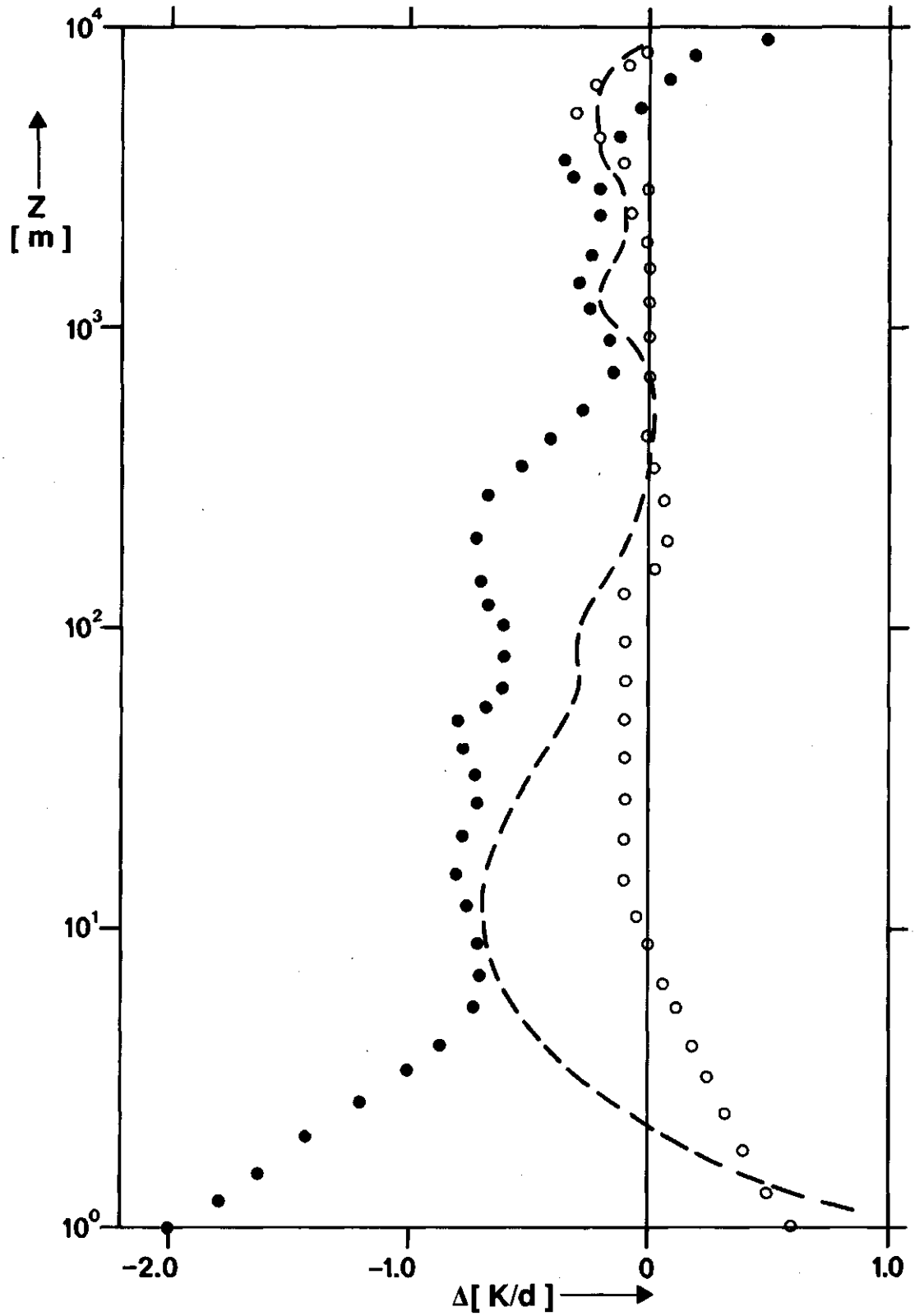

Fig. 3.3 *The difference between the exact cooling rate (based on the narrow band model) and the cooling rate using the emissivity model (closed circles), using the k-model which employs the double sum (open circles) and using the k-model which employs the single sum (dashed line) for a winter profile.*

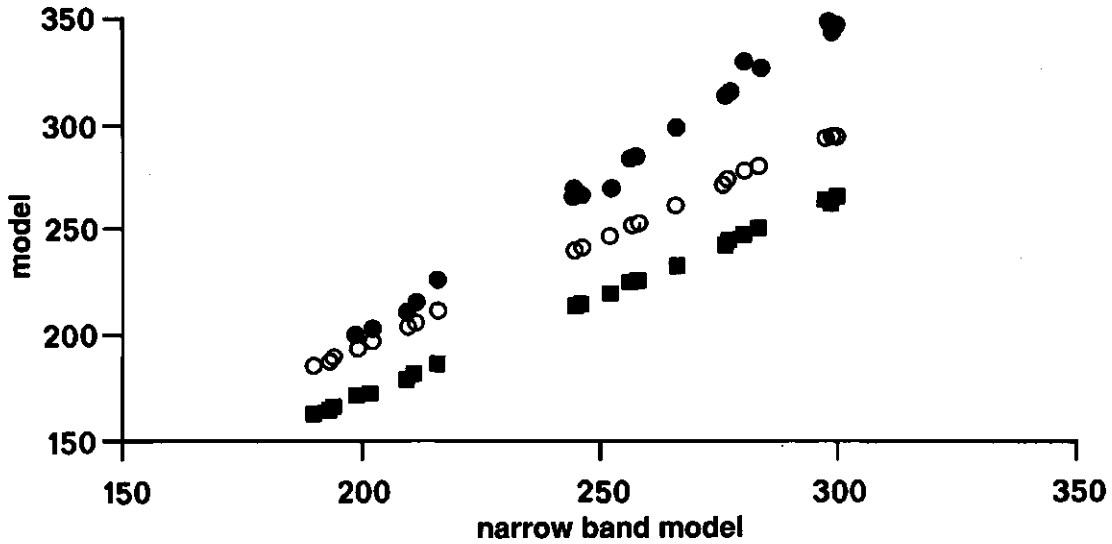

Fig. 3.2 *Comparison of the surface downward flux according to the emissivity model (closed circles), the k-model which employs the double sum (open circles) and the k-model which employs the single sum (closed squares) with the surface downward flux according to the narrow band model. (units W/m2)*

In Fig. 3.2 a scatter plot of the surface downward flux according to the k-models and emissivity model as a function of the narrow band model is given. Moreover in Table 3.1 the results of a linear regres-sion analysis can be found. The k-model which employs the double sum approximation agrees reasonably well with the NBM. The mean difference between the two models is 4.0 W/m2 with a rms of 0.8 W/m2 If the double sum is replaced by the single sum, the k-model systematically underestimates the downward flux by 30.7 W/m2. We attribute this behavior of the k-model to the performance in the stratosphere (cf. section 3a).

At high values of the surface downward flux the emissivity model diverge from the NBM (Fig. 3.2). The reason for this discrepancy is probably that the coefficient of Welch and Zdunkowski (1979) implicitly include some sort of temperature scaling, which is omitted in the NBM. Temperature scaling is important in the summer when high values of the surface downward flux are observed.

	model				
	1	2	3	4	5
Slope	1.51	1.01	0.94	1.00	0.94
Offset	-104.04	-7.45	-16.51	-5.55	-22.04
Av. dev	-21.46	4.04	30.67	5.83	34.21
rms	19.65	0.75	2.3	0.87	2.18

Table 3.1 *Results of the linear regression analysis: #1 the emissivity model; #2 the k-model double sum, 32 k-values per interval; #3 as #2 but now single sum; #4 as #2 but now 6 k-values; #5 as #3 but now 6 k-values (units W/m2)*

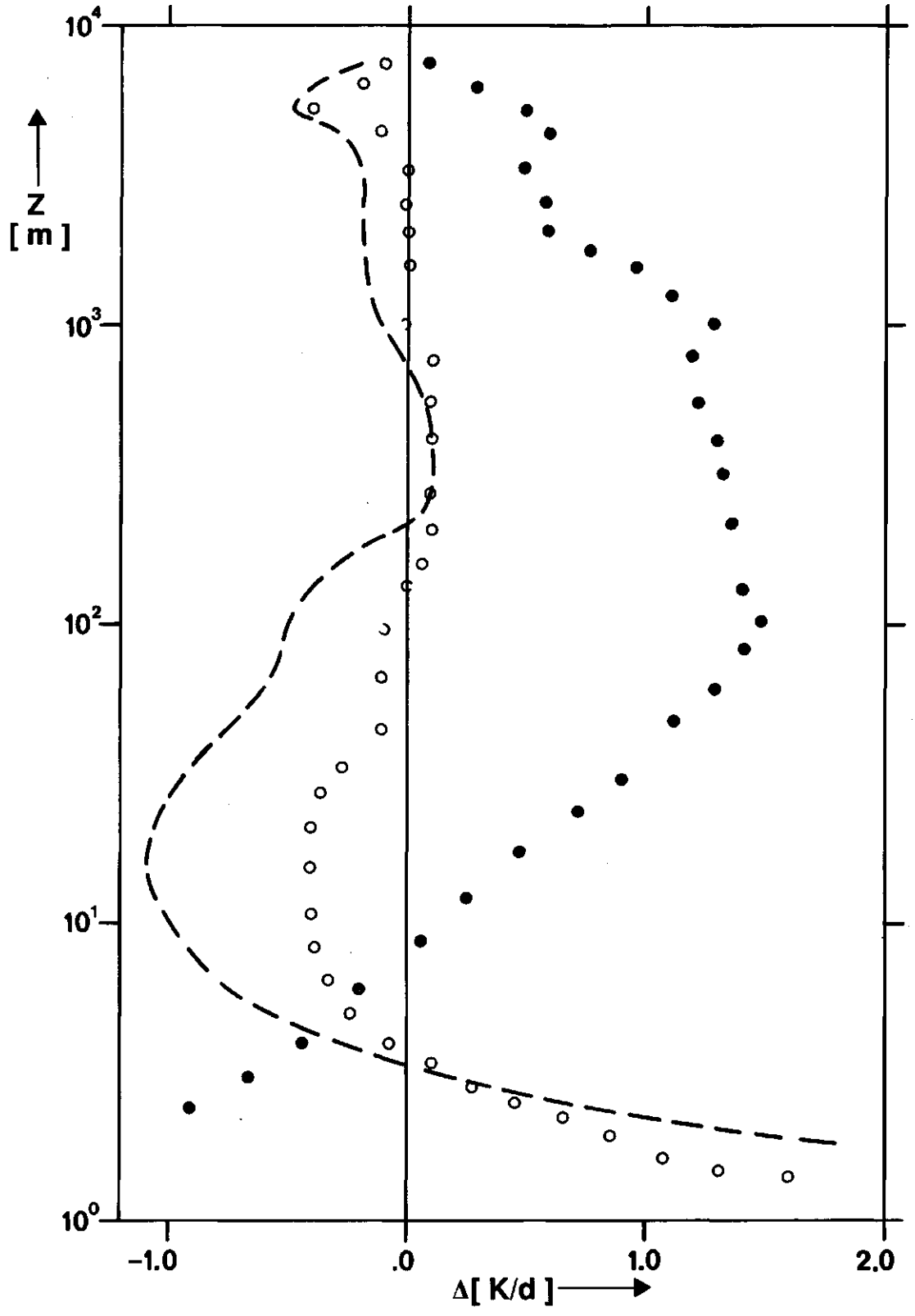

Fig. 3.4 *As Fig. 3.3 but now for a summer profile.*

In Figs. 3.3 and 3.4 the cooling rate profiles for a typical summer and winter case are given. In Tables 3.2 and 3.3 the average deviation and rms over all levels can be found.

	model				
	1	2	3	4	5
Av. dev.	-0.38	-0.03	0.09	0.25	0.20
rms	0.53	0.17	1.41	1.82	2.46

Table 3.2 *The average deviation and rms based on all levels of the winter profile. Numbers as in Table 3.1 (units W/m²).*

From Figs. 3.3 and 3.4 we see that except for layer near the surface all three models are in close agree-ment with the NBM. The two k-models perform slightly better than the emissivity model. Note that near the surface the radiative cooling rate is evaluated over thin layers, which is required to resolve the large vertical temperature gradients. As a result a relative small error in the two flux components results in a relative large error in the radiative cooling rate.

	model				
	1	2	3	4	5
Av. dev.	-0.58	0.18	0.13	0.18	0.07
rms	3.26	1.30	2.28	1.09	2.25

Table 3.3 *As Table 3.2 but now for a summer profile.*

4. Conclusions

An intercomparison study between infrared radiation codes for use in a boundary layer model is presented. The study involved an emissivity model and a k-distribution model. An accurate narrow band model (NBM) was used to provide the "exact" radiative fluxes. This accuracy of the NBM is at the expense of a large amount of computer time (Table 4.1). From the presented results we conclude that the required compu-tational time can be reduced without the loss of accuracy if the k-distribution method is applied to approximate the mean transmission. Dependent on the number of k-values per band the process time on a Mac II decreased from 1618 s to 262 s (32 k-values) or 25 s (6 k-values).

	model					
	0	1	2	3	4	5
process time (s)	1618	70	262	40	25	13

Table 4.1 *Process time on a Mac II for the total data set of 44 observed profiles. #0: narrow band model*

The amount of computer time can be reduced even further if gaseous overlap is approximated from a summation over absorber amount (cf. (3.11)). Then the process time decreased to 40 s (32 k-values) and 13 s (6 k-values). However, we assumed the weights in the finite sum approximation of the k-integral independent of height. Especially the performance of the single sum approximation of gaseous overlap is negatively influenced by this assumption.

ACKNOWLEDGEMENTS

Part of this study was performed during a two months visit at the Colorado State University. The author thanks G.L. Stephens for its hospitality and stimulation discussion. The author acknowledge financial support by the Netherlands organization for scientific research under contract # 752-365-008.

Appendix B. A new look at the Goody band model[6]

1. Abstract

In contrast to the usual statistical interpretation of the Goody band model, here we interpret the model to represent the mean transmission of a spectral interval which consists of a set of uniform absorbing, completely overlapping spectral lines. Because the interval width is much larger than the line width each line has a mean absorption which is much smaller than unity. This "flat line" interpretation clarifies the fact that the Goody band model can represent the mean transmission of a spectral interval which contains equidistant lines and that the performance of the Goody band model increases with decreasing interval width. In order to illustrate our conclusions, test calculations for the 15 μm CO_2-band are presented.

2. Introduction

The absorption and emission of infrared energy by water vapor (H_2O), carbon dioxide (CO_2) and ozone (O_3) determine most of the longwave radiative transfer through a cloudless atmosphere. At a single frequency, this radiative transfer is described by a transfer equation, which has a well established solution (Chandrasekhar, 1960; Liou, 1980). However, for all practical applications the solution for the whole longwave spectrum is required. Due to the rapid variation of the absorption coefficient with frequency, the direct integration of the transfer equation over frequency is very time consuming (WMO, 1984). A practical solution is obtained by considering spectral intervals for which an effective transmission τ can be defined

$$\tau(u) = \int_{\Delta\nu} \exp - \left\{ \sum_{i=1}^{n} S_i \, f\left(\left| \nu - \nu_{0i} \right| \right) u \right\} d\nu / \Delta\nu \qquad (2.1)$$

In eq. (2.1) S_i represents the line strength, ν_{0i} the line position, ν the frequency, f the line shape, u the absorber amount and n the number of lines within the interval. The complex arrangement of the spectral lines within the interval makes it impossible to obtain an analytical expression for τ. In practice τ is obtained either by measurements or from an idealized representation of the real spectrum (Liou, 1980).

For instance, if we assume that the overlap between spectral lines is negligible the mean transmission can be written as

$$\tau(u) = 1 - \sum_{i=1}^{n} A_i(u) \qquad (2.2)$$

where $A_i(u)$ denotes the mean absorption of the ith line, defined by

---

6 Published in Beitr. Phys. Atmosph. with P.G. Duynkerke as co-author

$$A_i(u) = \int_{\Delta\nu} 1 - \exp - \left\{ S_i f\left(\left| \nu - \nu_{0i} \right| \right) u \right\} d\nu / \Delta\nu \qquad (2.3)$$

In general we cannot make this simplification but we have to consider line overlap. Most models for the mean transmission take such overlap into account (Tiwari, 1978). One of those is the Goody or statistical band model (GBM hereafter). For an infinitely wide interval and a uniform distribution of the lines within the interval, Goody (1952) proposed for the mean transmission τ,

$$\tau(u) = \exp - \left\{ \sum_{i=1}^{n} A_i(u) \right\} \qquad (2.4)$$

A number of studies (Ellingson and Gille, 1978; Cess et al., 1986) demonstrated that the GBM (2.4) can represent the mean transmission quite accurately. Therefore, the GBM is frequently used to calculate the transfer of infrared radiation through the atmosphere (WMO, 1984; Stephens, 1984).

In principle the GBM may only be used to approximate the mean transmission for spectral intervals which contain a large number of randomly positioned lines. However, it has been demonstrated (Morcrette and Fouquart, 1985; Ellingson and Gille, 1978; Kiehl and Ramanathan, 1983) that the difference between the exact value of τ and the GBM decreases with decreasing interval width. For a statistical model such a behavior is quite surprising, since it has to be based on a large number of spectral lines. When we decrease the width of an interval we also decrease the number of lines within the interval. Hence a proper representation of the statistics can become questionable for smaller interval widths. Moreover, if we divide an absorption band (e.g. the 9.6 μm O_3-band) into many subintervals it is unrealistic to assume that each subinterval has more or less the same statistical properties (Wyatt et al., 1962). Also, if applied to an absorption band which contains equally spaced (Ellingson and Gille, 1978; Kiehl and Ramanathan, 1983; Crisp et al., 1986) or coincident lines (Cess et al., 1986), the GBM is still able to describe the mean transmission accurately. The ability of the GBM to describe the mean transmission function beyond the limitation imposed by Goody, cannot be fully explained from the statistical point of view. We therefore conclude that the statistical theory on which the GBM is based should be replaced by a modified one.

The major goal of this paper is to derive Equation (2.4) from a different point of view than the statistical view used by Goody. We will demonstrate in sections 3 and 4 that we can interpret the GBM to represent the mean transmission for a spectral interval, which contains uniformly absorbing and therefore completely overlapping spectral lines. With each individual line having a mean absorption much less than unity. This interpretation of the GBM makes it possible to give a better notion of the results obtained by Morcrette and Fouquart, than the usual statistical interpretation.

In section 3 we derive an expression for the mean transmission (named the π-equation) both along the statistical approach proposed by Goody and the new approach. From a set of test calculations for the 15 μm CO_2-band we demonstrate the accuracy of this equation. Though the expression for the mean transmission is the same in both approaches the different interpretation of the π-equation explains the obtained results.

In section 4 we will show that, if the equivalent width of each line is much smaller than the width of the spectral interval, the GBM (Equation (2.4)) can easily be derived from the π-equation. From a second set of test calculations for the 15 μm

CO_2-band we demonstrate the accuracy of the GBM.

3. The mean transmission function

3.1 The flat line approach

Consider a spectral interval of width $\Delta\nu$ containing n-spectral lines. The equivalent width of the ith line (W_i) is given by (Tiwari, 1978)

$$W_i(u) = A_i(u)\,\Delta\nu \tag{3.1}$$

The equivalent width is usually interpreted as the width of a rectangular line whose center is totally opaque, having the same total absorption as that of the actual line (see Fig. 3.1). But Equation (3.1) suggests that we can also interpret the equivalent width as the area of a rectangular line with sides equal to the width of the spectral interval and the mean absorption of the actual line (Fig. 3.1).

In the flat line approach of the GBM, we assume that the total absorption of a spectral line is represented by a rectangular shaped line with sides equal to the interval width and mean absorption of the real line, such that the surface of the rectangle is equal to the total absorption of the real line. Thus we assume that each absorbs uniformly over the entire interval. As a consequence of this assumption, there is complete overlap with every other line within the interval. Under these assumptions the mean transmission defined by Equation (2.1), may be written as

$$\tau(u) = \prod_{i=1}^{n}\left(1 - \frac{W_i(u)}{\Delta\nu}\right) \tag{3.2}$$

where the product is over all lines inside the interval. We refer to Equation (3.2) as the π-equation.

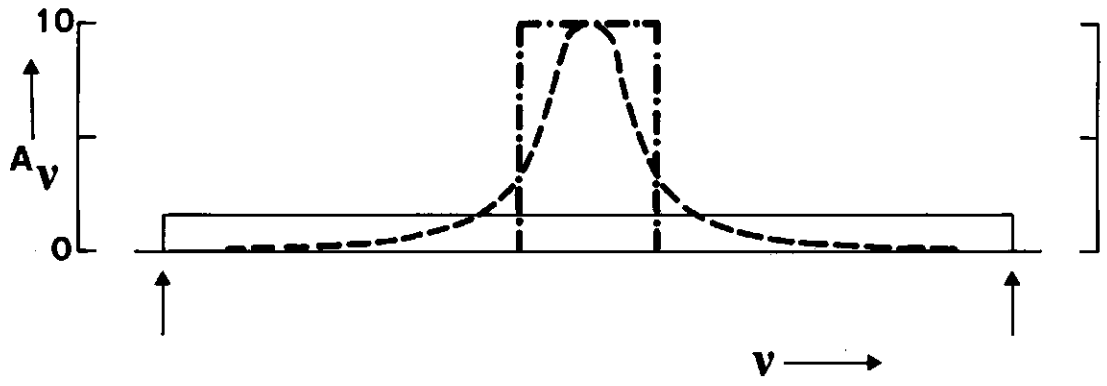

Fig. 3.1 *Equivalent width of a spectral line. The dashed line represents a Lorentz line, the dashed-dotted line the usual interpretation of the equivalent width and the solid line the flat line interpretation of the equivalent width. The area of the Lorentz line and the two rectangular lines are identical. The edges of the spectral interval are marked by two arrows.*

3.2 The statistical approach

Besides the above given flat line interpretation of the π-equation. we can also interpret this equation to be the mean transmission for a band containing randomly spaced lines as shown by Goody (1952). Consider a spectral interval of width $\Delta\nu$ containing one single line. Let P(n0) dn be the probability that the center of the line is between ν_0 and $\nu_0 + d\nu_0$. The distribution function $P(\nu_0)$ is normalized according to

$$\int_{\Delta\nu} P(\nu_0)\, d\nu = 1 \tag{3.3}$$

Then

$$P(\nu_0) \exp - \left\{ S\, f\left(\left| \nu - \nu_0 \right| \right) u \right\} d\nu_0 \tag{3.4}$$

represents the contribution to the transmission at frequency ν. After an integration over all possible line positions inside the interval we find the monochromatic transmission to be

$$\tau_\nu(u) = \int_{\Delta\nu} P(\nu_0) \exp - \left\{ S\, f\left(\left| \nu - \nu_0 \right| \right) u \right\} d\nu_0 \tag{3.5}$$

Assuming the interval wide enough to contain the entire line and the line position to be randomly distributed ($P(\nu) = 1/\Delta\nu$), Equation (3.5) becomes

$$\tau_\nu(u) = 1 - \frac{W(u)}{\Delta\nu} \tag{3.6}$$

with W(u) the equivalent width of the spectral line given by

$$W(u) = \int_{-\infty}^{\infty} 1 - \exp - \left[S\, f(\bar{\nu})\, u \right] d\bar{\nu} \tag{3.7}$$

and $\bar{\nu} = \left| \nu - \nu_0 \right|$.

Due to the specific choice of $P(\nu_0)$, $\tau_\nu(u)$ is no longer wavelength dependent. Therefore, the mean transmission defined in Equation (2.1) is equal to $\tau_\nu(u)$. For a number of lines, assuming that all lines are independent, we obtain Equation (3.2) for the mean transmission.

3.3 Test calculations

In the previous section we found that the flat line approach is consistent with the as-sumption of multiplicability of transmissivities, as does the statistical approach proposed by Goody (1952). Although the final expressions are identical the different assumptions used in both approaches makes that (3.2) is valid under different conditions for the two approaches.

In the statistical approach we must consider intervals which are wide enough to contain a large number of lines (in a statistical sense). Since a large number of lines is needed to obtain accurate statistical properties for the spectral interval considered. The flat line approach can handle one single line within the interval. When there is more than one line in the interval we assume complete overlap between the lines. This assumption is met more easily for narrow than for wide intervals. Therefore, in the flat line approach we may use the π-equation for narrow bands only.

In the statistical approach we also used a random distribution for the line position to derive the π-equation. From a statistical point of view we are not allowed to use the π-equation to describe the mean transmission of an interval which consists of lines which are not randomly placed. Since we did not make any assumptions regarding the line positions in the flat line approach, the use of the π-equation is not restricted to randomly placed lines only.

To examine the behavior of the π-equation in more detail, we performed a series of test calculations for the 15 μm CO_2-band. This band extends from 500 to 900 cm-1, and was divided into a number of equally wide subintervals. For each of these intervals a value for the mean transmission is calculated according to the π-equation. Then the mean transmission for the entire 15 μm band (τ_{15}) is calculated according to

$$\tau_{15}(u) = \frac{1}{m}\sum_{j=1}^{m}\tau_j(u) \qquad (3.8)$$

with τ_j the mean transmission of the jth subinterval and m the number of subintervals. Assuming a Lorentz shape for the spectral line and taking the intervals wide enough to contain the complete line, the equivalent width becomes

$$W(u) = 2\pi\alpha\, LR\left(\frac{Su}{2\pi\alpha}\right), \qquad (3.9)$$

with a the line half width and LR the Ladenberg-Reiche function

$$LR(x) = xe^{-x}\left(I_0(x) + I_1(x)\right) \qquad (3.10)$$

in which $I_0(x)$, $I_1(x)$ represent the modified Bessel function of zero and first order, respectively.

We made a direct calculation of τ_{15} from (2.1) to compare our results with. These "line by line" calculations employed the Lorentz line profile at a pressure of 1,013 * 10^5 Pa and a temperature of 296 K. We adopted a wavenumber cut off equal to 5 cm-1. The line parameters are adopted from the 1980 version of the atmospheric line compilation (Rothman, 1981). The results are given in Table 3.1.

A: τ_{15} directly calculated.

u	τ_{15}
10.00	0.4873
1.00	0.6314
0.10	0.7749
0.01	0.9139

B: τ_{15} according to the π-equation

	m	1	2	8	40	80	160	400
u	$\Delta\nu$	400	200	50	10	5	2.5	1
10.00		0.0002	0.0624	0.4512	0.4911	0.4937	0.4897	$-0.1304*10^{26}$
1.00		0.0898	0.3001	0.5972	0.6234	0.6337	0.6361	$0.5854*10^{6}$
0.10		0.5333	0.6030	0.7496	0.7700	0.7742	0.7711	0.7582
0.01		0.8662	0.8729	0.8968	0.9086	0.9144	0.9133	0.9137

Table 3.1 *The mean transmission of the 15 μm CO_2 band calculated according to a direct evaluation of Equation (2.1) and the π-equation (2.2). u is the absorber amount in kg m^{-2}, m the number of subintervals and $\Delta\nu$ the width of the subinterval in cm^{-1}.*

From Table 3.1 we see that there is only a good agreement between the results from the π-equation and the line by line calculations if the 15 μm band is divided into a large number of narrow subintervals. From a statistical point of view the bad agreement for wide intervals can be explained as follows. In the 15 μm band the strong lines are not uniformly distributed over the entire band, but are located near the center of the band. Therefore, we may not expect a good agreement with the exact results for the two calculations with wide subintervals. However, if we decrease the width of the subintervals we may neither expect a good agreement, since the CO_2-absorption lines are equally spaced instead of randomly. This is in contradiction with our test calculations. It is worth noticing that if applied to a different absorption band with a different structure, e.g. the water vapor rotation, the π-equation shows a similar behavior (cf. Morcrette and Fouquart, 1985). Therefore, a satisfactory explanation of the agreement between the π-equation and the line by line calculations in terms of statistical properties of the absorption band does not exist.

Within the context of the "flat-line" approach the results can be easily explained. For wide intervals ($\Delta\nu > 50$ cm^{-1}) we may not assume that each line uniformly absorbs over the entire interval. Moreover, there is incomplete overlap between the lines. Due to the presence of some strong lines, with a completely opaque line center, the π-equation will overestimate the total absorption. When we consider a line with a completely opaque center, it absorbs all photons with wavenumbers close to the line center. Therefore, the presence of another line at the same wavenumber does not affect the infrared energy transfer. Since this strong line absorbs in only a small part of the wide

interval, the π-equation cannot describe this type of overlap. A combination of high line density and large equivalent widths in the center of the 15 μm band, and a low line density in combination with small equivalent widths near the edges of the band amplifies the overestimation of the absorption by the π-equation.

This overestimation vanishes if the width of the interval is small enough for the strong lines to absorb uniformly over the entire subinterval. Moreover, the overestimation is restricted to the limited number of subintervals which contain strong lines. The transmission for those subintervals is practically zero, so that the mean transmission of the entire 15 μm band is hardly affected by this overestimation. This leads to a difference of less than 10% between the π-equation and the "line by line" calculation if 50 $cm^{-1} > \Delta\nu > 5$ cm^{-1} (see Table 3.1).

This difference is even less than 1% if the 15 μm band is divided into subintervals with a width equal to 2.5 cm^{-1}. However, intervals as small as 2.5 cm^{-1} may not be regarded as infinite. If the interval width becomes smaller than 2.5 cm^{-1} the use of the Ladenberg-Reiche function yields unrealistic values for $W_i(u)/\Delta\nu$ (>1). So that also the π-equation yields unrealistic values for τ_{15} as shown in Table 3.1.

4. The mean equivalent width

4.1 A simple interpolation formula

In the previous section we have seen that the π-equation is able to approximate the mean transmission function accurately. In comparison with line by line calculations, the use of the π-equation will save a tremendous amount of computer time. In the π-equation we still have to calculate the equivalent width of each individual line within the subinterval. Therefore the π-equation is still not very practical. If we assume that the interval contains only lines with an equivalent width, much smaller than the width of the spectral interval, we may approximate the π-equation by

$$\tau(u) = \prod_{i=1}^{n}\left(1-\frac{W_i(u)}{\Delta\nu}\right) = \prod_{i=1}^{n}\exp\left[\ln\left(1-\frac{W_i(u)}{\Delta\nu}\right)\right] \approx \exp\left(\frac{-n\overline{W}(u)}{\Delta\nu}\right), \quad (4.1)$$

with

$$\overline{W}(u) = \frac{1}{n}\sum_{i=1}^{n} W_i(u) \quad (4.2)$$

the mean equivalent width. Equation (4.1) was originally derived by Goody (1952) and therefore his name is attached to it. The use of Equation (4.1) in combination with an approximation for the mean equivalent width reduces the computation time even much further.

Based upon statistical assumptions of the absorption properties of a spectral interval, Goody (1952) and Malkmus (1967) derived two different relations between the mean equivalent width and u which are now widely used. Assuming a normalized exponential distribution

$$P(S)dS = \frac{1}{\bar{S}}e^{-S/\bar{S}}\,dS, \quad (4.3)$$

for the line strength within each band, Goody (1952) derived

$$\overline{W}(u) = \overline{S}u\left(1+\frac{\overline{S}u}{\pi\overline{\alpha}}\right)^{-0.5} \qquad (4.4)$$

where $\overline{S}$ is the mean line strength and $\overline{\alpha}$ the mean line width. Malkmus (1967) argued that the observed line strength distribution is better described by (see also Crisp et al. their Figure (2))

$$P(S)\,dS = \frac{N_0}{S}e^{-S/\overline{S}}\,dS \qquad (4.5)$$

where N_o is a "normalization factor"[7]. Using Equation (4.5) to describe line strength distribution Malkmus (1967) found

$$\overline{W}(u) = 2\pi\overline{\alpha}\,N_0\left[\left(1+\frac{\overline{S}u}{\pi\overline{\alpha}}\right)^{0.5} - 1\right]. \qquad (4.6)$$

We will show that the Equations (4.4) and (4.6) are two different interpolation formulas between the strong and weak absorption limit for a set of lines with a Lorentz shape.

Assume a spectral line with a Lorentz line and an interval wide enough to contain the entire line. Then the equivalent width of a spectral line is given by the Ladenberg-Reiche function (3.9). The Ladenberg-Reiche function has two well known limits. If

$$\frac{S_i u}{2\pi\alpha_i} << 1 \qquad \forall\ i \in 1.....n \qquad (4.7)$$

Equation (4.2) may be written as

$$\overline{W}(u) = \overline{S}u \qquad (4.8)$$

with

$$\overline{S} = \frac{1}{n}\sum_{i=1}^{n} S_i \qquad (4.9)$$

while for

---

[7] Note that N0 is loosely called a normalization factor since

$$\int_0^\infty \frac{N_0}{S}e^{-S/\overline{S}}\,dS$$

does not exist.

$$\frac{S_i u}{2\pi\alpha_i} >> 1 \qquad \forall\ i \in 1.....n \tag{4.10}$$

we may write

$$\overline{W}(u) = \sqrt{\overline{S}\overline{\pi\alpha}u} \tag{4.11}$$

with from Equation (4.9) and

$$\overline{\pi\alpha} = \frac{4}{n}\frac{\left(\sum_{i=1}^{n}\sqrt{S_i\alpha_i}\right)^2}{\sum_{i=1}^{n}S_i} \tag{4.12}$$

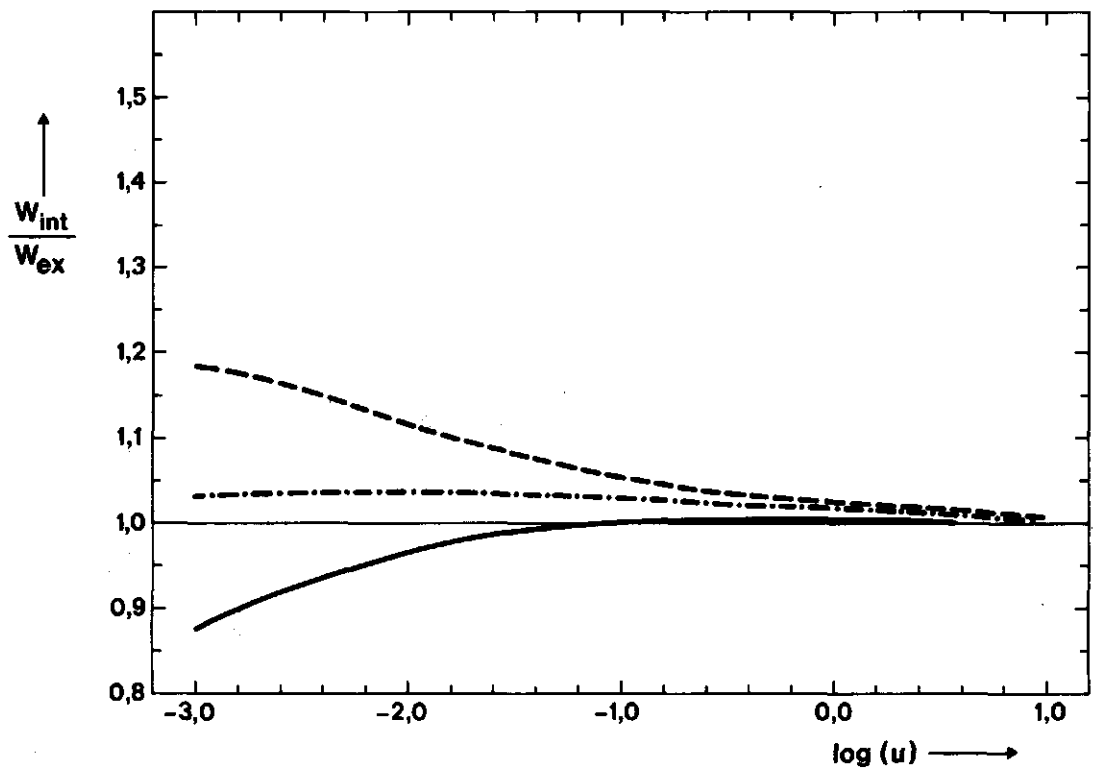

Fig. 4.1a *The total mean equivalent width $nW/\Delta\nu$ for all water vapor lines inside the 0-500 cm-1 spectral interval as a function of the absorber amount (u) according to the linear interpolation formula (Equation (4.13), the solid line), the quadratic interpolation formula (Equation (4.14), the dashed line) and according to the Malkmus interpolation formula (Equation (4.15), the dashed-dotted line) non dimensionalized with the exact total mean equivalent width (Equation (4.2)).*

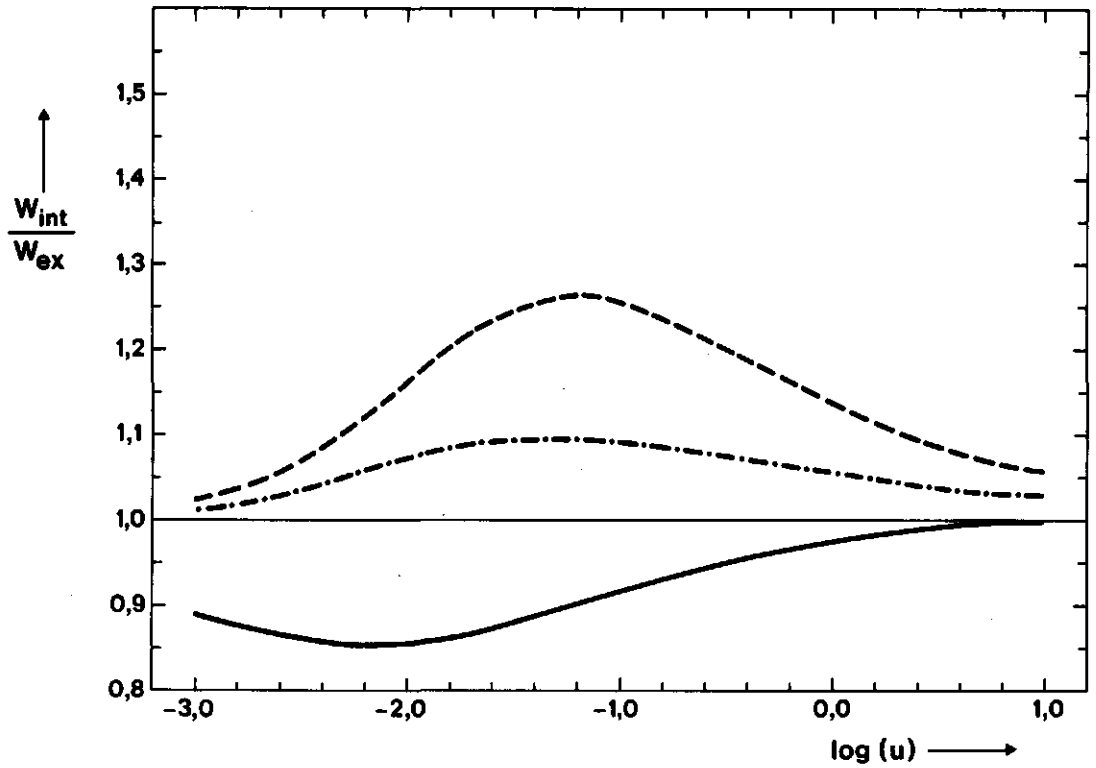

Fig. 4.1b *As Fig. 4.1a but for the water vapor lines in the 500-900 cm-1 spectral interval.*

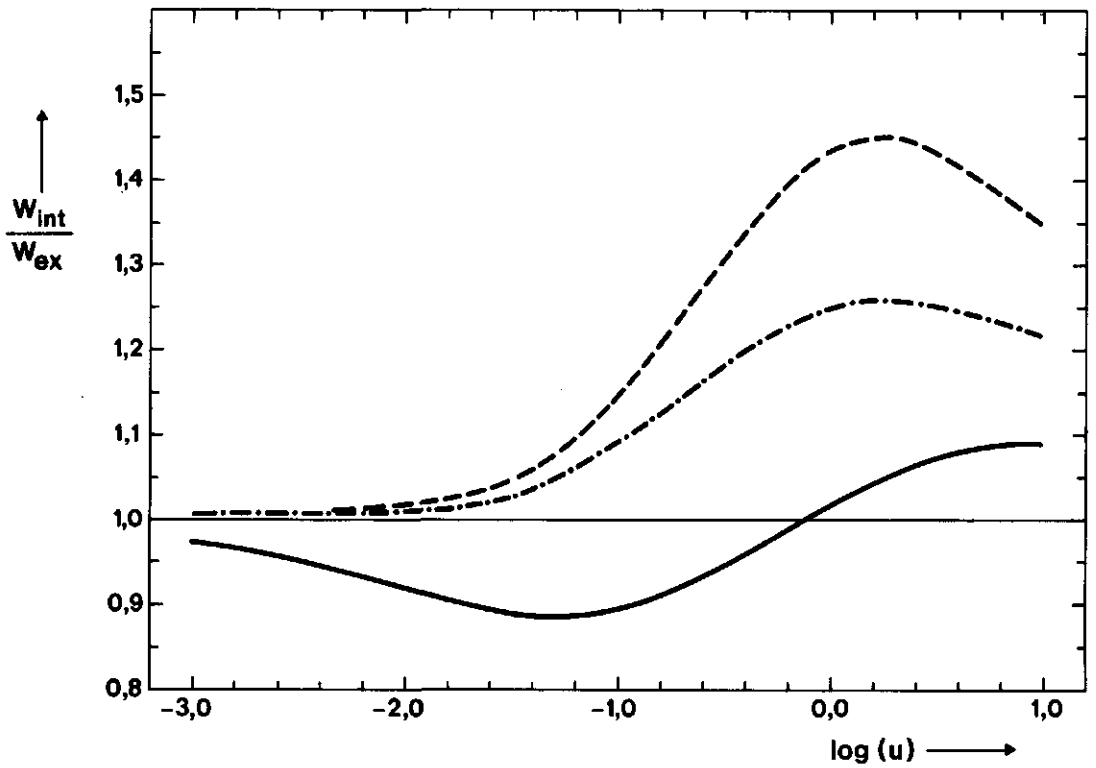

Fig. 4.1c *As Fig. 4.1a but for the water vapor lines in the 900-1300 cm-1 spectral interval.*

In the intermediate case we may approximate the behavior of $\overline{W}$ by a function of u using a simple interpolation formula. For instance, we can interpolate linearly

$$\frac{1}{\overline{W}(u)} \approx \frac{1}{\overline{S}u} + \frac{1}{\sqrt{\overline{S}\pi\alpha u}}, \tag{4.13}$$

or quadratically

$$\left(\frac{1}{\overline{W}(u)}\right)^2 = \left(\frac{1}{\overline{S}u}\right)^2 + \left(\frac{1}{\sqrt{\overline{S}\pi\alpha u}}\right)^2 \tag{4.14}$$

or we can use

$$\overline{W}(u) \approx L_{al}^2\left(\sqrt{\frac{1}{4S_{al}^2} + \frac{1}{L_{al}^2}} - \frac{1}{2S_{al}}\right) \tag{4.15}$$

where we abbreviated the linear absorption limit (4.8) by L_{al} and the square root absorption limit (4.11) by S_{al}.
In Figure 4.1 we compare the three interpolation formulas for three spectral intervals: the H2O rotation/vibration band (Figures 4.1a, b and c), the 15 μm CO_2-band (Figure 4.1d) and the 9.6 μm O_3 band (Figure 4.1e). From these Figures we see that the linear interpolation formula approximates the exact mean equivalent width slightly better than the two other formulas. Note that except in the limits of small and large u the use of an interpolation formula does not guarantee a correct description of $\overline{W}$ as a function of u for all u. To study the accuracy of the interpolation formulas in more detail we performed some calculations for the 15 μm CO_2-band in the next section.

4.2 Test calculations

For these calculations we used the same procedure as was described in section 3 3. We divided the 15 μm band into a set of equally wide subintervals. For each of these subintervals we calculated the mean transmission function according to one of the formulas given in Table 4.1. Then the mean transmission function for the entire 15 μm band is calculated from (3.8). The results of these test calculations are given in Table 4.2. To be consistent with our derivation of the GBM, we must compare the results of these test calculations with the calculations performed with the π-equation (section 3.3).

If we increase the interval width the ratio $W_i/\Delta\nu$ decreases. In that case the approximation of the π-equation by the GBM is justified (4.1). Thus we expect a better agreement between the π-equation and the GBM for wide intervals than for narrow intervals . This is shown by our test calculations.

Obviously the accuracy of the GBM is affected by the interpolation formula for . The calculations using formula B in Table 4.1 are in agreement with the calculations using the π-equation if the 15 μm band is divided into subintervals with a width of 50 cm-1 or larger. A good agreement is obtained for even narrower subintervals if we use formula C of Table 4.1.

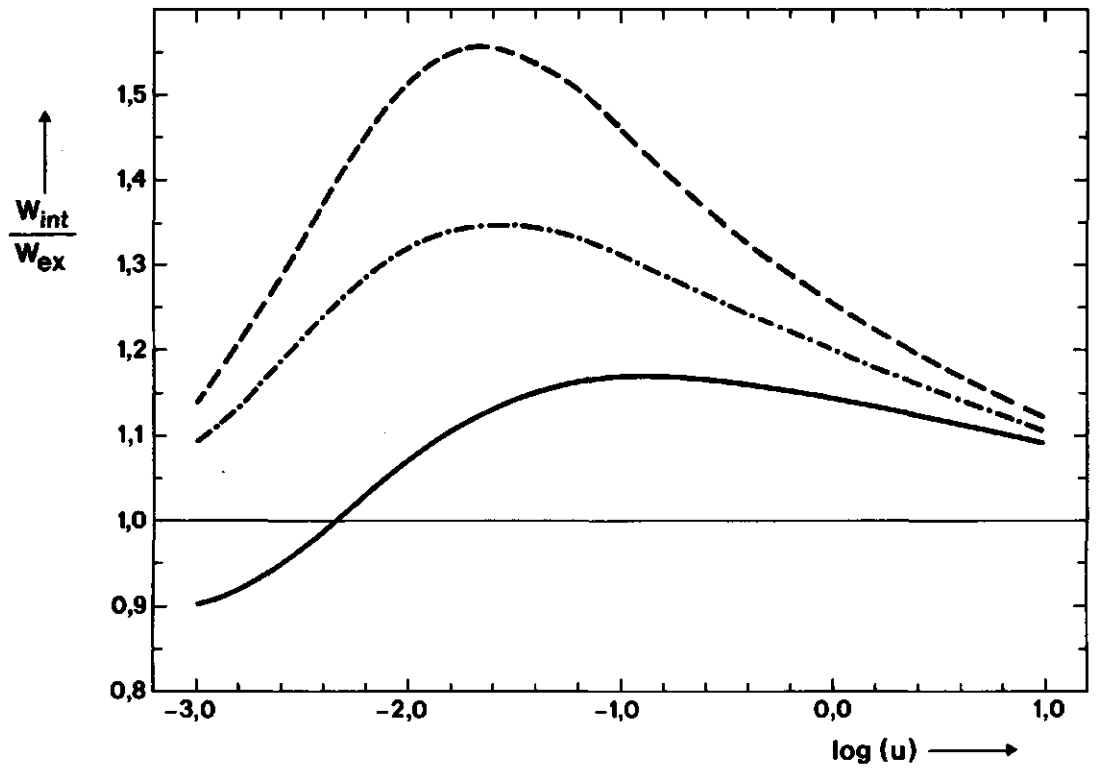

Fig. 4.1d *As Fig. 4.1a but for the 15 μm CO_2-band.*

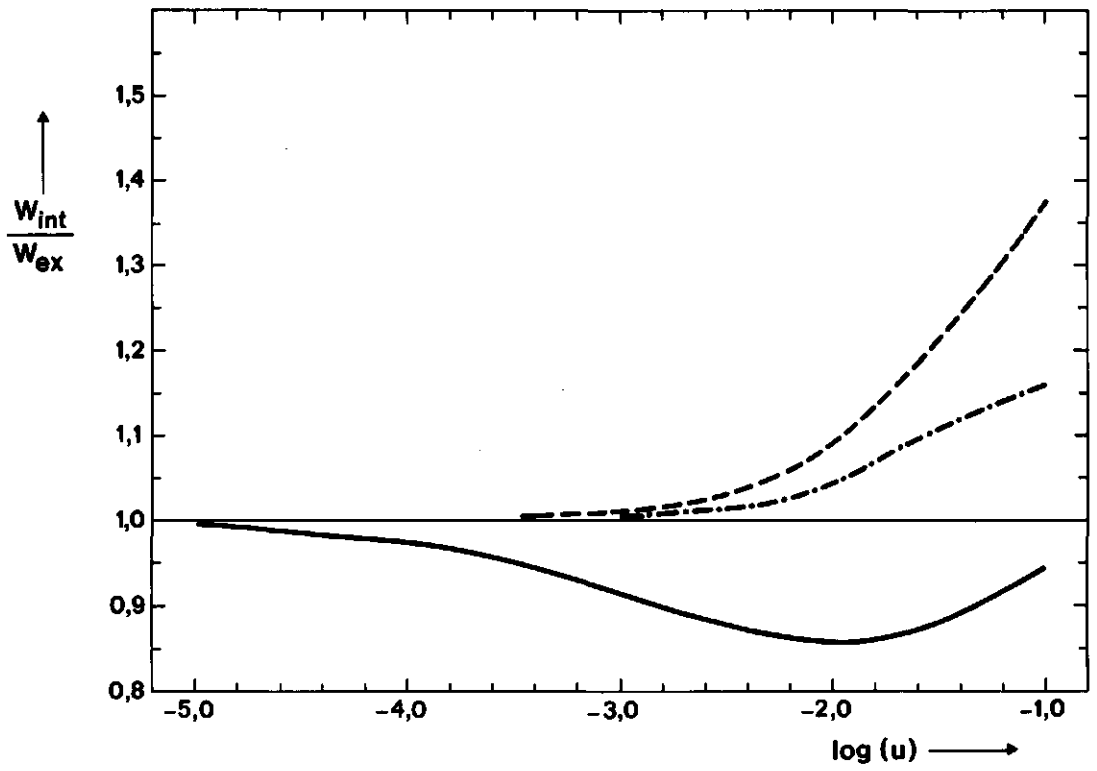

Fig. 4.1e *As Fig. 4.1a but for the 9.6 μm O_3-band.*

5. Summary and conclusions

Assuming a uniform distribution of the line position, an exponential distribution of the line strengths and infinitely wide spectral intervals, Goody (1952) was able to derive a simple formula for the mean transmission of a spectral interval. Morcrette and Fouquart (1985) showed that the performance of the Goody band model cannot be fully explained from this statistical point of view. For instance from their test calculations they concluded that the accuracy of the Goody band model increases with decreasing band width, which is in contradiction with the assumptions made by Goody (1952). Assuming that each line inside the interval absorbs uniformly over the entire interval, we showed that the mean transmission of a spectral interval can be calculated as a product of the transmission of each individual line inside the interval (the so called π-equation) Assuming that each line inside the interval has an equivalent width much smaller than the width of the spectral interval, we derived the Goody band model as an approximation of the π-equation. We therefore conclude that the GBM represents the mean transmission of a spectral interval which consists of a set of uniformly absorbing, completely overlapping, small ($W_i/\Delta\nu \ll 1$) spectral lines.

Since the assumption of complete overlap together with the assumption of uniform absorption is more likely fulfilled for narrow than for wide intervals, we expect a better agreement between the GBM and an exactly calculated mean transmission. This is demonstrated by a series of test calculations for the 15 μm band of CO_2.

The GBM is a simple relation between the mean transmission and mean equivalent width (4.1). The equivalent width, itself is a rather complicated function of the absorber amount and the absorption characteristics of each individual line. Goody (1952) and Malkmus (1967) assumed certain statistical distribution functions for the line strength in each interval to approximate the mean equivalent width. Equations (4.4) and (4.6) respectively. We showed that these same equations can be obtained using different interpolation formulas between the weak and strong absorption limit (Equations (4.14) and (4.15)). This interpretation of the formulas of Goody and Malkmus allows us to give a better formulation to approximate the mean equivalent width using non physical arguments. For instance, we showed that for most cases a linear interpolation formula gives a better approximation for the mean equivalent width than the formulas proposed by Goody and Malkmus. Finally, note that we did not make any assumptions with respect to the line positions. Thus we may use the GBM to simulate the mean transmission of a gas which consists of equally spaced lines (CO_2), randomly placed lines (H_2O) or coincident lines (CH_4).

ACKNOWLEDGEMENTS

We thank Drs H. van Dop, F.T.M. Nieuwstadt, J. Reiff and L. Wartena for reading the manuscript and stimulating discussions. Further we thank M. Kaltofen for preparing the paper and M. Brouwer for drawing the Figures. One of us (S.A.T.) acknowledges financial support by ZWO under contract # 752-365-008.

A: $W_i(u)$ according to the Ladenberg-Reiche function Equation (3.9)

$$\tau(u) = \exp - n\overline{\overline{W}}(u)/\Delta v$$

$$\overline{\overline{W}}(u) = \frac{1}{n}\sum_{i=1}^{n} W_i(u)$$

B: Linear interpolation, Equation (4.13)

$$\overline{\overline{W}}(u) = \left(\frac{1}{\overline{\overline{S}}u} + \frac{1}{\sqrt{\overline{\overline{S}}\pi\alpha u}} \right)^{-1}$$

C: Quadratic interpolation Equation (4.14)

$$\overline{\overline{W}}(u) = \frac{\overline{\overline{S}}u}{\sqrt{1 + \frac{\overline{\overline{S}}u}{\pi\alpha}}}$$

D: Malkmus interpolation Equation (4.15)

$$\overline{\overline{W}}(u) = 2\pi\alpha N_0 \left(\sqrt{1 + \frac{\overline{\overline{S}}u}{\pi\alpha}} - 1 \right)$$

Table 4.1 *The different formulas for τ used in the test calculations.*

A: τ_{15} according to formula A of Table 4.1.

	m	1	2	8	40	80	160	400
u	Δν	400	200	50	10	5	2.5	1
10.00		0.0002	0.0632	0.4519	0.4931	0.4988	0.5045	0.5190
1.00		0.0908	0.3008	0.5979	0.6262	0.6392	0.6472	0.6609
0.10		0.5338	0.6037	0.7502	0.7733	0.7811	0.7864	0.8084
0.01		0.8663	0.8730	0.8971	0.9098	0.9167	0.9184	0.9265

B: τ_{15} according to formula B of Table 4.1.

	m	1	2	8	40	80	160	400
u	Δν	400	200	50	10	5	2.5	1
10.00		0.0001	0.0490	0.4500	0.5014	0.5063	0.5114	0.5384
1.00		0.0635	0.2804	0.5941	0.6268	0.6397	0.6475	0.6670
0.10		0.4809	0.5818	0.7498	0.7785	0.7854	0.7904	0.8177
0.01		0.8576	0.8696	0.8990	0.9125	0.9192	0.9215	0.9320

C: τ_{15} according to formula C of Table 4.1.

	m	1	2	8	40	80	160	400
u	Dn	400	200	50	10	5	2.5	1
10.00		0.0001	0.0374	0.4216	0.4806	0.4858	0.4913	0.5101
1.00		0.0493	0.2345	0.5722	0.6039	0.6156	0.6232	0.6437
0.10		0.4008	0.5262	0.7191	0.7522	0.7609	0.7669	0.7957
0.01		0.8048	0.8268	0.8763	0.8938	0.9009	0.9035	0.9181

D: τ_{15} according to formula D of Table 4.1.

	m	1	2	8	40	80	160	400
u	Δν	400	200	50	10	5	2.5	1
10.00		0.0001	0.0429	0.4331	0.4877	0.4928	0.4981	0.5168
1.00		0.0561	0.2568	0.5801	0.6126	0.6249	0.6326	0.6522
0.10		0.4400	0.5508	0.7314	0.7620	0.7698	0.7754	0.8030
0.01		0.8273	0.8450	0.8847	0.9007	0.9076	0.9100	0.9231

Table 4.2 *The mean transmission of the 15 μm CO_2 band calculated according to the different formulas in Table 4.1. u is the absorber amount in kg m^{-2}, m the number of subintervals and Δν the width of the subinterval in cm^{-1}.*

Appendix C
List of symbols

a	Constant	100
A	Total absorption	17
b	Constant	100
B	Planck function	9
c_v	Constant	47
C_p	Heat capacity	45
e	Water vapor partial pressure	36
E	Turbulent kinetic energy	47
E_n	Exponential integral	25
f	Coriolis parameter	44
f	Line shape	18
f	Temperature and pressure function	29
f(k)	K-distribution function	21
g	Gravity acceleration	48
G	Soil heat flux	47
F_n	Net radiative flux	9
h	Boundary layer height	5
H	Sensible heat flux	55
I	Specific intensity	8
k	von Karman constant	49
$K_{m,h}$	Exchange coefficient for momentum and heat respectively	45
lE	Latent heat flux	55
$l_{m,h}$	Mixing length for momentum and heat respectively	45
N	Cloud cover	70
p	Pressure	29
P	Probability distribution function	86
q_v	Specific humidity	44
R_c	Canopy resistance	47
Ri_b	Bulk Richardson number	61
S	Line strength	18
T	Absolute temperature	9
T_0	Constant	100
Tm_s	Surface minimum temperature	66
u	Absorber amount	11
u*	Horizontal velocity scale, friction velocity	47
u_0	Constant	47
(u,v)	Velocity components in the (x,y) direction	44
(u_g,v_g)	Geostrophic wind components	44
w	Vertical velocity	5
w*	Vertical velocity	47
w_j	Quadrature weight	22

W	Equivalent width	34
z	Vertical coordinate	5
z_a	Screen level	36
z_0	Roughness length	5
α	Line halfwidth	8
β	Constant	100
$\beta_{m,h}$	Constant	49
κ	Absorption coefficient	9
κ^*	Mass absorption coefficient	11
η	Emission coefficient	9
θ	Potential temperature	5
θ	Propagation direction	8
θ_*	Temperature scale	47
λ	Thermal conductivity	47
Λ	Local Monin-Obuhkov length	49
μ	Cosine between vertical and propagation direction	8
$1/\bar{\mu}$	Diffusivity factor	23
ν	Frequency	9
ν_0	Line center	18
ρ	Density	11
σ	Scattering coefficient	9
σ	Stefan - Boltzmann constant	16
$\bar{\sigma}$	Continuum absorption coefficient	35
τ	Shear stress	49
τ	Transmission function	10
χ	Extinction coefficient	8
ω	Solid angle	9
ω	Angular frequency	47
$\phi_{m,h}$	Dimensionless shear and temperature gradient	49

Indices

c	continuum	d	deep soil
e	emissivity	h	boundary layer height
i	averaged over a spectral interval		
nb	narrow band	norad	without radiation
obs	observed	rad	with radiation
s	surface	sat	saturated
sl	single line	t	top
ν	at a single frequency		
prime	turbulent fluctuations	overbar	ensemble average
-	downward	+	upward

Constants

Most of the numerical values for the constants are adapted from Duynkerke and Driedonks (1987). The constants which are different from that paper are summarized below.

$\beta_{m,h}$	= 10	a	= 4.12 * 10-6 (kg-1m Pa-1)
k	= 0.4	b	= 7.7 * 10-6 (kg-1m Pa-1)
r	= 1.66	β	= 8.30 * 10-5 (m)
c_v	= 10	To	= 296. (K)
u_0	= 4.2 (ms-1)		

Appendix D
The transmission function

For wavenumbers between 0-400 and 1500-2800 cm-1 the band width ($\Delta\nu$) was chosen to be cm-1 whereas for wavenumbers in between 400-1500 cm-1 it was 10 cm-1. In total we considered 178 spectral intervals. In spectral intervals where two different gases or two different types of absorption mechanisms are active. The total transmission is calculated as the product of the transmission of each contributing gas or mechanism (Goody, 1964).

D.1 Gaseous absorption

The mean transmission for a frequency interval of width ($\Delta\nu$) for the rotational and vibrational lines of water vapor and carbon dioxide is modelled according to the Goody band model (Goody, 1952; Tjemkes and Duynkerke, 1988) and reads

$$\tau_i\,(z',z) = \exp -\left\{ \frac{n_i \overline{W}_i\,(z',z)}{\Delta\nu_i} \right\} \qquad (D1)$$

where n_i is the number of spectral lines within the interval $\Delta\nu_i$ and $\overline{W}_i$ is the mean line absorption also known as the mean equivalent width. The term $n_i\overline{W}_i$ represents the total absorption within the spectral interval. The mean equivalent width is approximated by a square interpolation between the weak and strong absorption limit of a line with a Lorentz profile

$$\frac{n_i \overline{W}_i(z',\,z)}{\Delta\nu_i} = \left\{ \left(\frac{1}{\overline{S}_i u} \right)^2 + \left(\frac{1}{\overline{S}_i u \pi \overline{\alpha}_i} \right) \right\}^{-1/2}, \qquad (D2)$$

with $\overline{S}_i$ the mean line strength, $\overline{\alpha}$ the mean line half width and u the absorber amount defined as

$$u = r \int_{z'}^{z} \rho(z'')\; dz'' \qquad (D3)$$

where r is the diffusivity factor which accounts for the integration over angles and which is taken to be 5/3, and ρ the density of water vapor or carbon dioxide (Liou, 1980). The mean line intensity and mean line half width are calculated from the 1980 compilation of the atmospheric line parameters. (Rothman, 1981). To account for the

integration over the inhomogeneous path (Liou, 1980) the extension of the Curtis Godson approximation as discussed by Rodgers and Walshaw (1966) is used.

D.2 Continuum absorption

For the band transmission of water vapor continuum we used the empirical fit proposed by Roberts et al. (1976)

$$\tau_i(z', z) = \exp- \left\{\bar{\sigma u}\right\}, \qquad (D4)$$

where $\bar{\sigma}$ is the absorption coefficient averaged over the band (Roberts et al. 1976)

$$\bar{\sigma} = \left\{a + be^{-\beta\nu_0}\right\} \; e \exp\left(T_0\left[\frac{1}{T} - \frac{1}{296}\right]\right), \qquad (D5)$$

with a, b, b, T_o constants, ν_0 the center of the band and e the water vapor partial pressure.

References

Abramowitz, M., and I.A. Stegun. 1964: *Handbook of mathematical functions*. Dover publications, inc., New York, 1046pp.

André, J. C., G. de Moor, P. Lacarriere, G. Thierry, and R. Du Vachat, 1978: "Modelling the 24 hour evolution of the mean and turbulent structures of the planetary boundary layer." *J. Atmos. Sci.*, **35**, p.1861 - 1883.

André, J. C., and L. Mahrt, 1982: "The nocturnal surface inversion and influence of clear air radiative cooling." *J. Atmos. Sci.*, **39**, p.864 - 878.

Beljaars, A. C. M., P. Scholtanus, and F.T.M. Nieuwstadt, 1983: "Surface similarity under nonuniform fetch conditions." *J. Climat. Appl. Meteor.*, **22**, p.1800 - 1810.

Blackadar, A. L. K., 1976: Modeling the nocturnal boundary layer. In *Third symposium on atmospheric turbulence diffusion and air quality*. AMS, Boston, Mass.

Bosveld, F. C., and A.C.M. Beljaars, 1988: Complex terrain effects on dry deposition. In *16th international technical meeting on air pollution modelling and its applications*. 1988, Plemun press.

Brunt, D., 1932: "Notes on radiation in the atmosphere: I." *Quart. J. Roy. Met. Soc.*, **58**, p.389 - 420.

Brutsaert, W., 1975: "On a derivable formula for longwave radiation from clear skies." *Water Resour. Res.*, **11**, p.742 - 744.

Businger, J. A., J.C. Wyngaard, Y. Izumi, and E.F. Bradley, 1971: "Flux profile relationships in the atmospheric surface layer." *J. Atmos. Sci.*, **28**, p.181 - 189.

Cess, R. D., D.P. Kratz, S.J. Kim, and J. Caldwell, 1986: "Infrared radiation models for atmospheric methane." *J. Geophys. Res.*, **91**, (d9), p.9857 - 9864.

Chandrasekhar, S. 1960: *Radiative transfer*. Dover Publications, inc., New York, 393 pp.

Chou, M. D., and A. Arking, 1980: "Computation of infrared cooling rates in the water vapor bands." *J. Atmos. Sci.*, **37**, p.855 - 867.

Coantic, M., and B. Seguin, 1971: "On the interaction of turbulent and radiative transfers in the surface layer." *Boundary-Layer. Meteorol.*, **1**, p.245 - 263.

Coantic, M., and O. Simonin, 1984: "Radiative effects on turbulent temperature spectra and budgets in the planetary boundary layer." *J. Atmos. Sci.*, **41**, p.2629 - 2651.

Crisp, D., S.B. Fels, and M.D. Schwarzkopf, 1986: "Approximate methods for funding CO2 15-μm band transmission in planetary atmospheres." *J. Geophys. Res.*, **91**, (d11), p.11851 - 11866.

Deardorff, J. W., 1978: "Efficient prediction of ground surface temperature and moisture, with inclusion of a layer of vegetation." *J. Geophys. Res.*, **1978,** p.1889 - 1903.

Domoto G.A., 1974: *J. Quant. Spec. Radiat. Transfer,* **14,** p.935.

Driedonks, A. G. M., 1981: Dynamics of the well-mixed atmospheric boundary layer. Thesis Free University, Amsterdam. Also KNMI-Scientific Report 81-2, 189pp.

Duynkerke, P. G., and A.G.M. Driedonks, 1987: "A model for the turbulent structure of the stratocumulus topped atmospheric boundary layer." *J. Atmos. Sci.,* **44,** p.43 - 64.

Ellingson, R. G., and J.C. Gille, 1978: "An infrared radiative transfer model. Part I: Model description and comparison of observations with calculations." *J. Atmos. Sci.,* **35,** p.523 - 545.

Elliott W.P., 1963: "The height variation of vertical heat flux near the ground." *Quart. J. Roy. Met. Soc.,* **89,** p.260 - 265.

Enger, L., A.S. Smedman, and U. Hogstrom, 1986: Intermittency in a stably stratified PBL. An experimal and numerical case study. In *Seventh symposium on turbulence and diffusion.* November 12-15,1986, Boulder, CO., AMS, Boston, Mass. 377pp.

Esournel, C., and D. Guedalia, 1985: "Influence of geostrophic wind on atmospheric nocturnal cooling." *J. Atmos. Sci.,* **42,** p.2695 - 2698.

Estournel, C., 1988: Etude de la phase nocturne de la couche limité atmospherique. Thesis Université Paul Sabatier, Toulouse.

Fischer, H., 1985: "Absorption und emission." *Promet,* **15,** (heft 2/3), p.16 - 19.

Fouquart, Y., and B. Bonnel, 1980: "Computations of solar heating of the earth's atmosphere: a new parametrization." *Beitr. Phys. Atmosph.,* **53,** p.35 - 62.

Funk, J. P., 1960: "Measured radiative flux divergence near the ground at night." *Quart. J. Roy. Met. Soc.,* **86,** p.382 - 389.

Garratt, J. R., and R.A. Brost, 1981: "Radiative cooling effects within and above the nocturnal boundary layer." *J. Atmos. Sci.,* **38,** p.2730 - 2746.

Goody, R. M. 1964: *Atmospheric radiation. I. Theoretical basis.* Oxford university press, London,

Goody, R. M., 1952: "A statistical model for water vapour absorption." *Quart. J. Roy. Met. Soc,* **78,** p.165 -169.

Hansen, J., G. Russell, D. Rind, P. Stone, A. Lacis, S. Lebedeff, R. Ruedy, and L. Travis, 1983: "Efficient three dimensional global models for climate studies: Models I and II." *Mon. Wea. Rev.,* **111,** (4), p.609 - 662.

Holtslag, A. A. M., and H.A.R. de Bruin, 1988: "Applied modelling of the nighttime surface energy balance over land." *J. Appl. Meteor.,* **22,** p.689 - 704.

Kiehl, J. T., and V. Ramanathan, 1982: "Radiative heating due to increaded CO2: The role of H2O continuum absorption in the 12-18 μm region." *J. Atmos. Sci.*, **39**, (12), p.2923 - 2926.

Kondratyev, K. Ya. 1969: *Radiation in the atmosphere.* Academic press, inc., New York, 912pp.

Lacser, A., and S.P.S. Arya, 1986: "A numerical model study of the structure and similarity scaling of the nocturnal boundary layer (NBL)." *Boundary-layer Meteorol.*, **35**, p.369 - 385.

Ladenberg, R., and F. Reiche, 1913: "Selektive Absorption." *Ann. Phys.*, **42**, p.181 - 209.

Lenschow, D. H., X.S. Li, C.J. Zhu, and B.B. Stankov, 1988: "The stably straified boundary layer over the great plains. I. Mean and turbulence structure." *Boundary-Layer Meteorol.*, **42**, p.95 - 121.

Liou, K. N. 1980: *An introduction to atmospheric radiation.* Academic press, inc., New York, 392pp.

Malkmus, W., 1967: "Random Lorentz bandmodel with exponential tailed 1/S kube ubtensity distribution function." *J. Opt. Soc. Am.*, **57**, p.323 - 329.

McClatchey, R. A., R.W. Fenn, J.E.A. Selby, F.E. Volz, and J.S. Garing. 1971: *Optical properties of the atmosphere.* AFGL Rep. 71-0279. AFGL, Hanscom AFB, MA.,

Monna, W. A. A., and J.G. van der Vliet. 1987: *Facilities for research and weather observations on the 213 m tower at Cabauw and remote locations.* KNMI Scientific Report 87-5. KNMI, de Bilt, The Netherlands, 27pp.

Morcrette, J. J., and Y. Fouquart, 1985: "On systematic errors in parameterized calculations of longwave radiation transfer." *Quart. J. Roy. Met. Soc.*, **111**, p.691 - 708.

Nieuwstadt, F. T. M., 1984: "The turbulent structure of the stable, nocturnal boundary layer." *J. Atmos. Sci.*, **41**, (14), p.2202 - 2216.

Ohring, G., and J.H. Joseph, 1978: "On the combined infrared cooling of two absorbing gases in the same spectral region." *J. Atmos. Sci.*, **35**, p.317 - 322.

Oke, T. R. 1978: *Boundary layer climates.* Methuen and Co. Ltd., London, 372pp.

Pollack, J. P., and C.P. McKay, 1985: "The impact of polar stratospheric clouds on the heating rates of the winter polar stratosphere." *J. Atmos. Sci.*, **42**, (3), p.245 - 262.

Quanhua, L., and J. Schmetz, 1988: "On the problem of an analytical solution to the diffusivity factor." *Beitr. Phys. Atmosph.*, **61**, (1), p.23 - 29.

Ramanathan, V., 1976: "Radiative transfer within the earth's troposhere and stratosphere: A simplified radiative convective model." *J. Atmos. Sci.*, **33**, p.1330 - 1346.

Robert, A. J., 1966: "The integration of a low order spectral form of the primitive meteorological equations." *J. Meteor. Soc. Japan,* **44,** p.237 - 244.

Roberts, R. E., J.E.A. Selby, and L.M. Biberman, 1976: "Infrared continuum absorption by atmospheric water vapor in the 8-12 μm window." *Appl. Opt.,* **15,** p.2085 - 2090.

Rodgers, C. D., 1967: "The use of emissivity in atmospheric radiation calculations." *Quart. J. Roy. Met. Soc.,* **93,** p.43 - 54.

Rodgers, C. D., and C.D. Walshaw, 1966: "The computation of infrared cooling rate in planetary atmospheres." *Quart. J. Roy. Met. Soc.,* **73,** p.67 - 92.

Rothman, L. S., 1981: "AFGL atmospheric line parameters compilation: 1980 version." *Appl. Opt.,* **20,** p.802 - 812.

Sasamori, T., 1968: "The radiative cooling calculations for application to general circulation experiments." *J. Appl. Meteor.,* **7,** (5), p.721 - 729.

Scott, N. A., and A. Chedin, 1981: "A fast line by line method for atmospheric absorption calculations. The automatized atmospheric absorption atlas." *J. Appl. Meteor.,* **20,** p.802 - 812.

Stephens G.L., 1984: "The parameterization of radiation for numerical weather prediction and climate models." *Mon. Wea. Rev.,* **112,** p.826 - 867.

Swinbank, W. C., 1963: "Longwave radiation from clear skies." *Quart. J. Roy. Met. Soc.,* **89,** p.339 - 348.

Ten Berge, H. F. M., 1986: Heat and water transfer at the bare soil surface: Aspects affecting thermal imagery. Thesis Agricultural University, Wageningen.

Tiwari, S. N., 1980: "Models for infrared atmospheric radiation." *Adv. Geophys.,* **20,** p.1 - 85.

Tjemkes S.A., 1988: A comparison of infrared radiation codes for the nocturnal boundary layer. In *IRS'88: Current problems in atmospheric radiation.* 18-24 August 1988, Lille (France), A. Deepak, Hampton, Vir.

Tjemkes, S. A., and P.G. Duynkerke, 1988a: "A new look at the goody band model." *Beitr. Phys. Atmosph.,* **61,** (2), p.105 - 113.

Tjemkes, S. A., and P.G. Duynkerke, 1988b: "The nocturnal boundary layer. Model calculations compared with observations." *J. Appl. Meteor.,* (accepted for publication).

Tjemkes, S. A., and P.G. Duynkerke, 1988c: The nocturnal boundary layer. Model calculations compared with observations. In *Eighth symposium on turbulence and diffusion.* April 26-29, 1988, San Diego, Calif., AMS, Boston, Mass. 420pp.

Tjemkes S.A., and F.T.M. Nieuwstadt, 1988: "An accurate radiation model." *submitted to J. Geophys. Res.*

van Ulden, A. P., and A.A.M. Holtslag, 1985: "Estimation of atmospheric boundary layer parameters for diffusion applications." *J. Climat. Appl. Meteor.,* **24,** (11), p.1196 - 1207.

van Wijk, W. R., and D.A. de Vries. 1963: Periodic temperature variations in a homogeneous soil. *Physics of plant environment.* ed. by van Wijk, W.R. North Holland publishing company, Amsterdam, 382pp.

Wang, W. C., and G.Y. Shi, 1988: "Total band absorptance and k-distribution function for atmospheric gases." *J. Quant. Spectrosc. Radiat. Transfer,* **39,** (5), p.387 - 397.

Welch R., and W. Zdunkowski, 1976: "A radiation model of the polluted atmospheric boundary layer." *J. Atmos. Sci.,* **33,** p.2170 - 2184.

Wessels, H. R. A., 1983: "Soil moisture measurements 1977 - 1981 at the Cabauw micrometeorology field." Personal memorandum,

World Meteorological Organization (WMO). 1984: *The intercomparison of radiation codes in climate models (ICRCCM).* Prep. by Y. Fouquart. World climate research program WCP-93. Geneva, Switzerland, 37pp.

Wyatt, P. J., V.R. Stull, and G.N. Plass, 1962: "Quàsi-random model for band absorption." *J. Opt. Soc. Am.,* **52,** p.1209 - 1217.

Yaglom, A. M., 1977: "Comments on wind and temperature flux-profile relationships." *Boundary-layer Meteorol.,* **11,** p.89 - 102.

Samenvatting en Conclusies.

Het voornaamste doel van deze studie is om het transport van langgolvige straling (golflengte tussen 3.6 en 100 μm) door een wolkenloze nachtelijke grenslaag te beschrijven.

De nachtelijke grenslaag is een dunne atmosferische laag (dikte ca. 200m) welke direct grenst aan het aardoppervlak en gedurende de nacht onwikkelt. Het warmte transport in de nachtelijke grenslaag vindt voornamelijk plaats door turbulente menging. Een model beschrijving van de grenslaag, waarin uitsluitend turbulente menging energie transporteert is bekend. Echter naast turbulente menging draagt langgolvige straling wezenlijk bij tot dit warmte transport. Met name nabij de grenslaag top, waar de turbulente menging zwak is en nabij het aardoppervlak, waar de stralings afkoeling bijzonder sterk is. Omdat langgolvige straling direct gekoppeld is aan de thermodynamische structuur van de grenslaag, zal afkoeling door langgolvige straling de turbulente structuur van de grenslaag beinvloeden. Mijn onderzoek concertreert zich op het transport van langgolvige straling door de grenslaag en de wisselwerking tussen straling en turbulentie met het doel dynamische processen in de nachtelijke grenslaag beter te begrijpen.

In deze studie wordt het transport van langgolvige straling beschreven met behulp van een smalbandig stralingsmodel. Hierin wordt het langgolvige spectrum opgedeeld in een groot aantal spectrale intervallen. Per interval wordt een gemiddelde flux berekend aan de hand van een stralings transport vergelijking. In het in hoofdstuk 3 beschreven stralingsmodel, met in appendix B aanvullende theorie, beschouw ik 178 spectrale intervallen met een typische breedte van 30 THz. Op grond van een vergelijking met 44 gevallen van gemeten neerwaartse fluxen aan het aardoppervlak en een vergelijking met onafhankelijke berekeningen, concludeer ik dat het smal bandig stralingsmodel de neerwaartse flux nabij het aardoppervlak met een gemiddelde fout van 3 W/m2 (≈ 1.5 %) en de koelingsnelheid met een gemiddelde fout van 0.2 K/dag (≈ 20 %) kan berekenen.

In hoofdstuk 4 wordt de wisselwerking tussen langgolvige straling en turbulente menging bestudeerd aan de hand van een vergelijkingstudie tussen modelberekeningen en waarnemingen in de nachtelijke grenslaag. De berekeningen werden uitgevoerd met behulp van het in hoofdstuk 3 beschreven smalbandig stralingmodel, om het transport van langgolvige straling te beschrijven, in combinatie met een E-l turbulentie model, om de luchtstroming in een horizontaal homogene grenslaag te beschrijven. De waarnemingen hebben betrekking op de thermodynamische en turbulente structuur van de onderste 200 m van de atmosfeer tesamen met metingen van de energiebalans van het oppervlak.

Hoewel niet alle details van de waarnemingen gereproduceerd kunnen worden, concludeer ik dat een bevredigende overeenkomst bestaat tussen modelberekening en waarneming. Op grond van deze berekeningen laat ik verder zien dat langgolvige straling alleen van belang is voor de structuur en evolutie van luchtlagen nabij de grenslaag top en nabij het oppervlak. Voor de overige luchtlagen in de nachtelijke grenslaag speelt langgolvige straling geen rol van betekenis. De structuur en evolutie van deze lagen wordt voornamelijk bepaald door turbulente menging. Verder blijkt uit deze berekeningen dat langgolvige straling de stabiliteit van de nachtelijk grenslaag verlaagt. Hierdoor kan de grenslaag ongeveer 25 % dikker worden.

De hoge nauwkeurigheid van het in hoofdstuk 3 beschreven smal bandige stralingsmodel, kost veel rekentijd. Daarom is dit model minder geschikt om in een grenslaagmodel voor de korte termijn weersverwachting te gebruiken. In appendix A

wordt een alternatief stralingsmodel, een zgn. k-distributie model, beschreven. Hierin wordt de gemiddelde transmissie van een spectraal interval uitgerekend met behulp van een beperkt aantal absorptie coefficienten (k's) Hierdoor is een k-distibutie model bijzonder snel, zonder significant verlies van nauwkeurigheid. Bovendien kan een k-distributie model eenvoudig uitgebreid worden om ook het transport van langgolvige straling door een bewolkte grenslaag te beschrijven. Hierdoor zijn k-distributie modellen bijzonder geschikt voor toepassing in numerieke grenslaag modellen.

Naast het bestuderen van de interactie tussen straling en turbulentie kan het in hoofdstuk 4 beschreven gekombineerde stralings-turbulentie model, ook gebruikt worden bij gevoeligheids analyses. Een voorbeeld van een dergelijke studie wordt gegeven in hoofdstuk 5. Hier wordt de invloed van de geostrofische wind op de minimum oppervlakte temperatuur beschreven. Op grond van model berekeningen wordt een eenvoudige formule voor de minimum oppervlakte temperatuur voor een verzadigde klei bodem voorgesteld. Uit een vergelijking met waarnemingen blijkt dat dit parametrisatie schema de minimum oppervlakte temperatuur met een nauwkerigheid van ongeveer 2.5 K kan berekenen.

De nachtelijke grenslaag is een dunne atmosferische laag. Omdat bijna alle menselijke activiteiten zich afspelen in de grenslaag is een goed begrip van de nachtelijke grenslaag van wezenlijk belang. Deze studie beperkt zich tot de wolkenloze nachtelijke grenslaag. Een situatie die niet vaak in Nederland voorkomt. Verder onderzoek aan de bewolkte grenslaag is daarom aan te bevelen.

Cirriculum Vitae

Naam	Stephen Arnoldus Tjemkes	
Geboortedatum	14 november 1958	
Geboorteplaats	Alkmaar	
Vooropleiding	1971 - 1978	Atheneum B a/h "Jan Arentz college" in Alkmaar
	1978 - 1984	Sterrenkunde a/d universiteit van Amsterdam
	Hoofdvak	Sterrenkunde
	1e Bijvak	Natuurkunde
	2e Bijvak	Meteorologie
Kandidaats examen	1981	
Doctoraal examen	1984 (met genoegen)	
Promotie onderzoek	1984 - 1988 op het Koninklijk Nederlands Meteorologisch Instituut (KNMI) in de Bilt, in dienst van de werkgemeenschap Meteorologie en Fysische Oceanografie (MFO). In 1986 gedurende twee maanden gast onderzoeker aan de Colorado State University in Amerika	